

AD-A076 535

MASSACHUSETTS INST OF TECH LEXINGTON LINCOLN LAB

F/G 17/9

TURBULENCE EFFECTS ON THE RECEIVER OPERATING CHARACTERISTICS OF--ETC(U)

JUL 79 B A CAPRON , J H SHAPIRO , R C HARNEY

F19628-78-C-0002

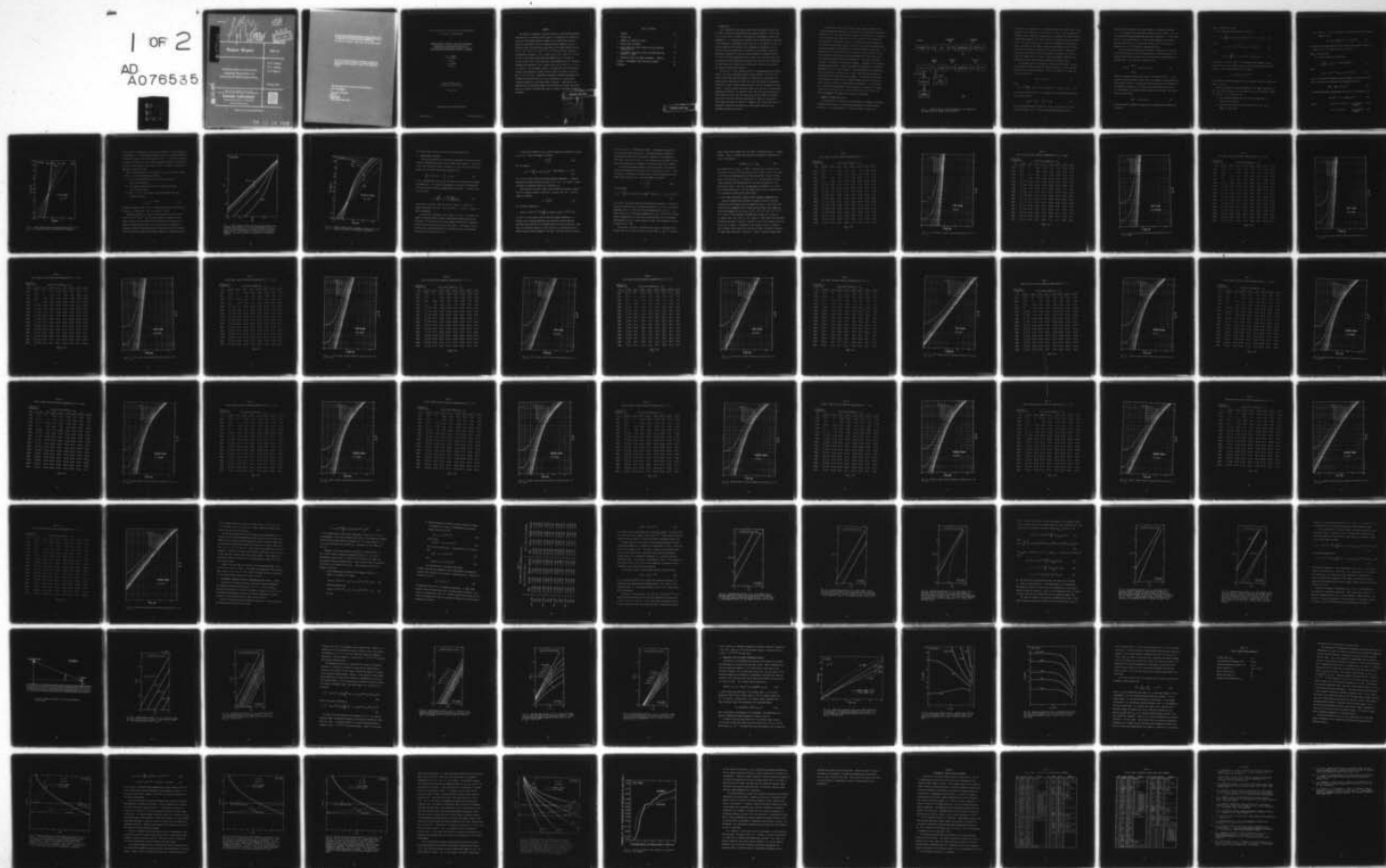
UNCLASSIFIED TST-33

ESD-TR-79-189

NL

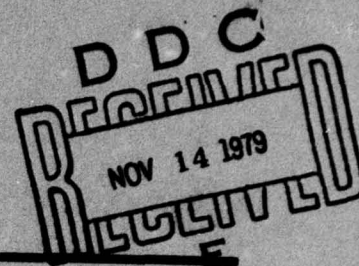
1 OF 2

AD
A076535



AD A 076535

LEVEL



Project Report

TST-33

Turbulence Effects on the Receiver
Operating Characteristics of a
Heterodyne-Reception Optical Radar

B. A. Capron
R. C. Harney
J. H. Shapiro

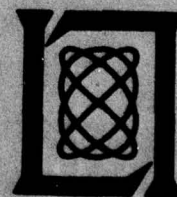
26 July 1979

Prepared for the Department of the Air Force
under Electronic Systems Division Contract F19628-78-C-0002 by

Lincoln Laboratory

MASSACHUSETTS INSTITUTE OF TECHNOLOGY

LEXINGTON, MASSACHUSETTS



Approved for public release; distribution unlimited.

79 11 13 027

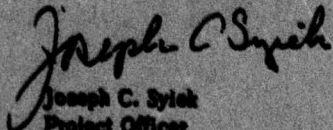
The work reported in this document was performed at Lincoln Laboratory, a center for research operated by Massachusetts Institute of Technology, with the support of the Department of the Air Force under Contract F19628-78-C-0002.

This report may be reproduced to satisfy needs of U.S. Government agencies.

The views and conclusions contained in this document are those of the contractor and should not be interpreted as necessarily representing the official policies, either expressed or implied, of the United States Government.

This technical report has been reviewed and is approved for publication.

FOR THE COMMANDER



Joseph C. Syiah
Project Officer
Lincoln Laboratory Project Office

MASSACHUSETTS INSTITUTE OF TECHNOLOGY
LINCOLN LABORATORY

TURBULENCE EFFECTS ON THE RECEIVER
OPERATING CHARACTERISTICS OF A
HETERODYNE-RECEPTION OPTICAL RADAR

B. A. CAPRON

R. C. HARNEY

Group 53

J. H. SHAPIRO

Consultant

PROJECT REPORT TST-33
(Tactical Systems and Technology)

26 JULY 1979

Approved for public release; distribution unlimited.

LEXINGTON

MASSACHUSETTS

ABSTRACT

The theory of atmospheric turbulence effects on the receiver operating characteristics of coherent optical radars is reviewed and the theoretical results for the target detection probability are numerically evaluated. Graphs are presented of the glint target detection probability P_D as a function of the carrier-to-noise ratio CNR at false alarm probabilities P_F of 10^{-1} , 10^{-3} , 10^{-5} , 10^{-7} , 10^{-9} , 10^{-11} , 10^{-13} , and 10^{-15} for turbulence log-amplitude variances σ_X^2 of 0, 0.0001, 0.001, 0.01, 0.05, 0.1, 0.2, and 0.5 and of the speckle target detection probability as a function of carrier-to-noise ratio at the same false alarm probabilities for turbulence log-amplitude variances σ^2 of 0, 0.0001, 0.001, 0.01, 0.05, 0.1, 0.2, 0.5, 1.0, and 2.0. For each graph a table is included which gives the carrier-to-noise ratio required to obtain various specific P_D values at given P_F and σ_X^2 (or σ^2) values. Experimental turbulence strength measurements are reviewed and selected results are used to determine the log-amplitude variances expected to occur under typical scenarios. These results are combined with the detection probability calculations to predict the performance of a realistic infrared radar under a variety of turbulent propagation conditions.

PRECEDING PAGE BLANK

NTIS GRA&I		<input checked="" type="checkbox"/> <input type="checkbox"/> <input type="checkbox"/>
DDC TAB		
Unannounced		
Justification		
By _____		
Distribution/ _____		
Availability Codes _____		
Dist	Availand/or special	
A		

TABLE OF CONTENTS

ABSTRACT	iii
1. INTRODUCTION	1
2. SUMMARY OF THEORETICAL RESULTS	2
3. COMPUTATIONAL PROCEDURES	12
4. GLINT TARGET AND SPECKLE TARGET RECEIVER OPERATING CHARACTERISTICS	15
5. EXPERIMENTAL TURBULENCE STRENGTH DETERMINATIONS AND TYPICAL σ_x^2 VALUES	52
6. TURBULENCE EFFECTS ON RADAR PERFORMANCE - EXAMPLES	71
APPENDIX. PROGRAMMABLE HAND CALCULATOR PROGRAMS	87
REFERENCES	90

PRECEDING PAGE BLANK

1. INTRODUCTION

Laser rangefinders and imaging radars offer new technical options for a variety of tactical target detection and imaging scenarios. Such systems will, of necessity, be subject to the vagaries of atmospheric optical wave propagation, i.e., absorption and scattering due to the molecular constituents of the atmosphere, hydrometeors (rain, snow, etc.), and aerosols, as well as phase and amplitude fluctuations due to atmospheric turbulence. As yet, there has been no comprehensive assessment of the limitations imposed by atmospheric propagation on optical radar performance, although extinction calculations [1] and measurements tend to favor use of the $10.6\mu\text{m}$ CO_2 laser wavelength over other candidate wavelengths (the $3.83\mu\text{m}$ DF laser wavelength has better extinction properties but existing DF lasers are not suitable for compact infrared radar systems).

At the M.I.T. Lincoln Laboratory there is an ongoing program to develop compact, CO_2 laser, heterodyne-reception radars [2]-[5]. As part of this effort we have undertaken development of a mathematical system model for a compact optical radar which includes the statistical effects of atmospheric propagation, target reflection characteristics, and the heterodyne detection process. To date, we have limited our analysis to the case of clear-weather propagation conditions. As detailed in Ref. [6], this choice enabled us to derive explicit results for the signal-to-noise ratio (SNR) of an imaging radar and the receiver operating characteristics (ROC) for single-pulse target detection within an analytical framework that includes the effects of atmospheric absorption and turbulence, target speckle and glint, and heterodyne-reception shot noise.

The SNR results reported in [6] were simple enough to permit direct numerical performance evaluation; the ROC results, in particular the detection probabilities for specular and diffuse targets in the presence of turbulence, were considerably more complicated. In this report we shall present ROC calculations for these cases. Section 2 is devoted to a brief summary of the relevant system theory from [6]. Section 3 describes the computational procedures employed in evaluating the detection probability expressions. The major portion of the report, Section 4, comprises tables and graphs of the glint target and speckle target detection probabilities versus carrier-to-noise ratio at selected false alarm probabilities for various turbulence strengths. Utilization of these results require knowledge of the turbulence log-amplitude variances. Several experimental determinations of turbulence parameters (C_n^2 or C_T^2) are available. These measurements are summarized in Section 5 and used to estimate the σ_x^2 values that might be obtained over horizontal and slant paths of varying lengths. The material in Sections 4 and 5 should be of direct value to system designers who need to accurately assess turbulence effects on target detection performance. To illustrate this, we present representative system calculations in Section 6. Finally, programs for performing speckle target calculations on HP-67, HP-97, and HP-29C programmable calculators are included in an Appendix.

2. SUMMARY OF THEORETICAL RESULTS

For the purposes of statistical system modeling, a monostatic heterodyne-reception optical radar is conveniently represented by the block diagram of Figure 1. This representation is valid for either a pulsed laser

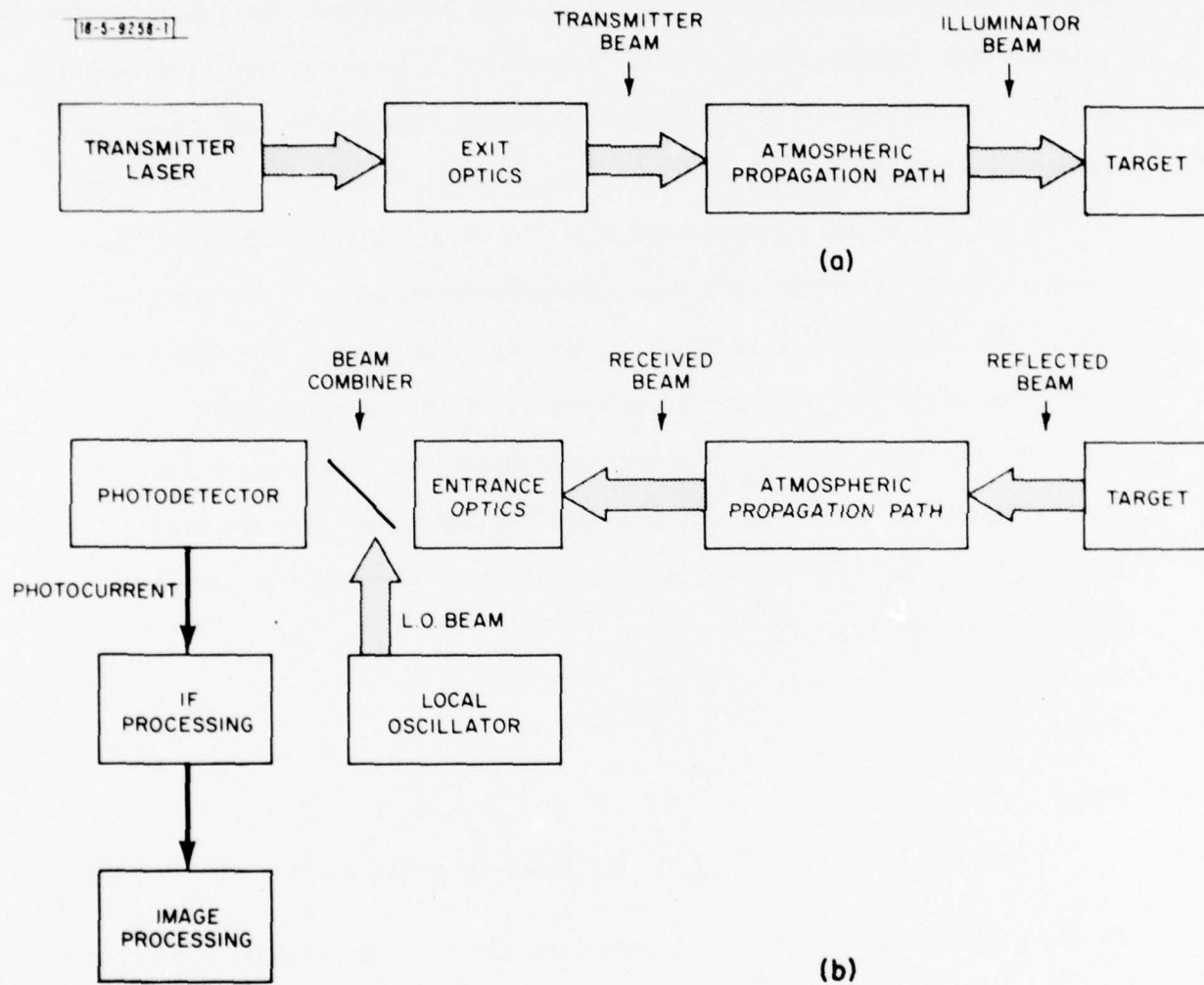


Fig. 1. Coherent optical radar configuration: (a) transmitter-to-target path, (b) target-to-receiver path.

transmitter or a scanned cw laser transmitter whose pixel dwell time is short compared to the atmospheric coherence time (~ 1 msec). In all weather conditions for which atmospheric backscatter can be ignored, the radar receiver's intermediate-frequency (IF) signal consists of a target return plus receiver noise. The target return may be influenced by atmospheric beam spreading (which can reduce the on-target irradiance) and atmospheric scintillation, as well as the reflection properties of the target itself. Because the radar employs heterodyne reception, atmospheric coherence-loss can also affect the target-return IF signal. Finally, atmospheric absorption will introduce an overall exponential extinction of the target return.

The parameter values envisaged for compact CO_2 laser radars are such that atmospheric beam spreading and receiver coherence loss are negligible under typical turbulence conditions. Thus, the receiver's IF signal has complex envelope [6]

$$\underline{r}(t) = \underline{y} + \underline{n}(t) \quad (1)$$

where

$$\underline{y} = P_T^{1/2} \int d\bar{\rho}' \underline{\varepsilon}_t^2(\bar{\rho}') \underline{I}(\bar{\rho}') \exp[2\chi(\bar{\rho}', \bar{0}) + 2j\phi(\bar{\rho}', \bar{0}) - \alpha L] \quad (2)$$

is the target return and $\underline{n}(t)$, a zero-mean circulo-complex Gaussian process with spectral density

$$S_{nn}(f) = h\nu_0/\eta \quad \text{for } |f| \leq W, \quad (3)$$

is the heterodyne-receiver shot noise. In Eqs. (2) and (3), P_T is the transmitter power, $\underline{\varepsilon}_t(\bar{\rho}')$ is the normalized (square-integral unity)

transmitter field pattern in the target plane vs. transverse coordinate $\bar{\rho}'$, \underline{I} is the complex field reflection coefficient of the target, χ and ϕ are the turbulence-induced log-amplitude and phase fluctuations, α is the atmospheric extinction coefficient, L is the distance between the transmitter and the target plane, $h\nu_0$ is the photon energy, $2W$ is the unilateral IF bandwidth, and η is the detector's quantum efficiency.

For the problem of deciding on the absence or presence of a target at a particular resolution cell and range based on a single observation, the optimum Neyman-Pearson processor uses a matched-filter envelope-detection threshold test. This test can be given the form

$$|\underline{r}(0)|^2 \begin{array}{c} \text{say } H_1 \\ \geq \\ \text{say } H_0 \end{array} -(2h\nu_0 W/\eta) \ln P_F \quad (4)$$

where W is adjusted so that the IF filter is the matched filter. In this expression H_0 and H_1 denote, respectively, the hypotheses target absent and target present, and $P_F = \Pr [\text{say } H_1 | H_0 \text{ true}]$ is the false alarm probability. The detection probability $P_D = \Pr [\text{say } H_1 | H_1 \text{ true}]$ achieved by the test Eq. (4) depends on the target character (specular or diffuse), the receiver carrier-to-noise ratio

$$\text{CNR} = \eta \langle |\underline{y}|^2 \rangle / 2h\nu_0 W \quad (5)$$

and the turbulence strength (as measured by the appropriate log-amplitude variance).

Case 1 Single-Glint Target

For a single-glint target we find that [6]

$$P_D = \int_{-\infty}^{\infty} d\chi \, p_X(\chi) \, Q_1 \left[(2 \text{CNR}_g^0)^{1/2} e^{2\chi}, (-2 \ln P_F)^{1/2} \right] \quad (6)$$

where

$$p_X(\chi) = (2\pi \sigma_X^2)^{-1/2} \exp \left[-(\chi + \sigma_X^2)^2 / 2\sigma_X^2 \right] \quad (7)$$

and

$$Q_1(\alpha, \beta) = \int_{\beta}^{\infty} du \, u \exp \left[-(u^2 + \alpha^2)/2 \right] I_0(\alpha u) \quad (8)$$

is Marcum's Q-function, CNR_g^0 is the turbulence-free propagation glint target carrier-to-noise ratio, and I_0 is the zeroth-order modified Bessel function. The log-amplitude variance is given by

$$\sigma_X^2 = 0.124 C_n^2 k^{7/6} L^{11/6} \quad (9)$$

for a uniform turbulence-strength (C_n^2) distribution along the optical path and $k = 2\pi \nu_0/c$.

We have discussed and presented examples of the CNR_g^0 calculation in [6]. Our present interest is in the behavior of P_D as a function of CNR_g^0 , σ_X^2 , and P_F . It is easily seen that:

- i) P_D increases monotonically with increasing CNR_g^0 when σ_X^2 and P_F are held fixed;
- ii) P_D increases monotonically with increasing P_F when σ_X^2 and CNR_g^0 are held fixed;

iii) when $\sigma_X^2 = 0$, Eq. (6) reduces to the well-known free-space propagation result

$$P_D = Q_1 [(2 \text{CNR}_g^0)^{1/2}, (-2 \ln P_F)^{1/2}] \quad (10)$$

To indicate the general behavior of Eq. (6) we have plotted in Figure 2 P_D vs. CNR_g^0 for $P_F = 10^{-7}$ and a variety of σ_X^2 values.

Case 2 Speckle Target

For a speckle target we find that [6]

$$P_D = \int_{-\infty}^{\infty} dU p_U(U) P_F (1 + \text{CNR}_S \exp[2U])^{-1} \quad (11)$$

where

$$p_U(U) = (2\pi \sigma^2)^{-1/2} \exp [-(U + \sigma^2)^2 / 2\sigma^2] \quad (12)$$

CNR_S is the turbulent-propagation speckle target carrier-to-noise ratio and is related to the turbulence-free propagation value by

$$\text{CNR}_S = \text{CNR}_S^0 \exp [4\sigma_X^2] \quad (13)$$

The aperture-averaged log-amplitude variance (σ^2) is related to σ_X^2 by

$$\exp [4\sigma^2] - 1 = \zeta (\exp[16\sigma_X^2] - 1) \quad (14)$$

where

$$\zeta \approx (d^2/\lambda L)/(1 + (d^2/\lambda L)) \quad \text{for resolved targets} \quad (15)$$

$$\approx 1/(1 + (d_t^2/\lambda L)) \quad \text{for unresolved targets} \quad (16)$$

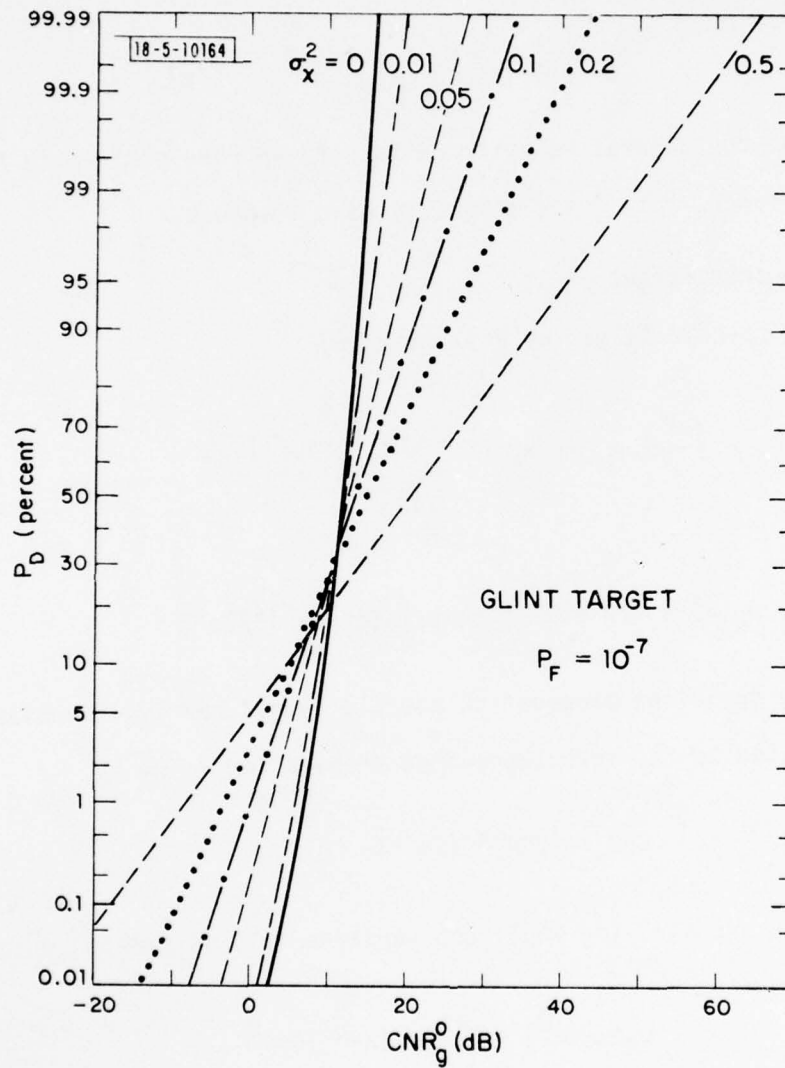


Fig. 2.-7 Glint target receiver operating characteristics for $P_F = 10^{-7}$ showing the effects of atmospheric turbulence.

is the aperture-averaging factor for aperture diameter d , target diameter d_t , and wavelength λ . The relationship between σ^2 and σ_X^2 for resolved targets is plotted in Figure 3 for several values of $d^2/\lambda L$. It should be noted that the curves of Figure 3 are also valid for unresolved targets if the quantity $(\lambda L/d_t^2)$ is substituted for the quantity $(d^2/\lambda L)$. Further calculations of CNR_S and σ^2 are given in [6].

We are interested herein in the behavior of P_D as a function of CNR_S , σ^2 , and P_F . It is easily demonstrated that:

- i) P_D increases monotonically with increasing CNR_S when σ^2 and P_F are held fixed;
- ii) P_D increases monotonically with increasing P_F when CNR_S and σ^2 are held fixed;
- iii) when $\sigma^2 = 0$, Eq. (11) reduces to the well-known free-space propagation result

$$P_D = P_F (1 + CNR_S^0)^{-1} \quad (17)$$

The general behavior of Eq. (11) is illustrated in Figure 4, where we have plotted P_D vs. CNR_S for $P_F = 10^{-7}$ and various σ^2 values.

Inasmuch as typical σ_X^2 values in the long-wave infrared may range from 10^{-4} to 10^{-1} and $\sigma^2 = 4\sigma_X^2$ for small targets or targets at short ranges, Figures 2 and 4 indicate that significant CNR increases may be needed to maintain high P_D values at low P_F values in the presence of turbulence. We will illustrate the use of these detection theory results after we describe the numerical procedures employed in generating Figures 2

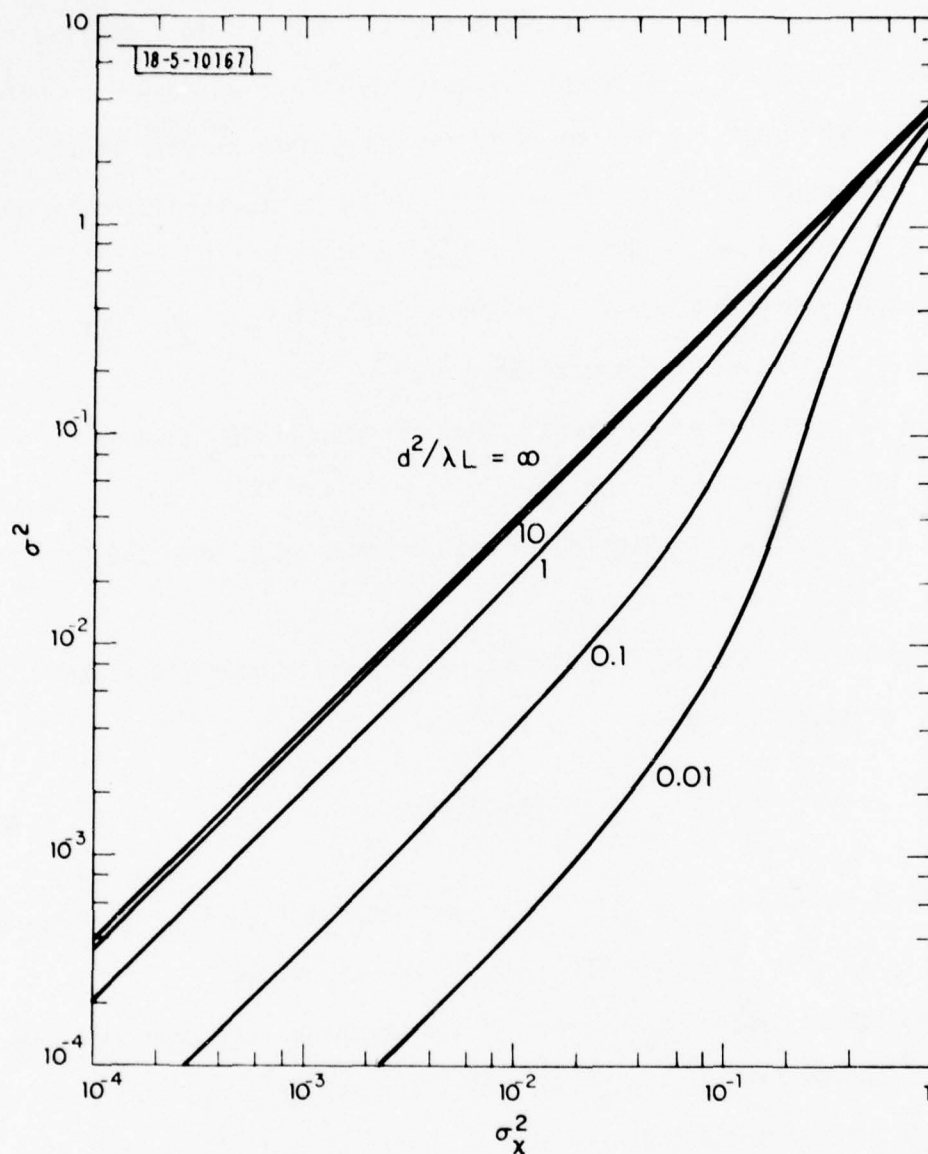


Fig. 3. Relationship of the aperture-averaged speckle target log-amplitude variance (σ^2) to the log-amplitude variance (σ_x^2) for resolved targets with various values of the Fresnel number ($d^2/\lambda L$). These curves are also valid for unresolved targets if the quantity ($d^2/\lambda L$) is replaced by the quantity ($\lambda L/d_t^2$).

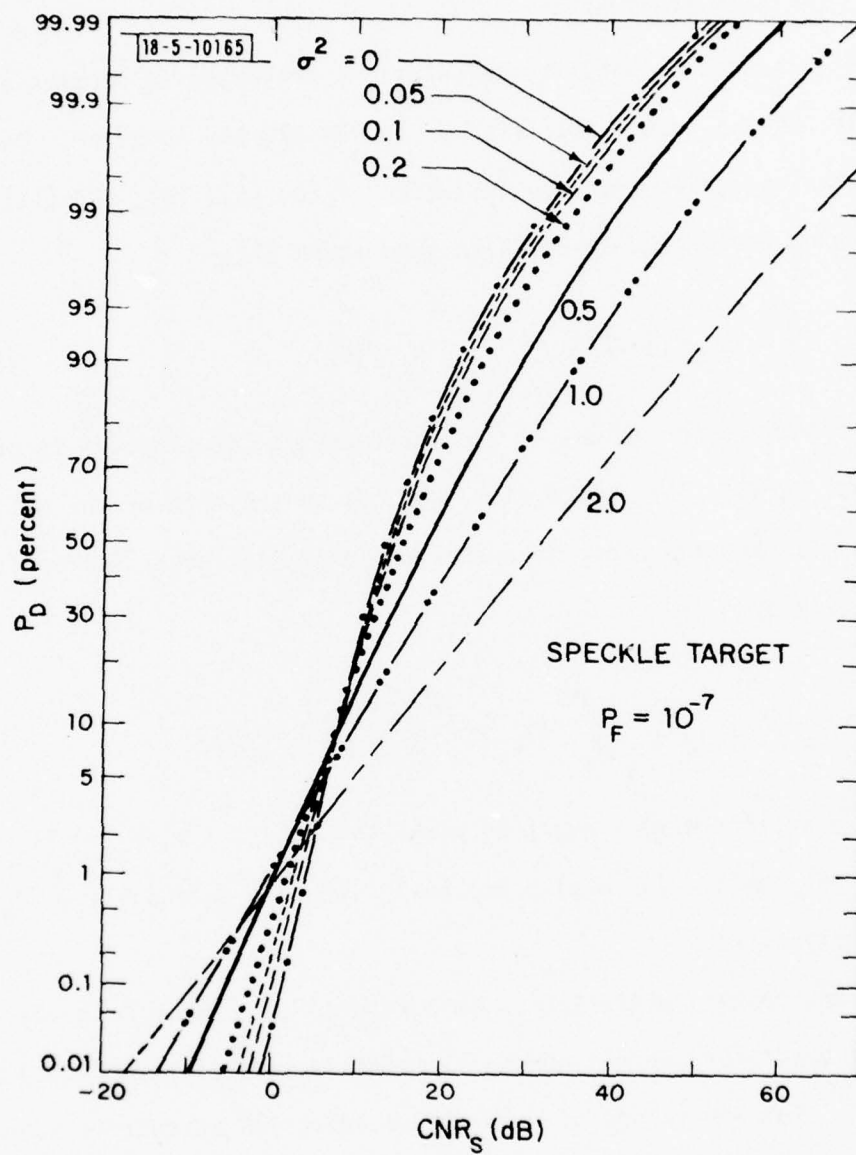


Fig. 4.-7 Speckle target receiver operating characteristics for $P_F = 10^{-7}$ showing the effects of atmospheric turbulence.

and 4 and present results for other false-alarm probabilities.

3. COMPUTATIONAL PROCEDURES

The detection probability calculations presented in Section 4 were performed in FORTRAN double precision on an IBM 370/168 computer. Due to the form of the integrals involved, solution of Eq. (6), (8), and (11) was performed using the method of Gaussian quadrature [7]:

$$\int_a^b dx w(x) f(x) \simeq \sum_{i=1}^N A_i f(x_i) \quad (18)$$

In this technique the values x_i are the zeroes of an appropriate orthogonal polynomial $P_N(x)$. The choice of P_N depends on the form of the weighting function $w(x)$ and the order of approximation N required. The coefficients A_i are given by

$$A_i = \int_a^b dx \frac{w(x) P_N(x)}{(x - x_i) dP_N(x_i)/dx} \quad (19)$$

In particular, for $w(x) = \exp [-x]$ with $a = 0$ and $b = \infty$, $P_N(x)$ is a Laguerre polynomial; for $w(x) = \exp [-x^2]$ with $a = -\infty$ and $b = \infty$, $P_N(x)$ is a Hermite polynomial.

For the results presented in this report, as σ^2 or σ_x^2 increased, the number of quadrature points needed to maintain sufficient accuracy also increased. For low values of N (≤ 64) standard IBM Scientific Subroutine Package routines were used to obtain the A_i and x_i . For larger values of N the A_i and x_i were calculated using a modified version of the program presented by Stroud and Secrest [7].

The detection probability for a diffuse target with turbulence is given by Eq. (11). Using the change of variables

$$\tau = \frac{U + \sigma^2}{\sigma \sqrt{2}} \quad (20)$$

Eq. (11) becomes

$$P_D = \pi^{-1/2} \int_{-\infty}^{\infty} d\tau \exp[-\tau^2] P_F (1 + \text{CNR}_S \exp[2\sigma(\tau \sqrt{2} - \sigma)])^{-1} \quad (21)$$

Eq. (21) has a form suitable for Gaussian-Hermite quadrature. A 16-point quadrature provided sufficient accuracy for $\sigma^2 \leq 0.2$. For larger σ^2 values the number of quadrature points was increased to 32.

Calculation of the glint target cases involved two separate integrals. The first integral, Marcum's Q-function, is given in Eq. (8). Using the change of variables

$$t = \frac{U^2 - \beta^2}{2} \quad (22)$$

Eq. (8) may be rewritten as

$$Q_1(\alpha, \beta) = \exp[-(\alpha^2 + \beta^2)/2] \int_0^{\infty} dt \exp[-t] I_0(\alpha(2t + \beta^2)^{1/2}) \quad (23)$$

Eq. (23) is in the correct form for Gaussian-Laguerre quadrature. A routine using a 32-point quadrature was sufficient to match Marcum's tabulated values [8] out to six decimal places for nearly every case. However, at the largest values of α for a given β , Q_1 approached but never reached unity and then proceeded to fall off. This fall off did not occur

until values of $Q_1 \approx 0.999999$ were reached. An asymptotic expansion for Q_1 has been previously derived [9]. The Gaussian-Laguerre quadrature proved more accurate than the asymptotic expansion in matching Marcum's value until the fall off occurs. In the program Q_1 was set equal to unity when a test showed that the asymptotic value was greater than 0.9999995.

This Gaussian-Laguerre quadrature routine was used to calculate the free-space propagation glint target results according to Eq. (10). It was also used as a subroutine in determining the turbulent-propagation glint target results from Eq. (6). Using the change of variables

$$\xi = \frac{x + \sigma_x^2}{\sigma_x \sqrt{2}} \quad (24)$$

Eq. (6) becomes

$$P_D = \pi^{-1/2} \int_{-\infty}^{\infty} d\xi \exp[-\xi^2] Q_1 [(2 \text{ CNR}_g^0)^{1/2} \exp[2\sigma_x(\xi \sqrt{2} - \sigma_x)], (-2 \ln P_F)^{1/2}] \quad (25)$$

Eq. (25) has the correct form for Gaussian-Hermite quadrature. Sufficient accuracy was obtained with a 24-point quadrature for $\sigma_x^2 \leq 0.01$, a 48-point quadrature for $\sigma_x^2 = 0.05$, and a 96-point quadrature for $\sigma_x^2 = 0.1$. For higher values of σ_x^2 a 198-point quadrature was used. In this last instance accuracy comparable to the preceding calculations was still not achieved. Unfortunately, A_i and x_i values needed for higher order quadrature could not be located for $N > 198$.

The accuracy criterion in determining the number of quadrature points used was that the calculated P_D value for given CNR , P_F , and σ_x^2 should not

change by more than 0.000001 when the number of quadrature points is roughly doubled. Tables 1 through 8 were obtained by numerically determining the roots of the equation

$$P_D(\text{CNR}; P_F, \sigma_X^2) = P_{D0} \quad (26)$$

for selected values of P_{D0} . In Tables 1 through 6 and 9 through 18, the calculations of P_D were sufficiently accurate to permit errors of less than ± 0.01 dB in the estimated value of CNR to be achieved in every instance. Tables 7 and 8 are for $\sigma_X^2 = 0.2$ and $\sigma_X^2 = 0.5$. At these high σ_X^2 values a weak sinusoidal oscillation about the true curve was observed in the calculated P_F curve. This error corresponded to a maximum of ± 0.1 dB in the calculated CNR values. For this reason Tables 7 and 8 are given to one less significant figure than the other tables.

4. GLINT TARGET AND SPECKLE TARGET RECEIVER OPERATING CHARACTERISTICS

Using the computational procedures discussed in Section 3 we have evaluated the glint target detection probability (P_D) as a function of the turbulence-free propagation glint target carrier-to-noise ratio (CNR_g°) for false alarm probability (P_F) values of 10^{-1} , 10^{-3} , 10^{-5} , 10^{-7} , 10^{-9} , 10^{-11} , 10^{-13} , and 10^{-15} and turbulence log-amplitude variance (σ_X^2) values of 0, 0.0001, 0.001, 0.01, 0.05, 0.1, 0.2, and 0.5. These results are presented as families of curves in Figures 5 through 12, each figure giving results for one of the σ_X^2 values. In addition to the figure, for each σ_X^2 value we have included a table which lists the value of CNR_g° (in decibels) required to obtain specified values of P_D and P_F . Tables 1 through 8 present data

TABLE 1

GLINT TARGET RECEIVER OPERATING CHARACTERISTICS $\sigma_x^2 = 0$

Detection Probability P_D	False Alarm Probability - P_F							
	10^{-1}	10^{-3}	10^{-5}	10^{-7}	10^{-9}	10^{-11}	10^{-13}	10^{-15}
.0001	**	**	-4.39	2.14	5.29	7.35	8.88	10.08
.0010	**	$-\infty$	0.68	4.79	7.20	8.89	10.18	11.22
.0100	**	-1.77	4.31	7.19	9.06	10.44	11.53	12.43
.1000	$-\infty$	4.08	7.60	9.65	11.09	12.19	13.09	13.85
.3000	-0.70	6.65	9.37	11.07	12.31	13.27	14.07	14.75
.5000	2.50	8.06	10.42	11.94	13.06	13.95	14.69	15.32
.7000	4.75	9.27	11.35	12.72	13.75	14.58	15.27	15.86
.8000	5.86	9.93	11.86	13.16	14.14	14.93	15.60	16.17
.8500	6.47	10.31	12.17	13.42	14.38	15.15	15.79	16.35
.9000	7.18	10.76	12.53	13.74	14.66	15.41	16.04	16.58
.9500	8.14	11.39	13.05	14.19	15.07	15.78	16.38	16.90
.9800	9.09	12.05	13.59	14.67	15.50	16.18	16.76	17.26
.9900	9.68	12.46	13.94	14.98	15.78	16.44	17.00	17.48
.9950	10.17	12.82	14.24	15.25	16.02	16.67	17.21	17.69
.9990	11.12	13.52	14.84	15.78	16.51	17.12	17.64	18.09
.9999	12.15	14.31	15.52	16.39	17.07	17.64	18.13	18.56

CNR_g^o in dB

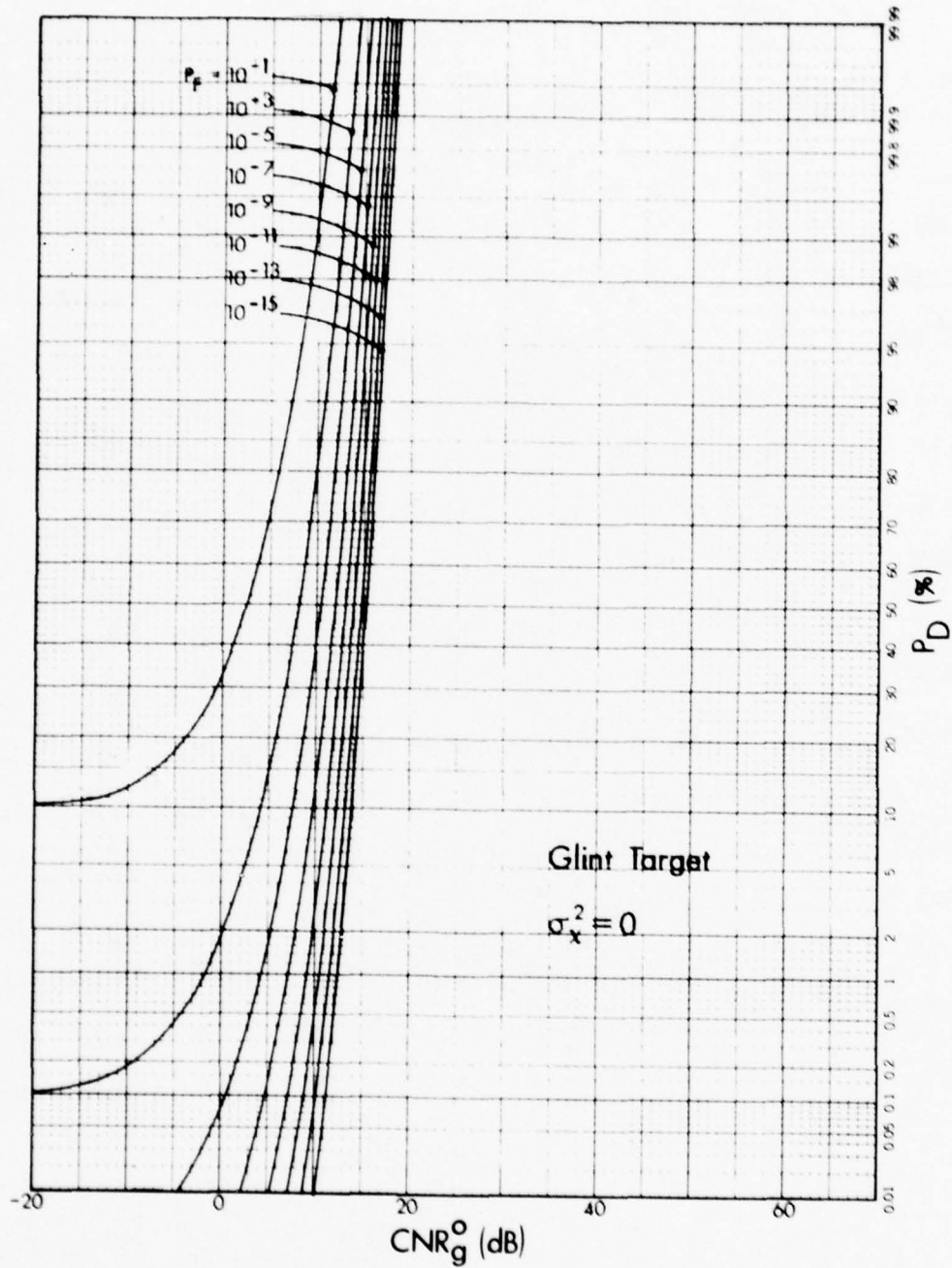


Fig. 5. Glint target receiver operating characteristics for $\sigma_x^2 = 0$.

TABLE 2

GLINT TARGET RECEIVER OPERATING CHARACTERISTICS $\sigma_X^2 = 0.0001$

Detection Probability P_D	False Alarm Probability - P_F							
	10^{-1}	10^{-3}	10^{-5}	10^{-7}	10^{-9}	10^{-11}	10^{-13}	10^{-15}
.0001	**	**	-4.40	2.13	5.27	7.33	8.85	10.05
.0010	**	$-\infty$	0.68	4.78	7.18	8.86	10.15	11.19
.0100	**	-1.77	4.30	7.18	9.04	10.42	11.51	12.40
.1000	$-\infty$	4.07	7.59	9.64	11.08	12.18	13.08	13.83
.3000	-0.71	6.65	9.37	11.07	12.30	13.27	14.06	14.74
.5000	2.50	8.06	10.42	11.94	13.06	13.95	14.69	15.32
.7000	4.76	9.27	11.35	12.73	13.76	14.58	15.27	15.87
.8000	5.86	9.93	11.87	13.17	14.15	14.95	15.61	16.18
.8500	6.48	10.31	12.18	13.44	14.39	15.16	15.81	16.37
.9000	7.19	10.77	12.55	13.76	14.68	15.43	16.05	16.60
.9500	8.15	11.40	13.07	14.21	15.09	15.80	16.41	16.93
.9800	9.11	12.07	13.62	14.70	15.53	16.21	16.79	17.29
.9900	9.69	12.49	13.97	15.01	15.81	16.47	17.04	17.53
.9950	10.19	12.85	14.28	15.28	16.06	16.71	17.26	17.73
.9990	11.15	13.56	14.88	15.82	16.56	17.17	17.69	18.15
.9999	12.18	14.35	15.57	16.45	17.14	17.71	18.20	18.63

CNR_g^o in dB

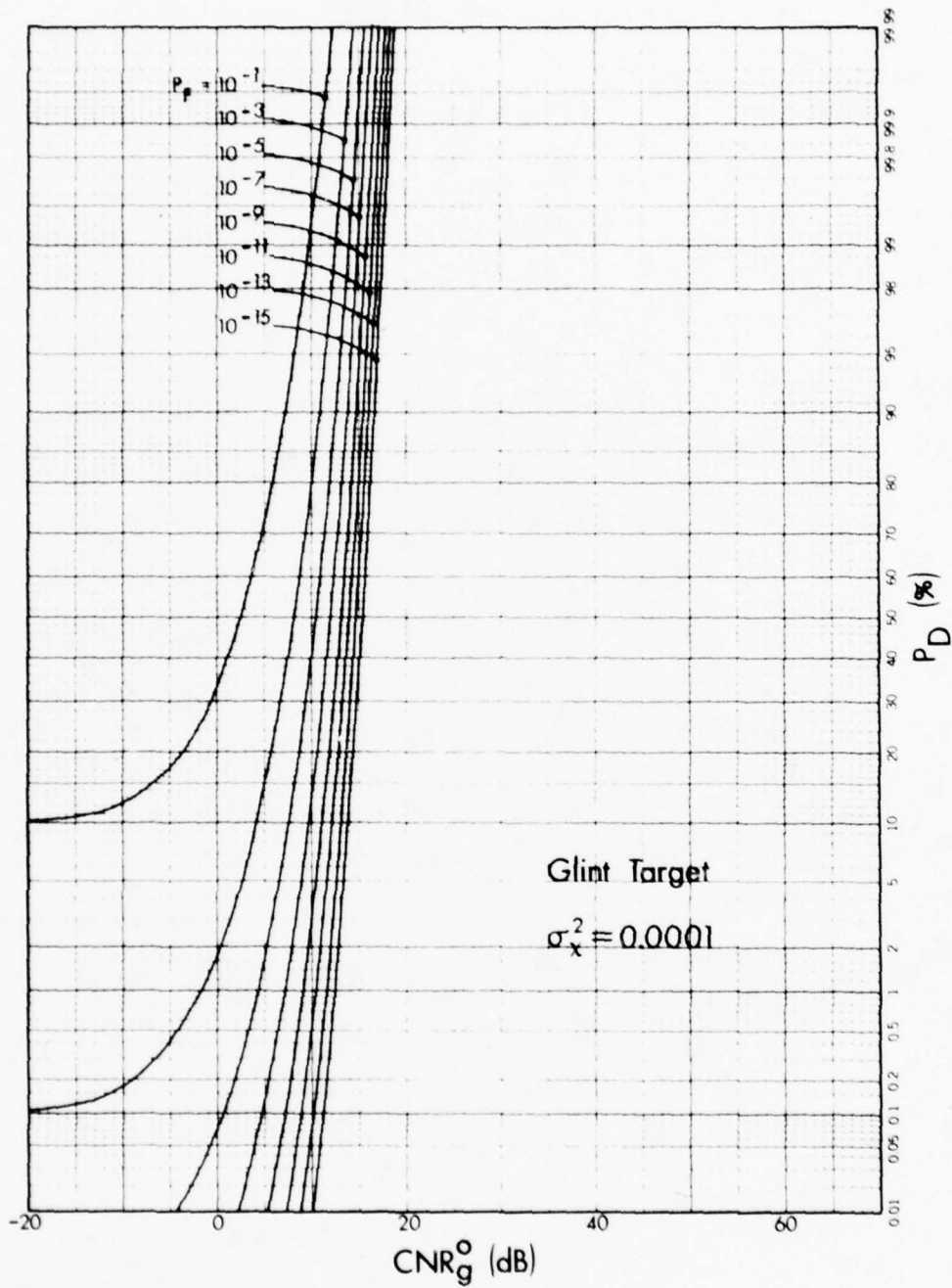


Fig.6. Glint target receiver operating characteristics for $\sigma_x^2 = 0.0001$.

TABLE 3

GLINT TARGET RECEIVER OPERATING CHARACTERISTICS $\sigma_X^2 = 0.001$

Detection Probability P_D	False Alarm Probability - P_F							
	10^{-1}	10^{-3}	10^{-5}	10^{-7}	10^{-9}	10^{-11}	10^{-13}	10^{-15}
.0001	**	**	-4.44	2.02	5.12	7.14	8.62	9.79
.0010	**	$-\infty$	0.61	4.66	7.03	8.68	9.94	10.95
.0100	**	-1.81	4.22	7.06	8.91	10.26	11.32	12.20
.1000	$-\infty$	4.03	7.53	9.56	10.98	12.07	12.96	13.71
.3000	-0.72	6.63	9.34	11.03	12.26	13.22	14.01	14.68
.5000	2.50	8.06	10.42	11.94	13.06	13.95	14.69	15.32
.7000	4.77	9.31	11.39	12.78	13.81	14.64	15.34	15.93
.8000	5.90	9.99	11.94	13.25	14.25	15.05	15.72	16.29
.8500	6.52	10.39	12.27	13.54	14.51	15.29	15.94	16.51
.9000	7.25	10.86	12.66	13.89	14.82	15.58	16.22	16.78
.9500	8.24	11.53	13.22	14.39	15.28	16.01	16.63	17.16
.9800	9.23	12.24	13.82	14.93	15.78	16.48	17.07	17.59
.9900	9.84	12.69	14.21	15.28	16.11	16.79	17.36	17.87
.9950	10.37	13.09	14.55	15.59	16.39	17.06	17.63	18.12
.9990	11.38	13.86	15.23	16.21	16.97	17.61	18.15	18.63
.9999	12.49	14.75	16.02	16.93	17.66	18.26	18.78	19.23

CNR_g^o in dB

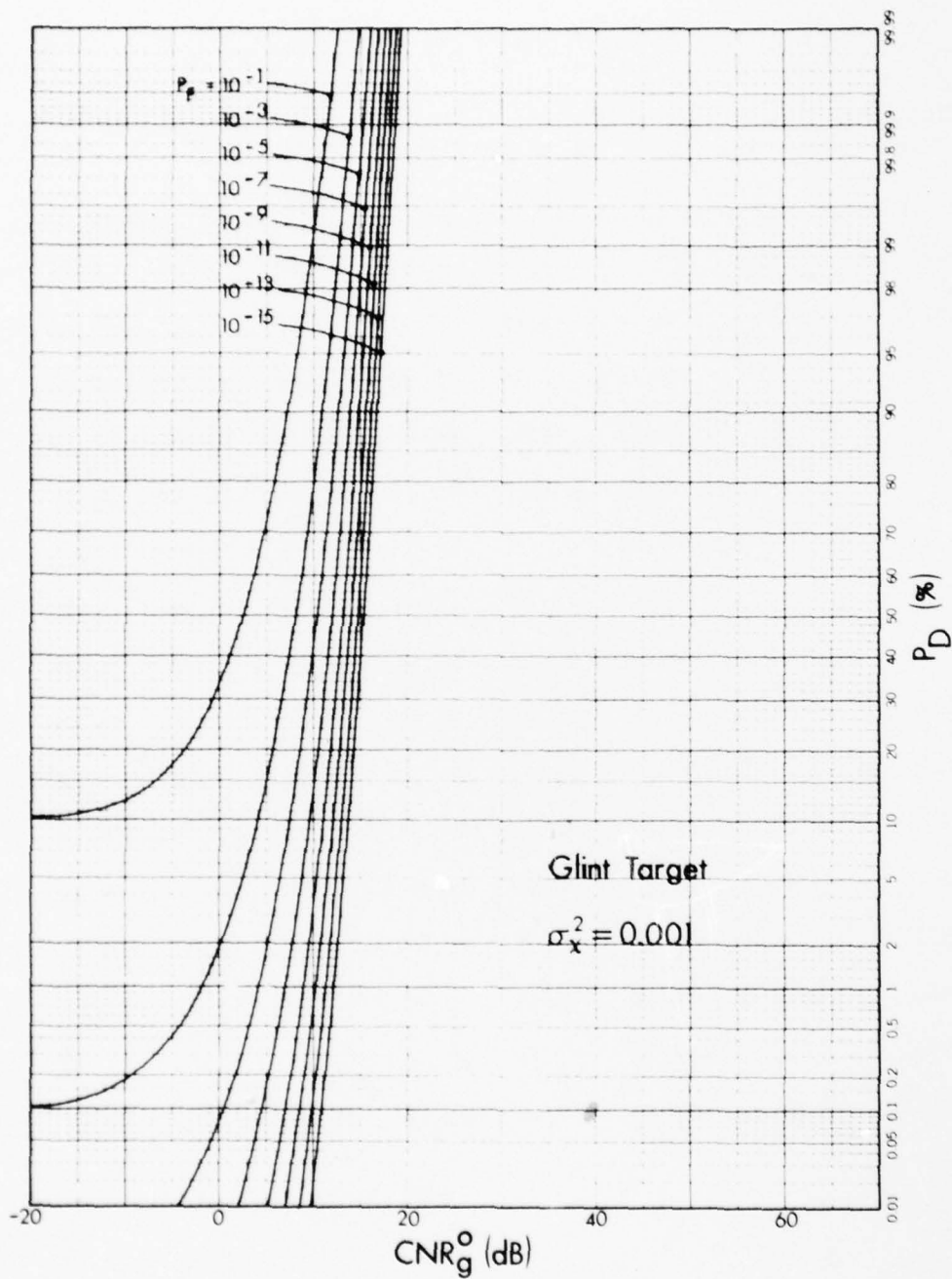


Fig. 7. Glint target receiver operating characteristics for $\sigma_x^2 = 0.001$.

TABLE 4

GLINT TARGET RECEIVER OPERATING CHARACTERISTICS $\sigma_X^2 = 0.01$

Detection Probability P_D	False Alarm Probability - P_F							
	10^{-1}	10^{-3}	10^{-5}	10^{-7}	10^{-9}	10^{-11}	10^{-13}	10^{-15}
.0001	**	**	-4.93	0.96	3.63	5.31	6.52	7.47
.0010	**	$-\infty$	-0.13	3.51	5.56	6.97	8.04	8.90
.0100	**	-2.22	3.42	5.99	7.64	8.85	9.80	10.58
.1000	$-\infty$	3.62	6.96	8.88	10.23	11.26	12.10	12.80
.3000	-0.84	6.44	9.11	10.78	11.98	12.93	13.71	14.37
.5000	2.50	8.12	10.50	12.03	13.16	14.06	14.81	15.45
.7000	4.97	9.66	11.82	13.25	14.32	15.18	15.90	16.51
.8000	6.25	10.54	12.59	13.97	15.01	15.85	16.55	17.15
.8500	6.98	11.06	13.06	14.41	15.43	16.25	16.95	17.54
.9000	7.85	11.71	13.64	14.95	15.95	16.76	17.44	18.03
.9500	9.06	12.65	14.49	15.76	16.73	17.52	18.18	18.76
.9800	10.34	13.67	15.43	16.65	17.59	18.36	19.01	19.57
.9900	11.15	14.34	16.04	17.24	18.16	18.91	19.55	20.11
.9950	11.87	14.94	16.61	17.77	18.68	19.42	20.05	20.60
.9990	13.29	16.16	17.74	18.86	19.74	20.46	21.07	21.61
.9999	14.94	17.61	19.11	20.18	21.02	21.72	22.31	22.83

 CNR_g° in dB

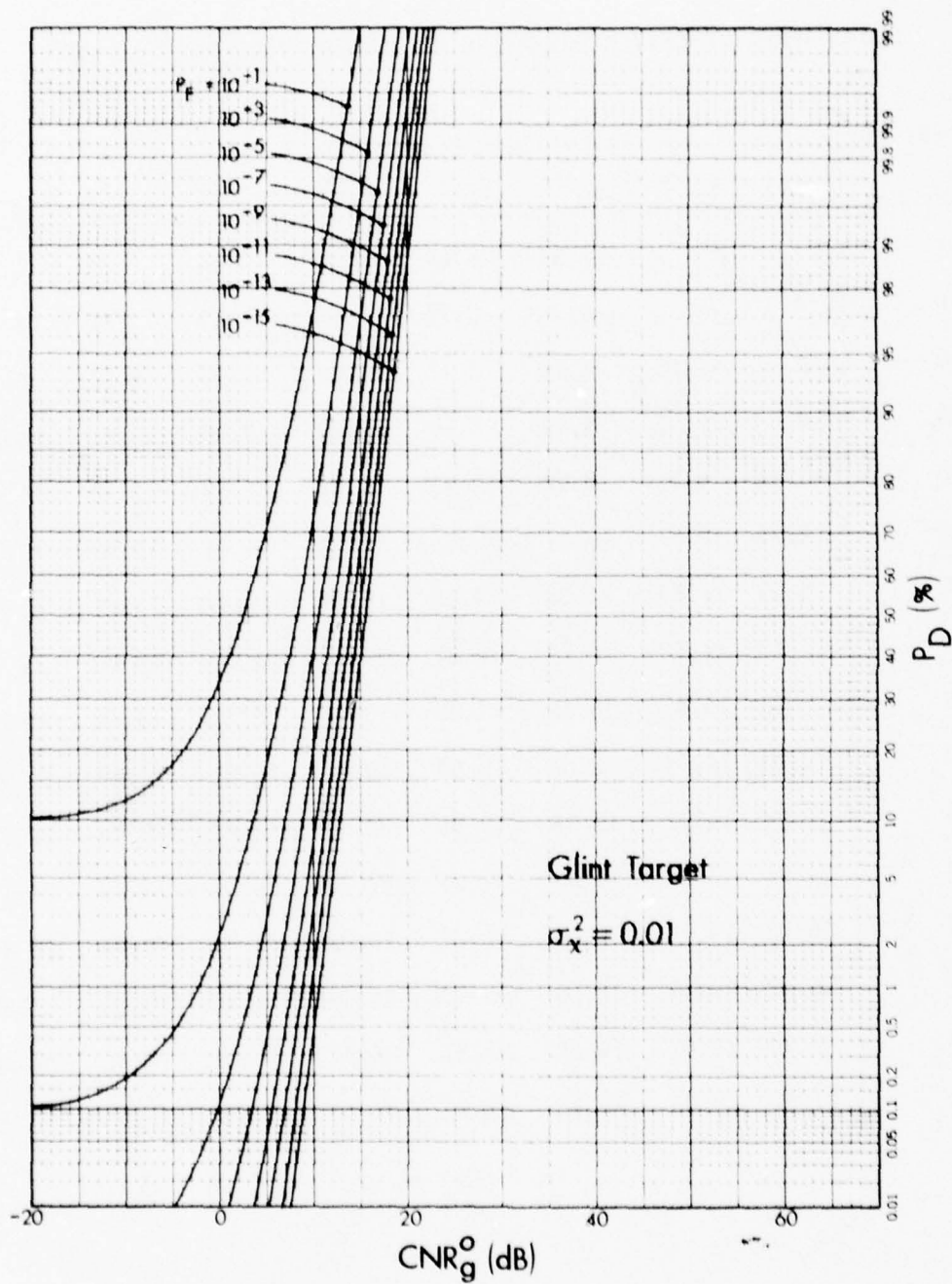


Fig. 8. Glint target receiver operating characteristics for $\sigma_x^2 = 0.01$.

TABLE 5

GLINT TARGET RECEIVER OPERATING CHARACTERISTICS $\sigma_x^2 = 0.05$

Detection Probability P_D	False Alarm Probability - P_F							
	10^{-1}	10^{-3}	10^{-5}	10^{-7}	10^{-9}	10^{-11}	10^{-13}	10^{-15}
.0001	**	**	-7.54	-3.64	-1.86	-0.64	0.29	1.05
.0010	**	$-\infty$	-3.36	-0.70	0.86	1.99	2.88	3.62
.0100	**	-4.05	0.58	2.71	4.11	5.17	6.01	6.72
.1000	$-\infty$	2.35	5.45	7.24	8.51	9.48	10.28	10.95
.3000	-1.18	6.17	8.82	10.46	11.66	12.59	13.36	14.01
.5000	2.76	8.67	11.11	12.68	13.83	14.74	15.49	16.13
.7000	5.99	11.09	13.38	14.88	15.99	16.87	17.61	18.24
.8000	7.78	12.53	14.74	16.21	17.30	18.17	18.89	19.52
.8500	8.83	13.41	15.58	17.02	18.10	18.96	19.68	20.30
.9000	10.13	14.51	16.62	18.04	19.11	19.96	20.67	21.29
.9500	11.98	16.12	18.16	19.55	20.59	21.43	22.14	22.75
.9800	14.01	17.91	19.89	21.24	22.26	23.09	23.79	24.39
.9900	15.33	19.11	21.04	22.37	23.38	24.20	24.88	25.47
.9950	16.52	20.19	22.09	23.40	24.40	25.21	25.89	26.48
.9990	18.94	22.41	24.24	25.51	26.49	27.29	27.96	28.55
.9999	21.82	25.09	26.86	28.09	29.04	29.82	30.48	31.05

CNR_g^c in dB

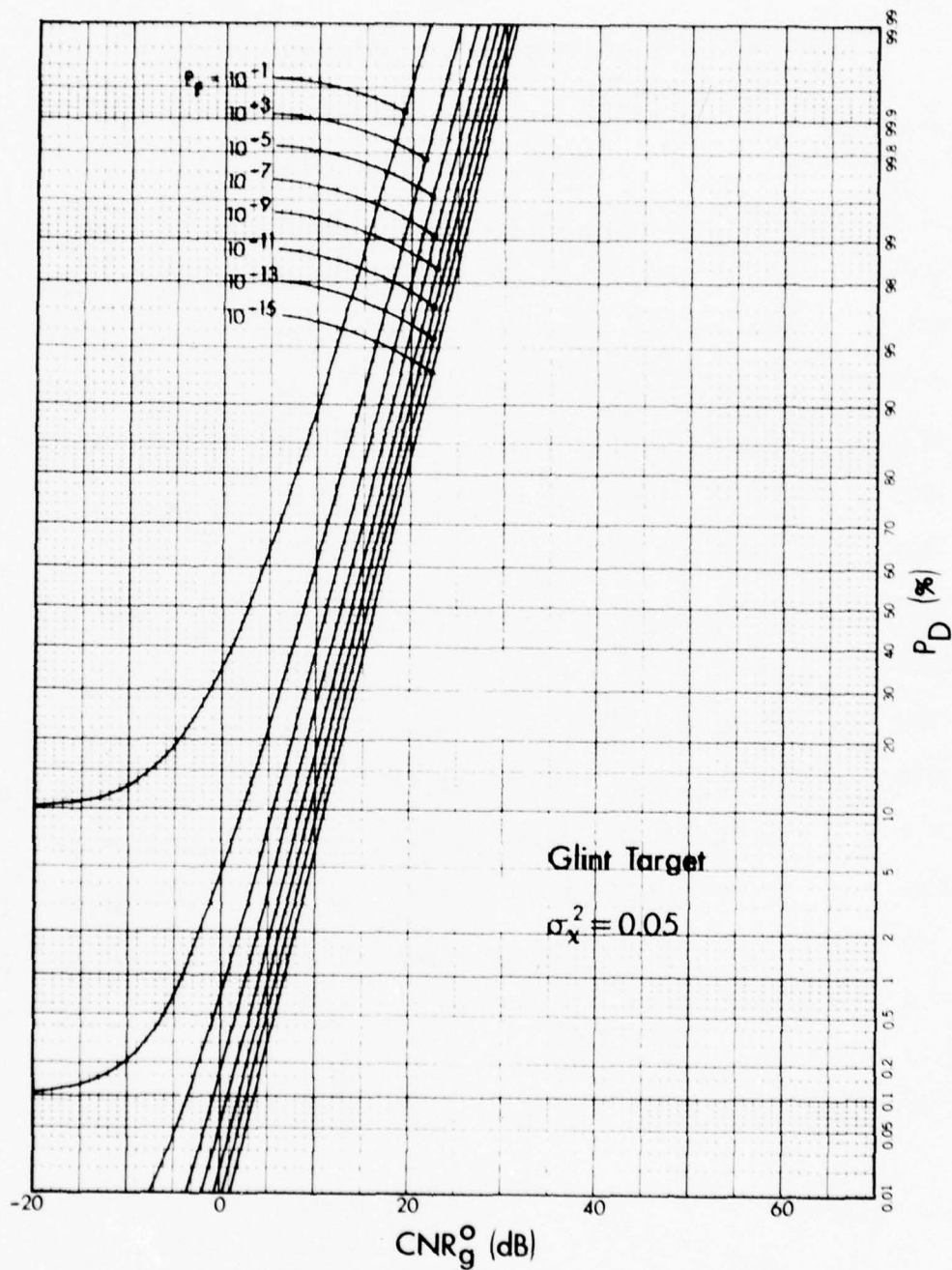


Fig. 9. Glint target receiver operating characteristics for $\sigma_x^2 = 0.05$.

TABLE 6

GLINT TARGET RECEIVER OPERATING CHARACTERISTICS $\sigma_X^2 = 0.1$

Detection Probability P_D	False Alarm Probability - P_F							
	10^{-1}	10^{-3}	10^{-5}	10^{-7}	10^{-9}	10^{-11}	10^{-13}	10^{-15}
.0001	**	**	-11.07	-8.09	-6.56	-5.46	-4.59	-3.87
.0010	**	$-\infty$	-6.64	-4.36	-2.94	-1.88	-1.04	-0.33
.0100	**	-6.00	-1.86	0.11	1.44	2.45	3.27	3.96
.1000	$-\infty$	1.43	4.42	6.17	7.41	8.36	9.15	9.81
.3000	-1.32	6.24	8.89	10.53	11.71	12.64	13.41	14.06
.5000	3.31	9.48	11.96	13.54	14.69	15.60	16.35	16.99
.7000	7.28	12.66	15.02	16.54	17.66	18.56	19.30	19.93
.8000	9.52	14.57	16.86	18.35	19.46	20.34	21.08	21.71
.8500	10.86	15.74	17.98	19.46	20.56	21.44	22.17	22.79
.9000	12.51	17.21	19.41	20.86	21.95	22.82	23.54	24.16
.9500	14.91	19.36	21.51	22.93	24.01	24.86	25.58	26.19
.9800	17.55	21.77	23.86	25.26	26.31	27.16	27.87	28.48
.9900	19.29	23.38	25.42	26.81	27.85	28.69	29.39	30.01
.9950	20.86	24.84	26.86	28.22	29.26	30.09	30.79	31.39
.9990	24.07	27.85	29.81	31.14	32.16	32.98	33.67	34.27
.9999	27.92	31.51	33.39	34.70	35.69	36.51	37.18	37.77

CNR_g^o in dB

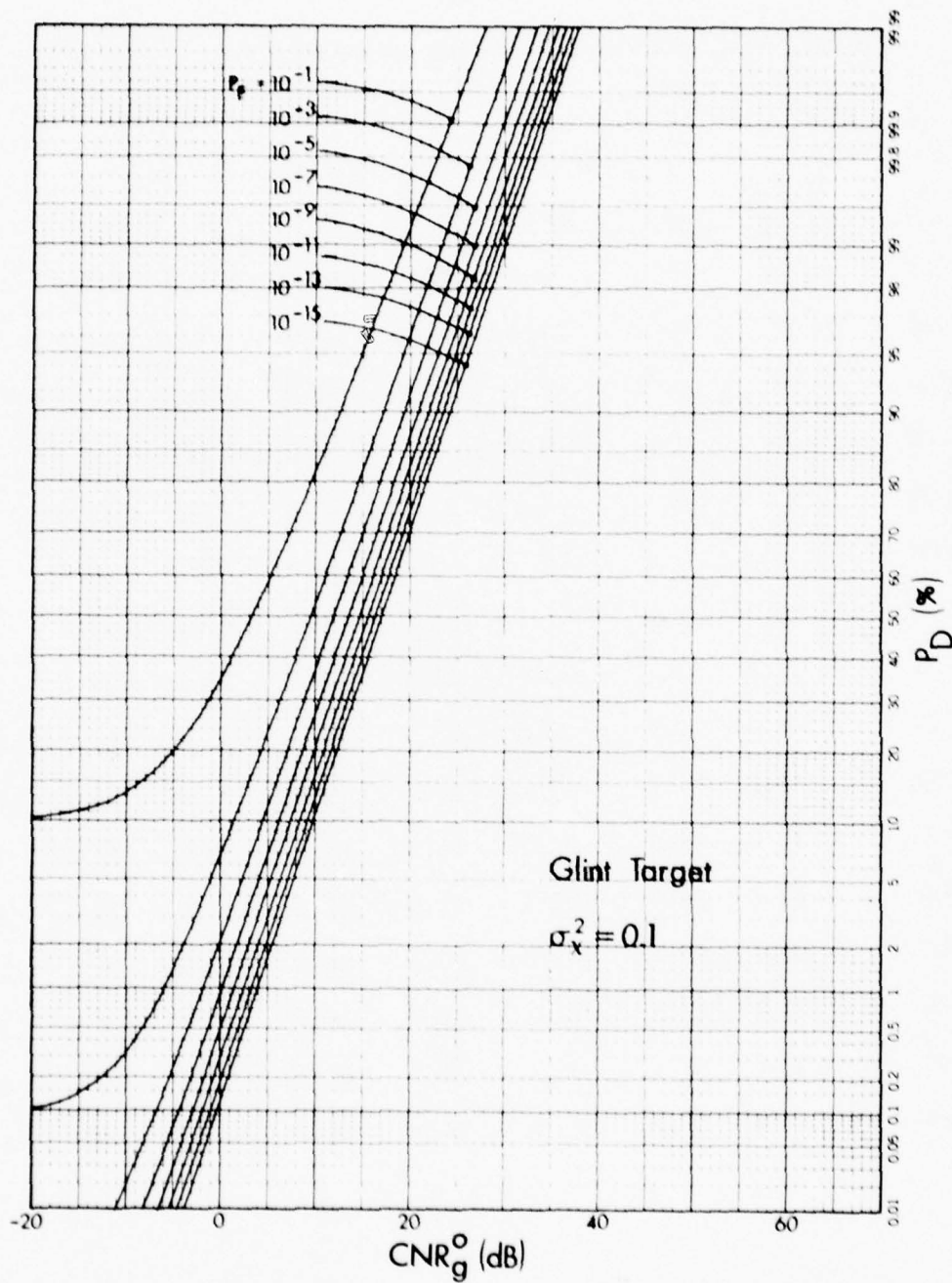


Fig. 10. Glint target receiver operating characteristics for $\sigma_x^2 = 0.1$.

TABLE 7

GLINT TARGET RECEIVER OPERATING CHARACTERISTICS $\sigma_X^2 = 0.2$

Detection Probability P_D	False Alarm Probability - P_F							
	10^{-1}	10^{-3}	10^{-5}	10^{-7}	10^{-9}	10^{-11}	10^{-13}	10^{-15}
.0001	**	**	-16.9	-14.4	-13.0	-12.0	-11.2	-10.5
.0010	**	$-\infty$	-11.4	-9.4	-8.0	-7.0	-6.2	-5.5
.0100	**	-8.9	-5.1	-3.3	-2.0	-1.0	-0.2	0.5
.1000	$-\infty$	0.5	3.4	5.1	6.3	7.2	8.0	8.7
.3000	-1.1	6.8	9.5	11.1	12.3	13.2	14.0	14.6
.5000	4.6	11.2	13.7	15.3	16.4	17.3	18.1	18.7
.7000	9.7	15.5	17.9	19.4	20.6	21.5	22.2	22.8
.8000	12.7	18.1	20.4	21.9	23.1	24.0	24.7	25.3
.8500	14.4	19.7	22.0	23.5	24.6	25.5	26.2	26.9
.9000	16.6	21.7	23.9	25.4	26.5	27.4	28.2	28.8
.9500	19.8	24.6	26.8	28.3	29.4	30.3	31.0	31.6
.9800	23.3	27.9	30.1	31.5	32.6	33.5	34.2	34.8
.9900	25.7	30.1	32.3	33.7	34.8	35.6	36.4	37.0
.9950	27.8	32.1	34.3	35.7	36.7	37.6	38.3	38.9
.9990	32.1	36.3	38.4	39.7	40.8	41.6	42.4	43.0
.9999	37.4	41.3	43.3	44.7	45.7	46.6	47.3	47.9

CNR_g^o in dB

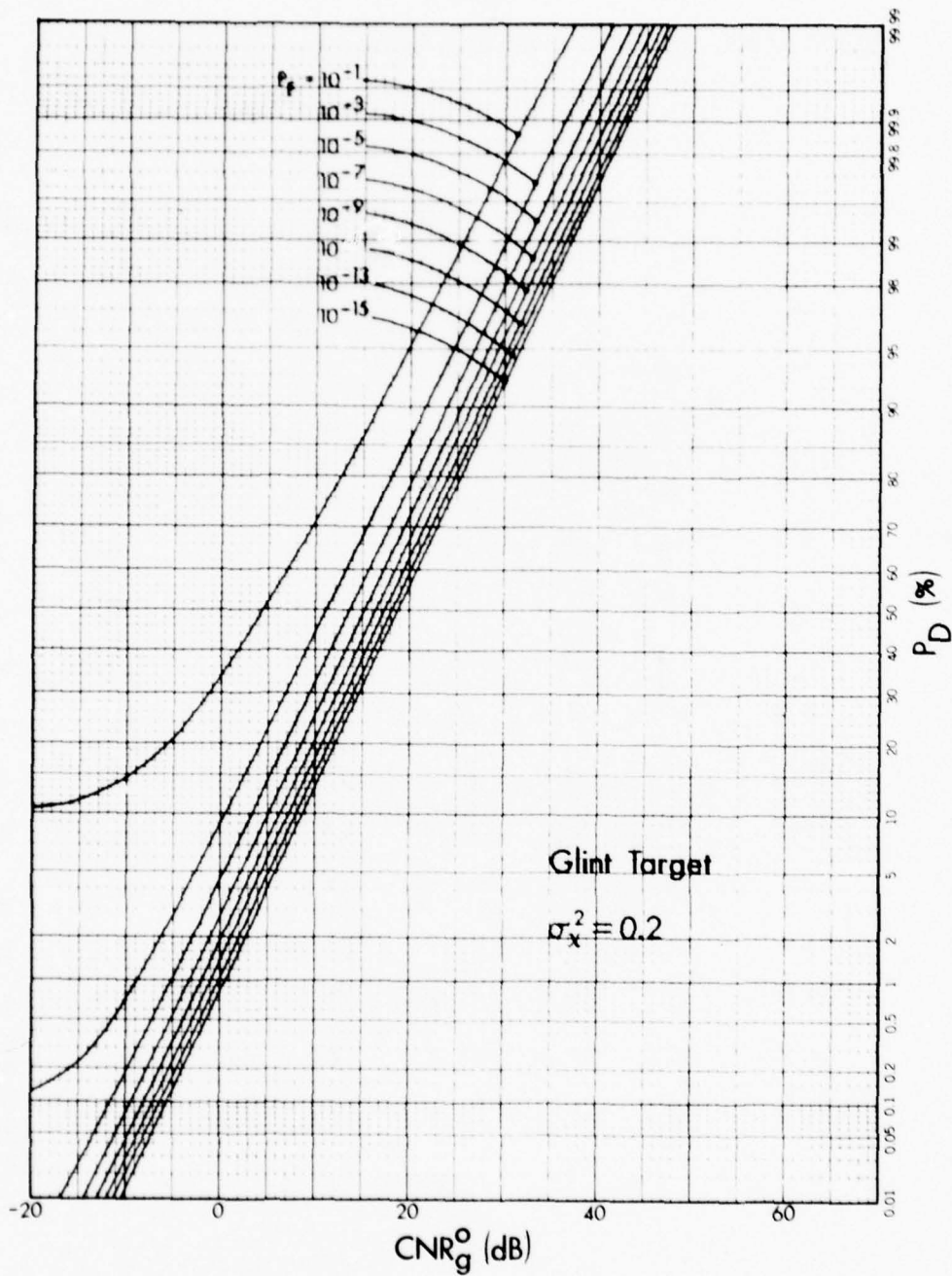


Fig. 11. Glint target receiver operating characteristics for $\sigma_x^2 = 0.2$.

TABLE 8

GLINT TARGET RECEIVER OPERATING CHARACTERISTICS $\sigma_X^2 = 0.5$

Detection Probability P_D	False Alarm Probability - P_F							
	10^{-1}	10^{-3}	10^{-5}	10^{-7}	10^{-9}	10^{-11}	10^{-13}	10^{-15}
.0001	**	**	<-20	<-20	<-20	<-20	<-20	<-20
.0010	**	$-\infty$	-19.7	-17.9	-16.6	-15.6	-14.8	-14.1
.0100	**	-13.7	-10.1	-8.4	-7.1	-6.2	-5.4	-4.7
.1000	$-\infty$	0.1	2.9	4.6	5.8	6.7	7.5	8.2
.3000	0.8	9.7	12.4	14.0	15.2	16.1	16.8	17.5
.5000	9.2	16.3	18.9	20.5	21.6	22.5	23.3	23.9
.7000	16.6	22.9	25.4	27.0	28.1	29.1	29.8	30.5
.8000	21.0	26.9	29.4	30.9	32.1	32.9	33.7	34.3
.8500	23.6	29.4	31.8	33.3	34.5	35.4	36.1	36.7
.9000	26.9	32.5	34.8	36.4	37.5	38.4	39.1	39.7
.9500	31.7	37.1	39.3	40.8	42.0	42.9	43.6	44.3
.9800	37.1	42.1	44.4	45.9	47.1	47.9	48.6	49.3
.9900	40.6	45.5	47.8	49.3	50.4	51.3	52.1	52.7
.9950	43.8	48.7	50.9	52.4	53.5	54.4	55.1	55.7
.9990	50.5	55.1	57.3	58.7	59.8	60.7	61.4	62.0
.9999	58.5	62.9	65.1	66.5	67.6	68.5	69.2	69.8

CNR_g^o in dB

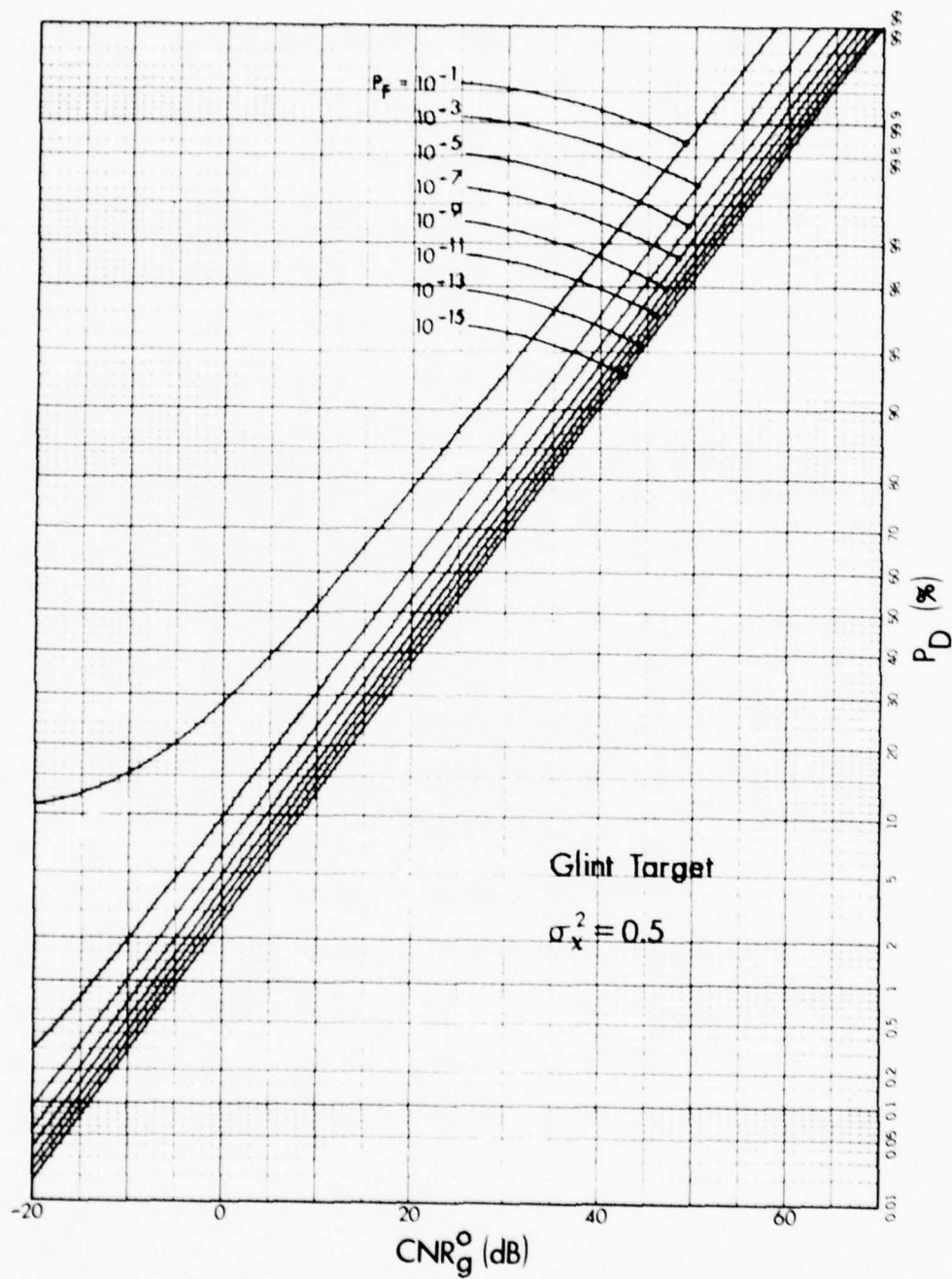


Fig. 12. Glint target receiver operating characteristics for $\sigma_x^2 = 0.5$.

TABLE 9
SPECKLE TARGET RECEIVER OPERATING CHARACTERISTICS $\sigma^2 = 0$

Detection Probability P_D	False Alarm Probability - P_F							
	10^{-1}	10^{-3}	10^{-5}	10^{-7}	10^{-9}	10^{-11}	10^{-13}	10^{-15}
.0001	**	**	-6.02	-1.25	0.97	2.43	3.52	4.39
.0010	**	$-\infty$	-1.76	1.25	3.01	4.26	5.23	6.02
.0100	**	-3.01	1.76	3.98	5.44	6.53	7.40	8.13
.1000	$-\infty$	3.01	6.02	7.78	9.03	10.00	10.79	11.46
.3000	-0.40	6.76	9.33	10.93	12.10	13.02	13.78	14.42
.5000	3.66	9.53	11.93	13.47	14.61	15.51	16.25	16.89
.7000	7.37	12.64	14.95	16.45	17.57	18.45	19.19	19.82
.8000	9.69	14.76	17.04	18.53	19.63	20.51	21.24	21.87
.8500	11.20	16.18	18.44	19.92	21.02	21.90	22.63	23.25
.9000	13.19	18.10	20.35	21.82	22.92	23.79	24.52	25.14
.9500	16.42	21.26	23.49	24.96	26.05	26.93	27.65	28.28
.9800	20.53	25.33	27.55	29.01	30.11	30.98	31.70	32.33
.9900	23.58	28.37	30.59	32.05	33.14	34.01	34.74	35.36
.9950	26.61	31.39	33.61	35.07	36.16	37.03	37.76	38.38
.9990	33.62	38.39	40.61	42.07	43.16	44.03	44.76	45.38
.9999	43.62	48.39	50.61	52.07	53.16	54.04	54.76	55.38

CNR_s in dB

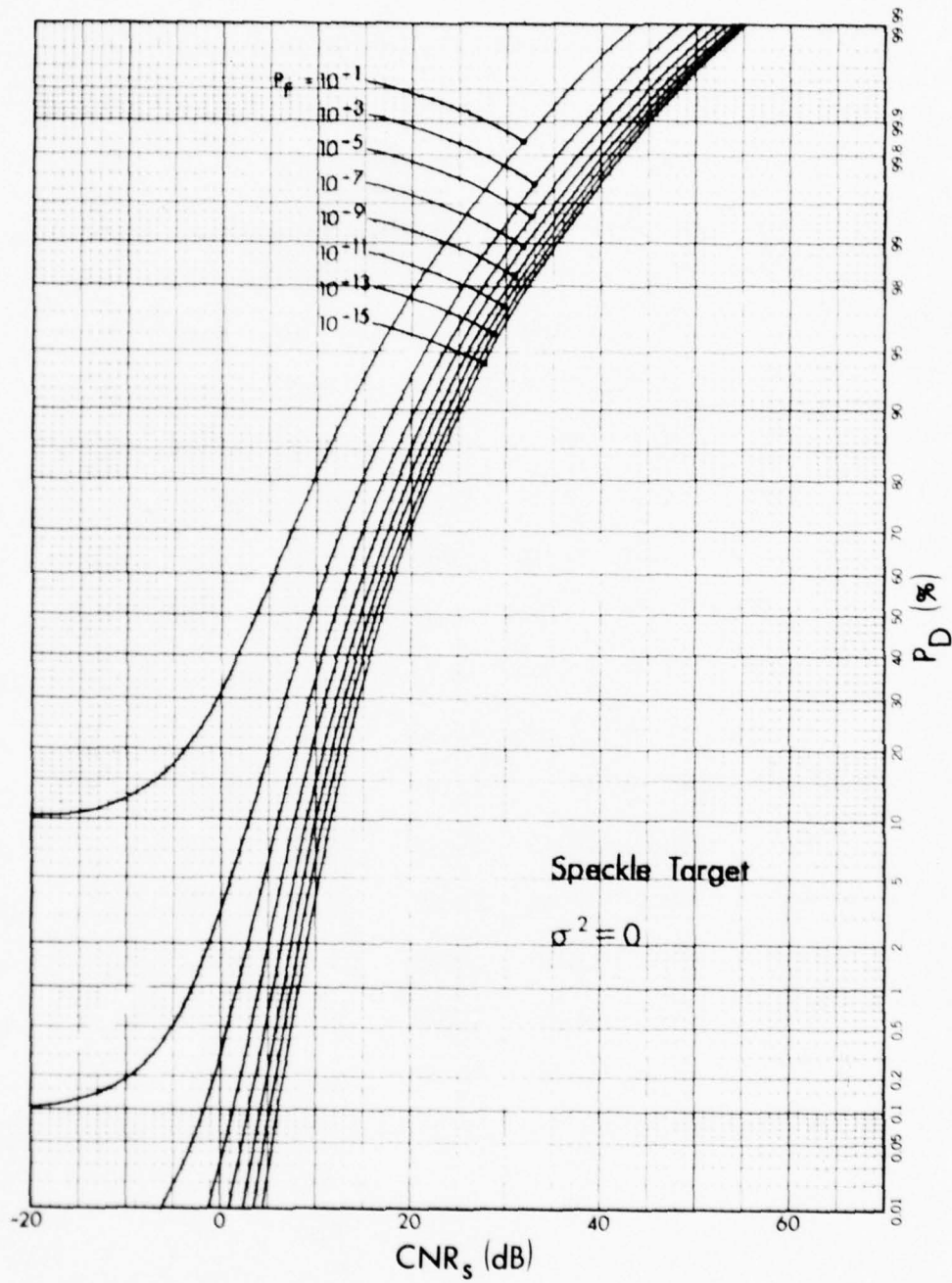


Fig. 13. Speckle target receiver operating characteristics for $\sigma^2 = 0$.

TABLE 10
SPECKLE TARGET RECEIVER OPERATING CHARACTERISTICS $\sigma^2 = 0.0001$

Detection Probability P_D	False Alarm Probability - P_F							
	10^{-1}	10^{-3}	10^{-5}	10^{-7}	10^{-9}	10^{-11}	10^{-13}	10^{-15}
.0001	**	**	-6.02	-1.25	0.97	2.43	3.52	4.39
.0010	**	$-\infty$	-1.76	1.25	3.01	4.26	5.23	6.02
.0100	**	-3.01	1.76	3.98	5.44	6.53	7.40	8.13
.1000	$-\infty$	3.01	6.02	7.78	9.03	10.00	10.79	11.46
.3000	-0.40	6.76	9.33	10.93	12.10	13.02	13.78	14.42
.5000	3.66	9.53	11.93	13.48	14.61	15.51	16.25	16.89
.7000	7.37	12.64	14.95	16.45	17.57	18.45	19.19	19.82
.8000	9.70	14.77	17.04	18.53	19.63	20.51	21.24	21.87
.8500	11.20	16.18	18.44	19.92	21.02	21.90	22.63	23.26
.9000	13.19	18.10	20.35	21.82	22.92	23.79	24.52	25.14
.9500	16.43	21.26	23.49	24.96	26.05	26.93	27.66	28.28
.9800	20.53	25.33	27.55	29.02	30.11	30.98	31.71	32.33
.9900	23.58	28.37	30.59	32.05	33.14	34.01	34.74	35.36
.9950	26.61	31.39	33.61	35.07	36.16	37.04	37.76	38.38
.9990	33.62	38.39	40.61	42.07	43.16	44.03	44.76	45.38
.9999	43.59	48.36	50.58	52.04	53.14	54.01	54.73	55.35

CNR_s in dB

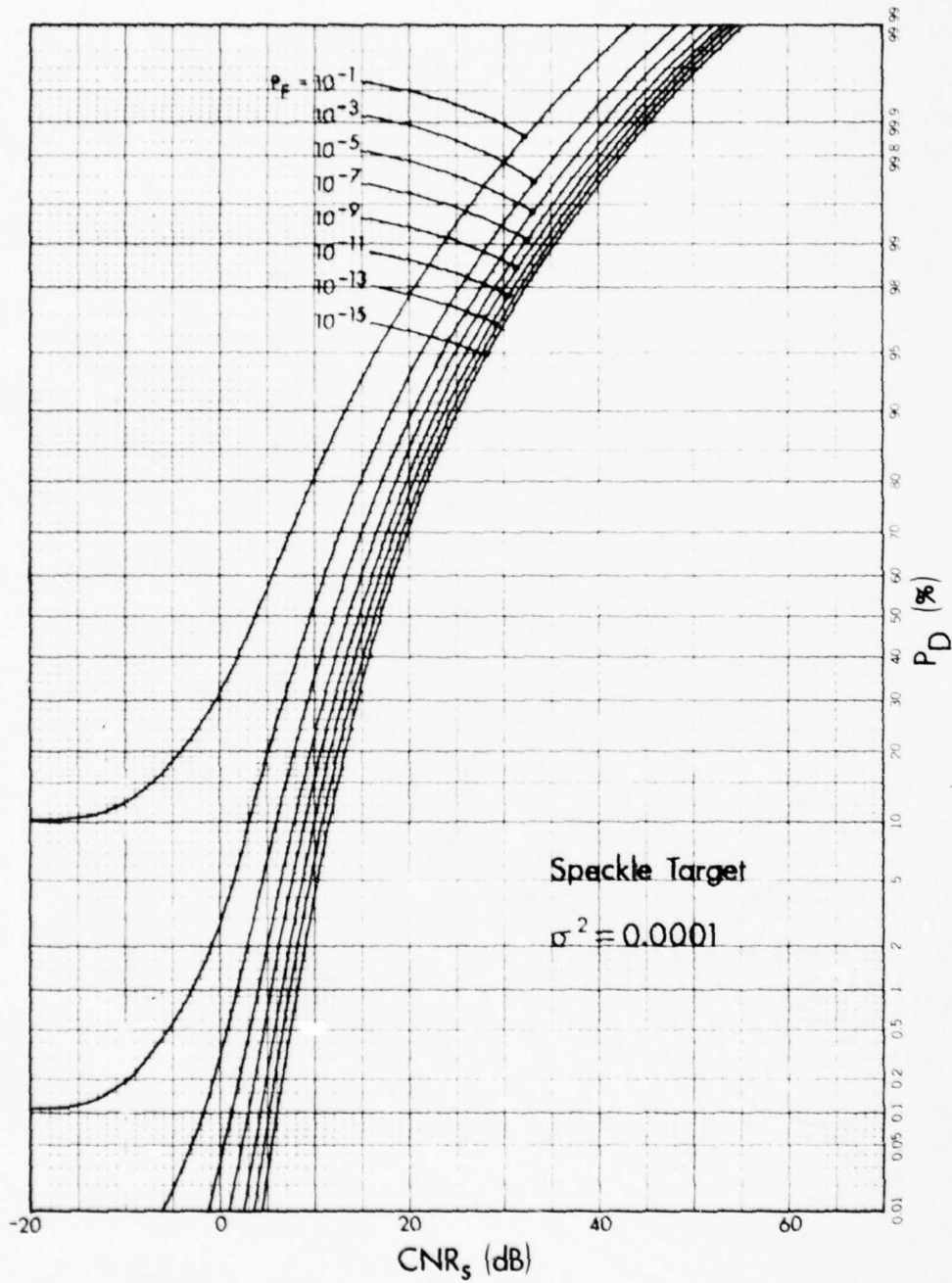


Fig. 14. Speckle target receiver operating characteristics for $\sigma^2 = 0.0001$.

TABLE 11
SPECKLE TARGET RECEIVER OPERATING CHARACTERISTICS $\sigma^2 = 0.001$

Detection Probability P_D	False Alarm Probability - P_F							
	10^{-1}	10^{-3}	10^{-5}	10^{-7}	10^{-9}	10^{-11}	10^{-13}	10^{-15}
.0001	**	**	-6.03	-1.28	0.93	2.39	3.48	4.35
.0010	**	$-\infty$	-1.78	1.23	2.98	4.23	5.20	5.99
.0100	**	-3.02	1.75	3.96	5.42	6.51	7.38	8.11
.1000	$-\infty$	3.01	6.02	7.78	9.03	10.00	10.79	11.46
.3000	-0.40	6.76	9.33	10.94	12.10	13.02	13.78	14.43
.5000	3.67	9.54	11.94	13.48	14.62	15.52	16.26	16.90
.7000	7.38	12.65	14.97	16.47	17.58	18.47	19.20	19.83
.8000	9.71	14.78	17.06	18.54	19.65	20.53	21.26	21.88
.8500	11.21	16.20	18.46	19.94	21.04	21.91	22.64	23.27
.9000	13.21	18.12	20.36	21.83	22.93	23.81	24.54	25.16
.9500	16.44	21.28	23.51	24.98	26.07	26.94	27.67	28.29
.9800	20.55	25.34	27.57	29.03	30.12	31.00	31.72	32.34
.9900	23.60	28.38	30.60	32.07	33.16	34.03	34.76	35.38
.9950	26.63	31.41	33.63	35.09	36.18	37.05	37.78	38.40
.9990	33.63	38.41	40.62	42.09	43.18	44.05	44.77	45.40
.9999	43.61	48.38	50.60	52.06	53.15	54.02	54.75	55.37

CNR_s in dB

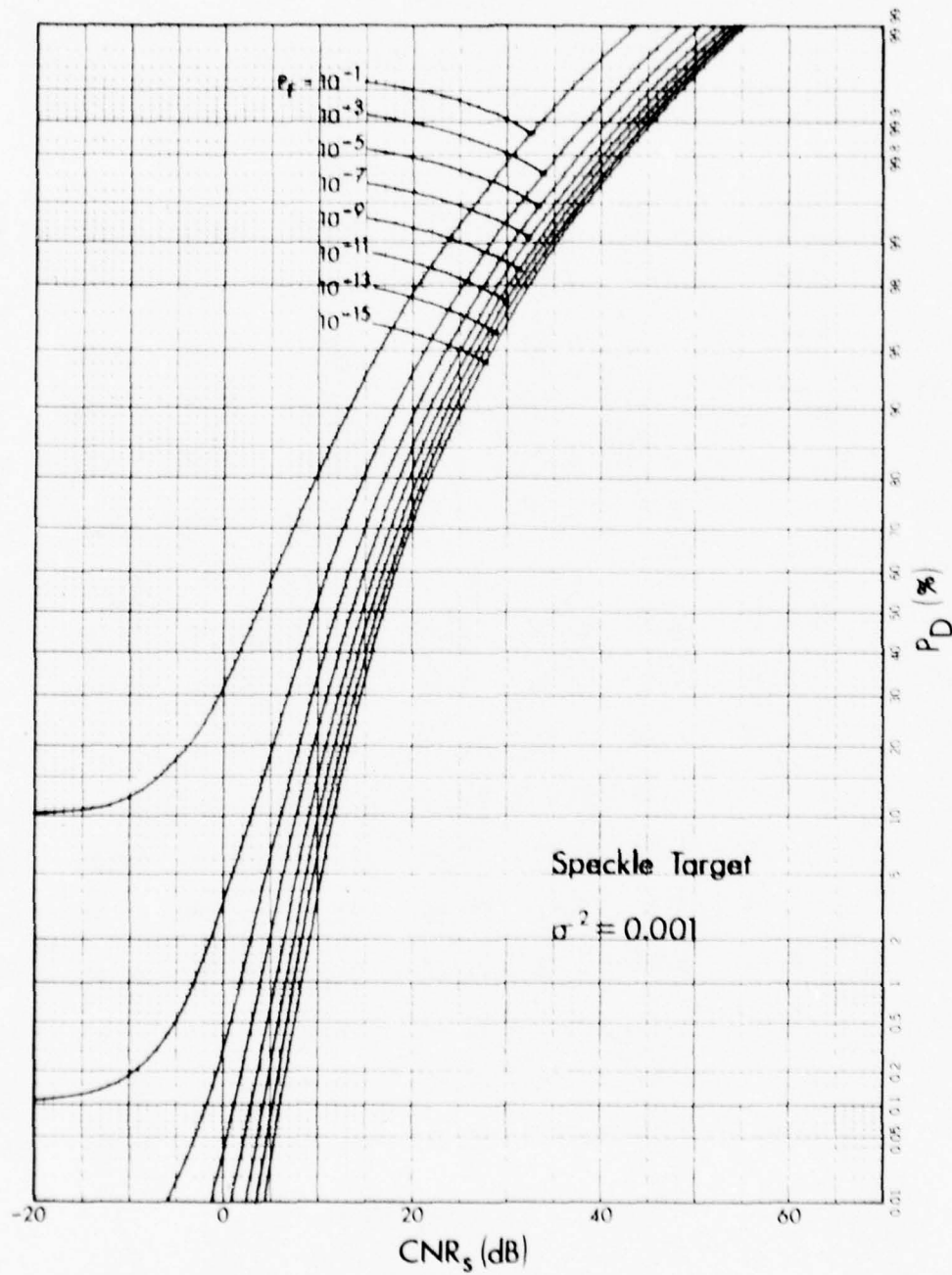


Fig. 15. Speckle target receiver operating characteristics for $\sigma^2 = 0.001$.

TABLE 12
SPECKLE TARGET RECEIVER OPERATING CHARACTERISTICS $\sigma^2 = 0.01$

Detection Probability P_D	False Alarm Probability - P_F							
	10^{-1}	10^{-3}	10^{-5}	10^{-7}	10^{-9}	10^{-11}	10^{-13}	10^{-15}
.0001	**	**	-6.15	-1.52	0.63	2.04	3.10	3.95
.0010	**	$-\infty$	-1.93	1.01	2.73	3.96	4.91	5.69
.0100	**	-3.09	1.63	3.82	5.27	6.35	7.22	7.94
.1000	$-\infty$	2.99	6.00	7.76	9.01	9.98	10.77	11.44
.3000	-0.37	6.81	9.39	10.99	12.16	13.08	13.84	14.49
.5000	3.74	9.63	12.04	13.58	14.72	15.62	16.36	17.00
.7000	7.49	12.78	15.09	16.59	17.71	18.59	19.33	19.96
.8000	9.83	14.91	17.19	18.68	19.78	20.66	21.40	22.02
.8500	11.34	16.34	18.60	20.08	21.18	22.06	22.79	23.41
.9000	13.35	18.26	20.51	21.98	23.08	23.95	24.68	25.31
.9500	16.59	21.43	23.66	25.13	26.22	27.10	27.82	28.44
.9800	20.70	25.50	27.72	29.19	30.28	31.15	31.88	32.50
.9900	23.75	28.54	30.76	32.22	33.31	34.19	34.91	35.53
.9950	26.78	31.56	33.78	35.24	36.34	37.21	37.93	38.55
.9990	33.79	38.56	40.78	42.24	43.33	44.20	44.93	45.55
.9999	43.77	48.54	50.75	52.22	53.31	54.18	54.90	55.53

CNR_s in dB

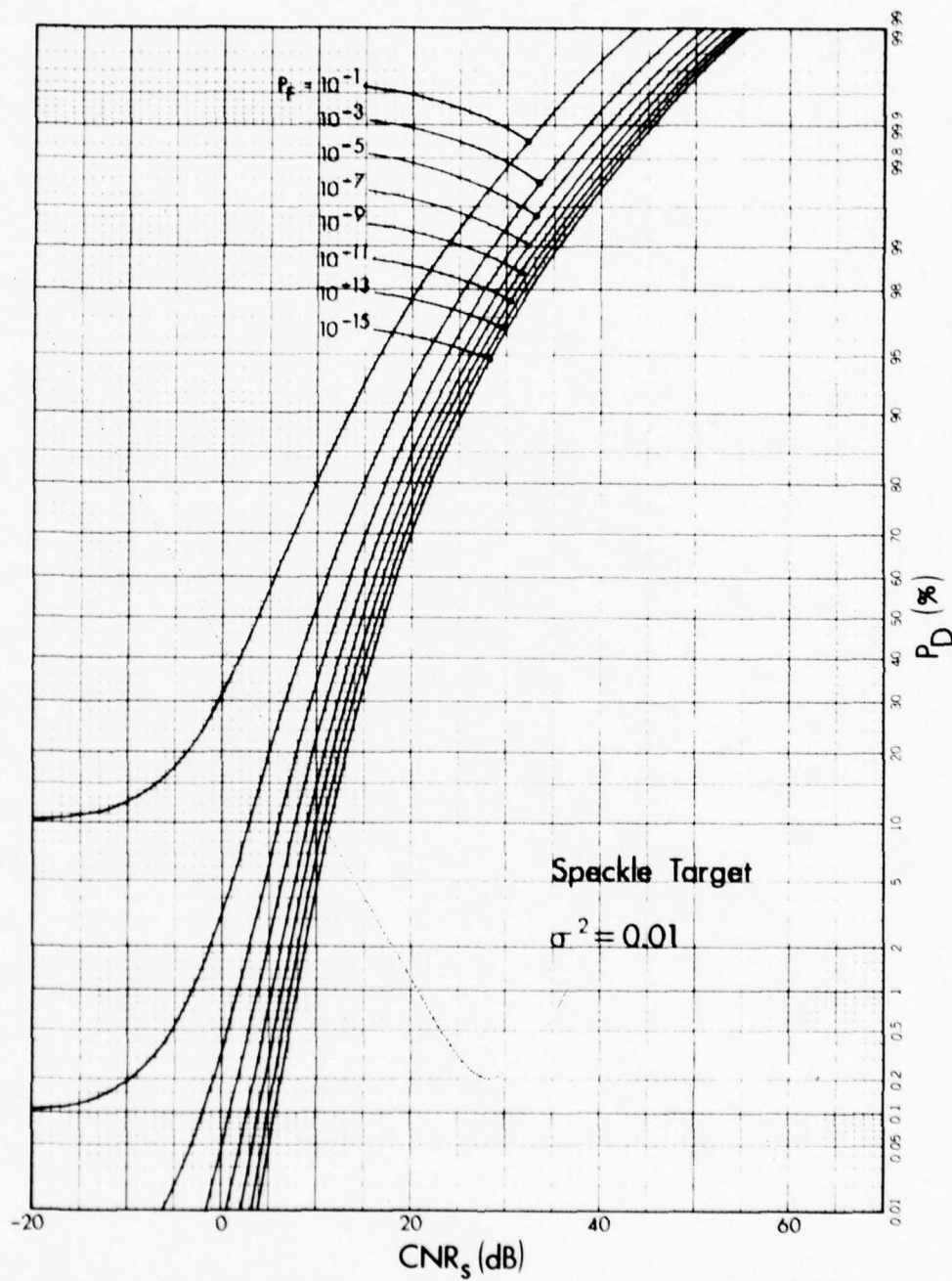


Fig. 16. Speckle target receiver operating characteristics for $\sigma^2 = 0.01$.

TABLE 13
SPECKLE TARGET RECEIVER OPERATING CHARACTERISTICS $\sigma^2 = 0.05$

Detection Probability P_D	False Alarm Probability - P_F							
	10^{-1}	10^{-3}	10^{-5}	10^{-7}	10^{-9}	10^{-11}	10^{-13}	10^{-15}
.0001	**	**	-6.68	-2.54	-0.61	0.69	1.67	2.47
.0010	**	$-\infty$	-2.58	0.15	1.76	2.93	3.84	4.59
.0100	**	-3.37	1.15	3.27	4.68	5.74	6.59	7.30
.1000	$-\infty$	2.95	5.94	7.70	8.94	9.91	10.70	11.36
.3000	-0.22	7.04	9.63	11.24	12.42	13.34	14.10	14.74
.5000	4.06	10.03	12.45	14.00	15.14	16.04	16.79	17.43
.7000	7.96	13.31	15.63	17.14	18.26	19.14	19.88	20.51
.8000	10.38	15.50	17.79	19.28	20.39	21.27	22.00	22.63
.8500	11.93	16.95	19.22	20.70	21.81	22.69	23.42	24.04
.9000	13.97	18.90	21.16	22.63	23.73	24.61	25.33	25.96
.9500	17.25	22.10	24.33	25.80	26.89	27.77	28.50	29.12
.9800	21.38	26.18	28.41	29.87	30.96	31.84	32.56	33.18
.9900	24.44	29.23	31.45	32.91	34.00	34.88	35.60	36.22
.9950	27.48	32.25	34.47	35.94	37.03	37.90	38.63	39.25
.9990	34.48	39.26	41.47	42.94	44.03	44.90	45.62	46.25
.9999	44.46	49.23	51.45	52.91	54.00	54.87	55.60	56.22

CNR_s in dB

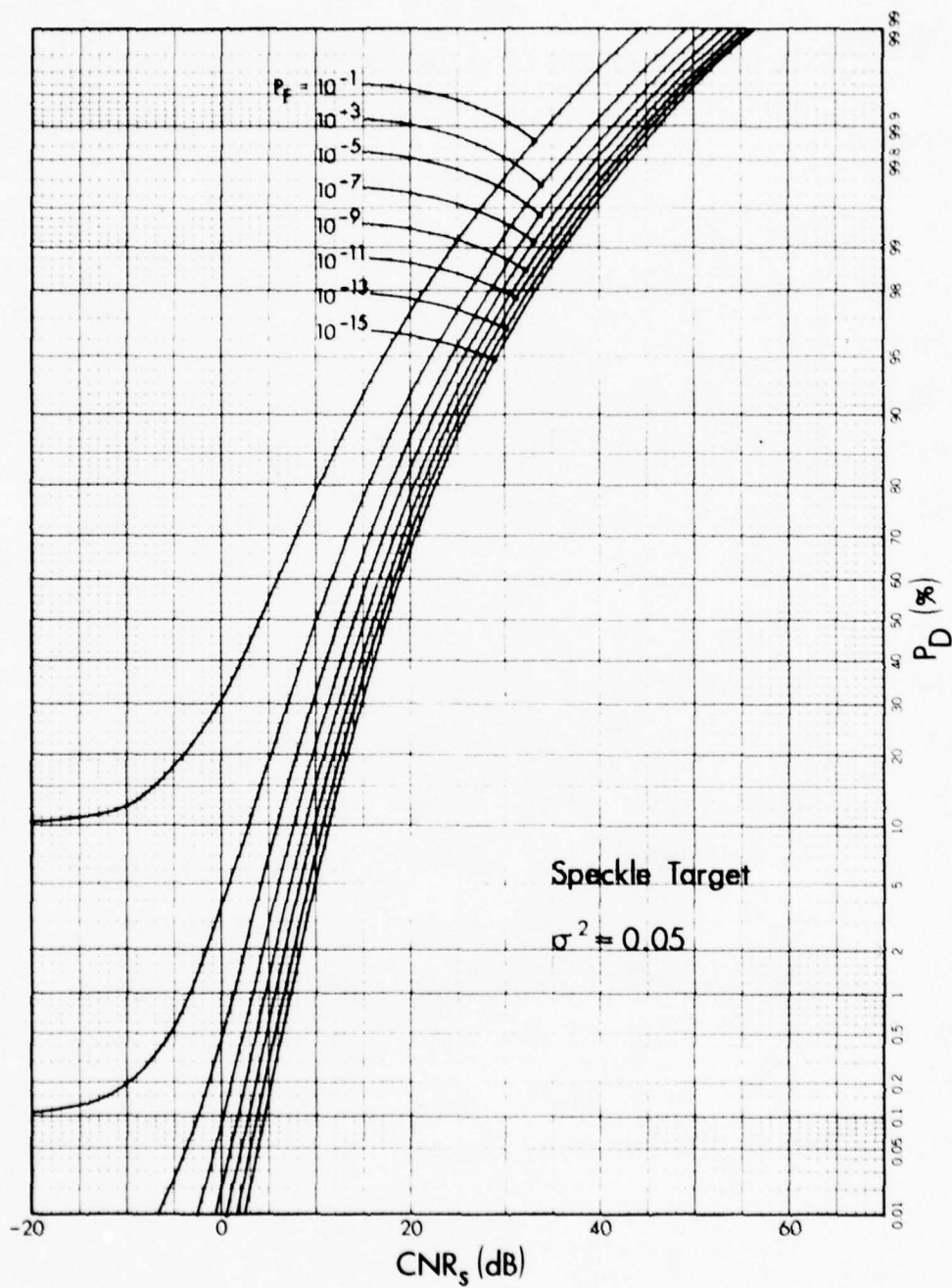


Fig. 17. Speckle target receiver operating characteristics for $\sigma^2 = 0.05$.

TABLE 14

SPECKLE TARGET RECEIVER OPERATING CHARACTERISTICS $\sigma^2 = 0.1$

Detection Probability P_D	False Alarm Probability - P_F							
	10^{-1}	10^{-3}	10^{-5}	10^{-7}	10^{-9}	10^{-11}	10^{-13}	10^{-15}
.0001	**	**	-7.39	-3.69	-1.93	-0.71	0.23	0.99
.0010	**	$-\infty$	-3.33	-0.78	0.76	1.88	2.77	3.50
.0100	**	-3.70	0.66	2.71	4.09	5.13	5.96	6.66
.1000	$-\infty$	2.94	5.91	7.66	8.90	9.86	10.65	11.31
.3000	-0.03	7.33	9.93	11.55	12.72	13.65	14.41	15.06
.5000	4.45	10.51	12.95	14.51	15.65	16.56	17.30	17.94
.7000	8.54	13.95	16.29	17.80	18.92	19.81	20.55	21.18
.8000	11.05	16.22	18.52	20.01	21.12	22.00	22.74	23.37
.8500	12.65	17.71	19.99	21.47	22.58	23.46	24.19	24.81
.9000	14.74	19.70	21.96	23.43	24.53	25.41	26.14	26.76
.9500	18.06	22.93	25.17	26.64	27.73	28.61	29.33	29.96
.9800	22.23	27.04	29.26	30.73	31.82	32.69	33.42	34.04
.9900	25.30	30.09	32.31	33.77	34.87	35.74	36.46	37.09
.9950	28.34	33.12	35.34	36.80	37.89	38.77	39.49	40.11
.9990	35.35	40.12	42.34	43.80	44.90	45.77	46.49	47.11
.9999	45.33	50.10	52.32	53.78	54.87	55.74	56.47	57.09

 CNR_s in dB

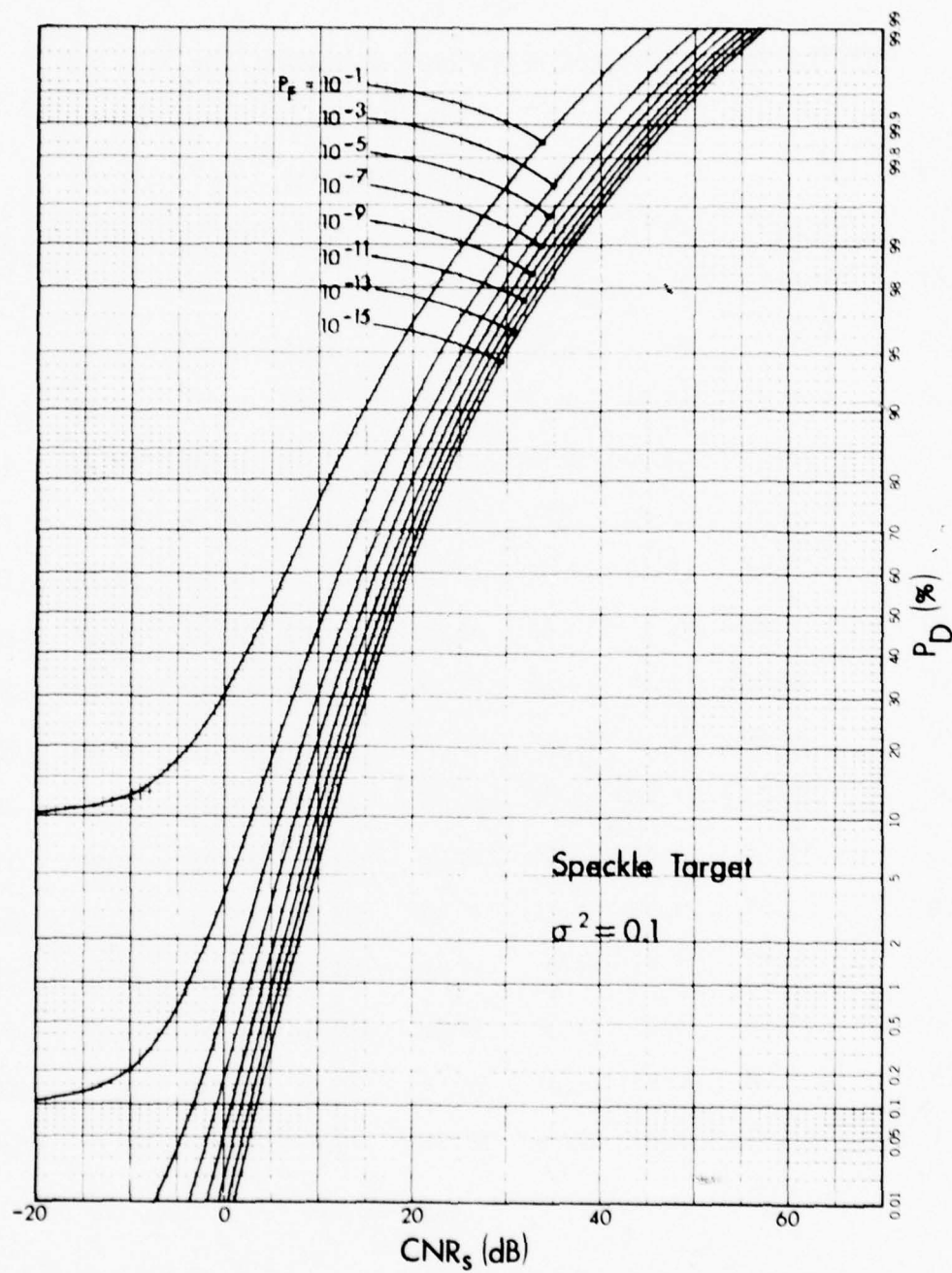


Fig. 18. Speckle target receiver operating characteristics for $\sigma^2 = 0.1$.

TABLE 15

SPECKLE TARGET RECEIVER OPERATING CHARACTERISTICS $\sigma^2 = 0.2$

Detection Probability P_D	False Alarm Probability - P_F							
	10^{-1}	10^{-3}	10^{-5}	10^{-7}	10^{-9}	10^{-11}	10^{-13}	10^{-15}
.0001	**	**	-8.80	-5.64	-4.04	-2.91	-2.02	-1.28
.0010	**	$-\infty$	-4.60	-2.26	-0.81	0.27	1.12	1.83
.0100	**	-4.26	-0.12	1.86	3.20	4.21	5.03	5.72
.1000	$-\infty$	3.00	5.95	7.68	8.91	9.86	10.65	11.31
.3000	0.41	7.93	10.54	12.16	13.34	14.26	15.02	15.67
.5000	5.25	11.45	13.92	15.48	16.63	17.54	18.29	18.93
.7000	9.68	15.20	17.56	19.08	20.20	21.10	21.84	22.47
.8000	12.36	17.62	19.93	21.44	22.55	23.44	24.17	24.80
.8500	14.04	19.18	21.48	22.97	24.08	24.96	25.69	26.32
.9000	16.23	21.25	23.52	25.01	26.11	26.99	27.72	28.34
.9500	19.67	24.57	26.81	28.29	29.38	30.26	30.99	31.61
.9800	23.91	28.73	30.96	32.43	33.52	34.40	35.12	35.74
.9900	27.01	31.81	34.03	35.49	36.59	37.46	38.18	38.81
.9950	30.06	34.85	37.07	38.53	39.62	40.49	41.22	41.84
.9990	37.08	41.86	44.08	45.54	46.63	47.50	48.23	48.85
.9999	47.07	51.84	54.06	55.52	56.61	57.48	58.21	58.83

 CNR_S in dB

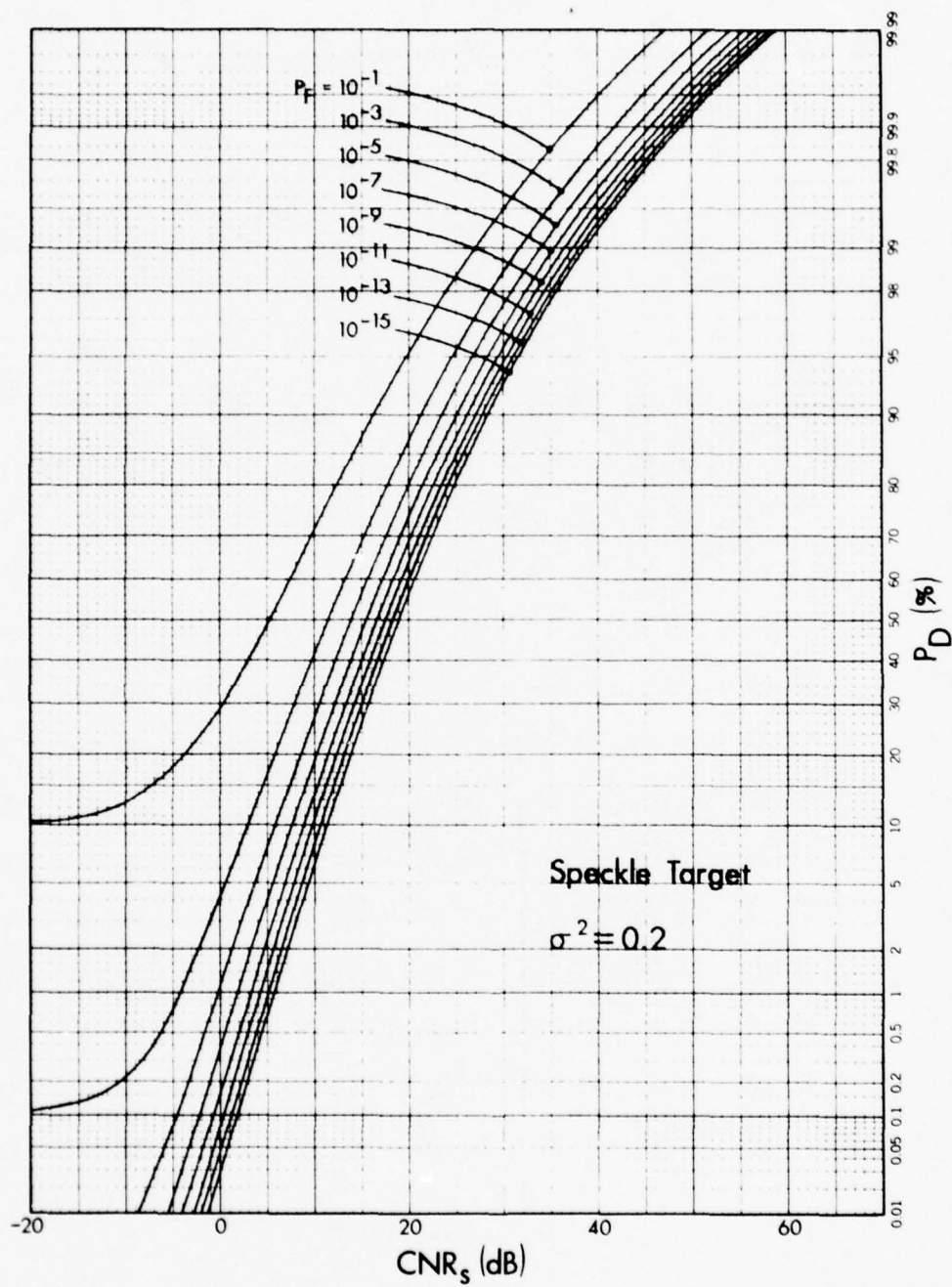


Fig. 19. Speckle target receiver operating characteristics for $\sigma^2 = 0.2$.

TABLE 16
SPECKLE TARGET RECEIVER OPERATING CHARACTERISTICS $\sigma^2 = 0.5$

Detection Probability P_D	False Alarm Probability - P_F							
	10^{-1}	10^{-3}	10^{-5}	10^{-7}	10^{-9}	10^{-11}	10^{-13}	10^{-15}
.0001	**	**	-12.30	-9.73	-8.31	-7.25	-6.41	-5.71
.0010	**	$-\infty$	-7.26	-5.18	-3.83	-2.81	-1.98	-1.30
.0100	**	-5.30	-1.46	0.40	1.67	2.67	3.47	4.15
.1000	$-\infty$	3.60	6.50	8.20	9.41	10.36	11.14	11.80
.3000	1.91	9.80	12.43	14.05	15.23	16.15	16.91	17.56
.5000	7.68	14.18	16.68	18.26	19.41	20.32	21.07	21.71
.7000	12.94	18.71	21.11	22.65	23.78	24.68	25.42	26.06
.8000	16.07	21.55	23.91	25.43	26.55	27.44	28.18	28.81
.8500	18.02	23.35	25.68	27.19	28.31	29.20	29.93	30.56
.9000	20.50	25.69	27.99	29.48	30.60	31.48	32.21	32.84
.9500	24.30	29.32	31.59	33.07	34.17	35.05	35.78	36.41
.9800	28.83	33.72	35.97	37.44	38.54	39.41	40.14	40.76
.9900	32.05	36.89	39.13	40.59	41.69	42.56	43.29	43.91
.9950	35.18	39.99	42.22	43.68	44.78	45.65	46.38	47.00
.9990	42.28	47.06	49.28	50.74	51.83	52.70	53.43	54.05
.9999	52.27	57.05	59.27	60.73	61.82	62.69	63.42	64.04

CNR_s in dB

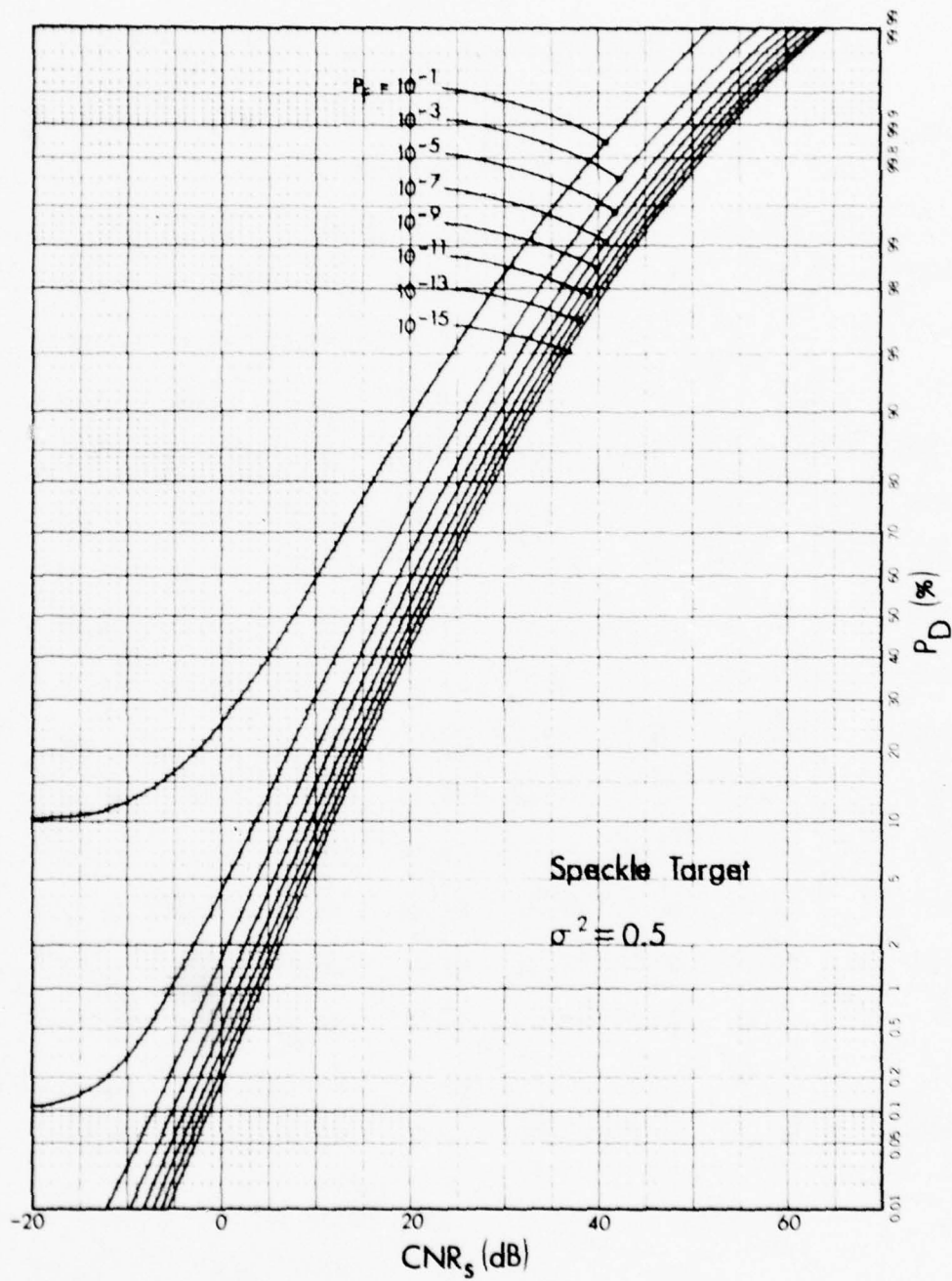


Fig. 20. Speckle target receiver operating characteristics for $\sigma^2 = 0.5$.

TABLE 17
SPECKLE TARGET RECEIVER OPERATING CHARACTERISTICS $\sigma^2 = 1.0$

Detection Probability P_D	False Alarm Probability - P_F							
	10^{-1}	10^{-3}	10^{-5}	10^{-7}	10^{-9}	10^{-11}	10^{-13}	10^{-15}
.0001	**	**	-16.06	-13.74	-12.40	-11.39	-10.57	-9.88
.0010	**	$-\infty$	-9.66	-7.72	-6.43	-5.44	-4.63	-3.96
.0100	**	-5.81	-2.16	-0.37	0.89	1.85	2.64	3.31
.1000	$-\infty$	5.30	8.16	9.84	11.04	11.98	12.75	13.41
.3000	4.78	13.14	15.77	17.39	18.56	19.48	20.24	20.89
.5000	11.76	18.62	21.14	22.72	23.88	24.79	25.54	26.19
.7000	18.13	24.20	26.63	28.18	29.32	30.23	30.97	31.61
.8000	21.90	27.64	30.04	31.57	32.70	33.60	34.34	34.97
.8500	24.21	29.79	32.16	33.68	34.81	35.70	36.44	37.08
.9000	27.13	32.54	34.88	36.39	37.51	38.40	39.14	39.77
.9500	31.53	36.73	39.03	40.53	41.64	42.53	43.26	43.89
.9800	36.62	41.65	43.92	45.40	46.51	47.39	48.12	48.74
.9900	40.14	45.08	47.34	48.81	49.91	50.79	51.52	52.15
.9950	43.48	48.36	50.61	52.08	53.18	54.05	54.78	55.40
.9990	50.84	55.65	57.88	59.34	60.43	61.31	62.03	62.65
.9999	60.94	65.72	67.94	69.40	70.49	71.37	72.09	72.71

CNR_s in dB

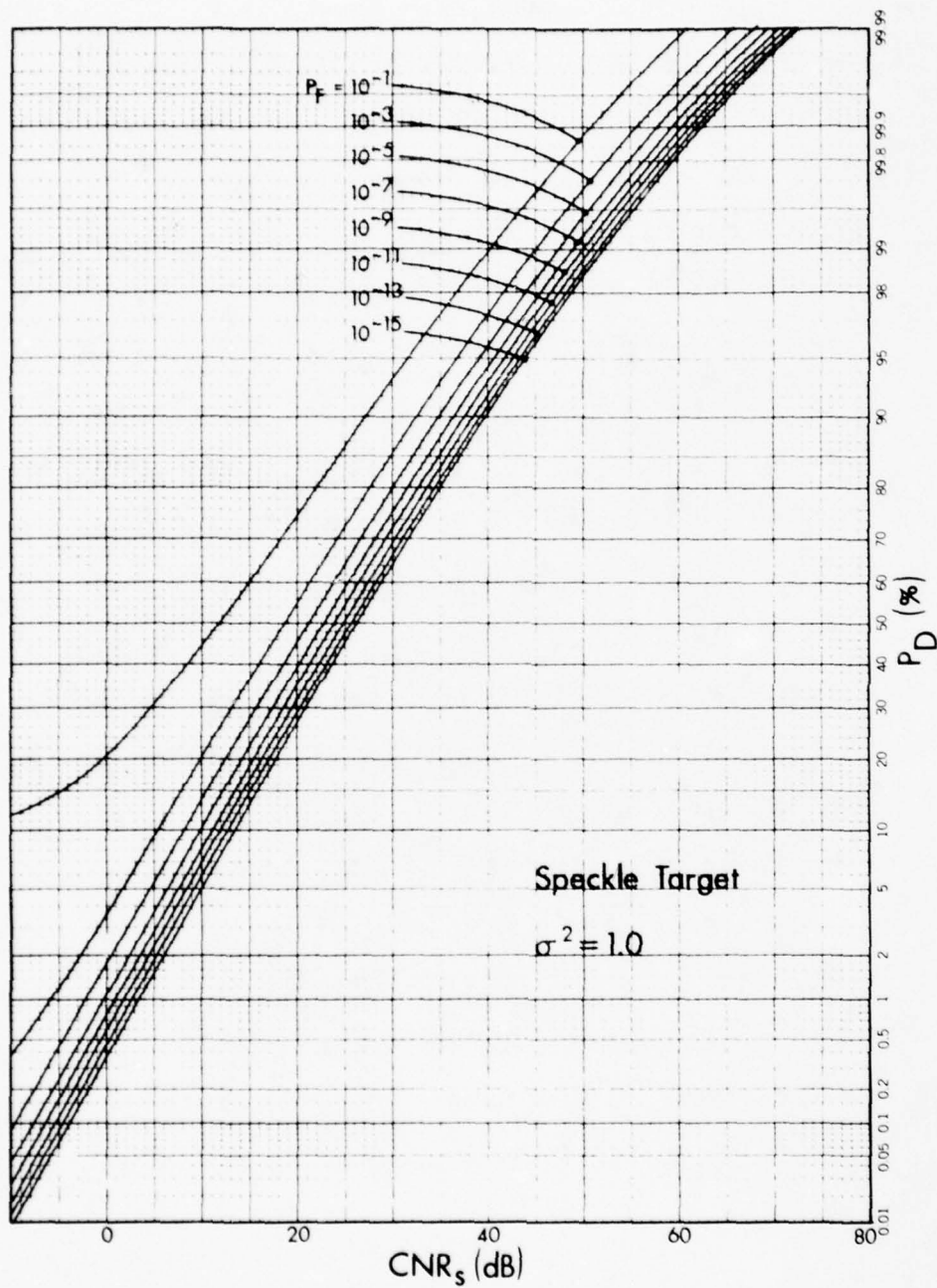


Fig. 21. Speckle target receiver operating characteristics for $\sigma^2 = 1.0$.

TABLE 18
SPECKLE TARGET RECEIVER OPERATING CHARACTERISTICS $\sigma^2 = 2.0$

Detection Probability P_D	False Alarm Probability - P_F							
	10^{-1}	10^{-3}	10^{-5}	10^{-7}	10^{-9}	10^{-11}	10^{-13}	10^{-15}
.0001	**	**	-19.74	-17.52	-16.25	-15.27	-14.48	-13.81
.0010	**	$-\infty$	-11.16	-9.32	-8.06	-7.09	-6.30	-5.63
.0100	**	-4.64	-1.07	0.68	1.90	2.86	3.64	4.30
.1000	$-\infty$	9.92	12.75	14.41	15.61	16.55	17.32	17.97
.3000	11.15	20.22	22.84	24.45	25.62	26.54	27.30	27.94
.5000	20.03	27.38	29.92	31.50	32.66	33.57	34.32	34.96
.7000	28.15	34.60	37.07	38.63	39.77	40.67	41.42	42.06
.8000	32.92	39.01	41.44	42.99	44.13	45.03	45.78	46.41
.8500	35.82	41.74	44.15	45.68	46.82	47.71	48.46	49.09
.9000	39.48	45.19	47.58	49.11	50.24	51.13	51.87	52.51
.9500	44.90	50.38	52.73	54.25	55.37	56.26	56.99	57.63
.9800	51.06	56.34	58.65	60.15	61.27	62.15	62.89	63.52
.9900	55.23	60.39	62.68	64.18	65.29	66.17	66.90	67.53
.9950	59.11	64.17	66.45	67.94	69.04	69.93	70.66	71.28
.9990	67.34	72.27	74.52	75.99	77.09	77.97	78.70	79.32
.9999	78.06	82.88	85.11	86.58	87.67	88.55	89.27	89.90

CNR_s in dB

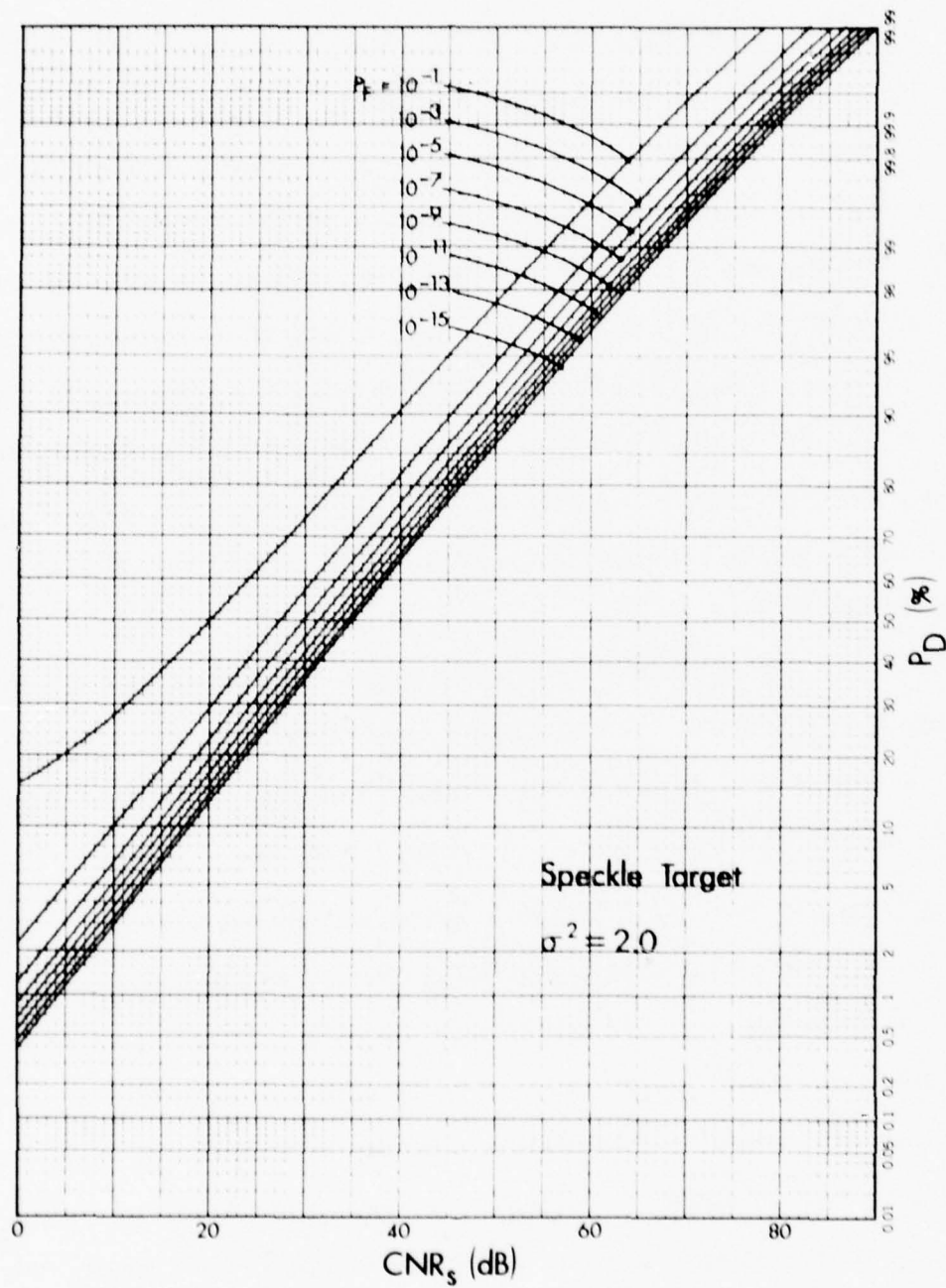


Fig. 22. Speckle target receiver operating characteristics for $\sigma^2 = 2.0$.

for the commonly desired P_D values of 0.0001, 0.001, 0.01, 0.1, 0.3, 0.5, 0.7, 0.8, 0.85, 0.90, 0.95, 0.98, 0.99, 0.995, 0.999, and 0.9999 and the same P_F values used in the figures.

We have also evaluated the speckle target detection probability as a function of the turbulent-propagation speckle target carrier-to-noise ratio (CNR_s) for the same false alarm probabilities used in the glint target case and turbulence log-amplitude variance (σ^2) values of 0, 0.0001, 0.001, 0.01, 0.05, 0.1, 0.2, 0.5, 1.0, and 2.0. These results are presented in Figures 13 through 22. For each σ^2 value we have included a table which lists the value of CNR_s required to obtain specified P_D and P_F values. These results are presented in Tables 9 through 18 for the same P_D and P_F values used in the glint target results.

Tables 1 through 6 have an uncertainty in the calculated CNR_g° values of less than ± 0.01 dB. Tables 7 and 8 have an uncertainty in the calculated CNR_g° values of less than ± 0.1 dB. Tables 9 through 18 have an uncertainty in the calculated CNR_s values of less than ± 0.01 dB.

5. EXPERIMENTAL TURBULENCE STRENGTH DETERMINATIONS AND TYPICAL σ_X^2 VALUES

Utilization of the data presented in Section 4 requires knowledge of the turbulence log-amplitude variance (σ_X^2 or σ^2). In this section we provide an assessment of the range of turbulence strengths (C_n^2 or C_T^2) and corresponding log-amplitude variances that may be encountered in typical scenarios in which coherent optical radars may be utilized.

Within the weak-perturbation propagation regime (i.e., before the onset of saturated scintillation) we have that

$$\sigma_X^2 = 0.56 k^{7/6} \int_0^L dz C_n^2(z) (z/L)^{5/6} (L-z)^{5/6} \quad (27)$$

is the log-amplitude variance due to turbulence. In Eq. (27), $k = 2\pi/\lambda$ is the wavenumber at the laser wavelength, and $C_n^2(z)$ is the turbulence strength profile along the path from the transmitter ($z = 0$) to the target ($z = L$). For a horizontal path with a profile $C_n^2 = \text{constant}$, Eq. (27) reduces to Eq. (9).

Equations (9) and (27) presume that $C_n^2(z)$ is a fixed profile. In fact, $C_n^2(z)$ exhibits random time dependence [10], [11]. To a first approximation we may use Eq. (9) and (27) with $C_n^2(z)$ or C_n^2 taken to be the average turbulence strength profile. Only limited results are available [10]-[16] for the variability of $C_n^2(z)$. Some selected results from a summary in [10] are:

- i) Soviet measurements [12] made on the steppes in July and August at a height of 2.5 m gave

$$\text{Pr}[5.4 \times 10^{-14} \text{ m}^{-2/3} \leq C_n^2 \leq 5.4 \times 10^{-13} \text{ m}^{-2/3}] = 0.84 \quad (28)$$

during the daytime and

$$\text{Pr}[5.4 \times 10^{-15} \text{ m}^{-2/3} \leq C_n^2 \leq 5.4 \times 10^{-14} \text{ m}^{-2/3}] = 0.70 \quad (29)$$

at night.

ii) NOAA measurements [13] made in Eastern Colorado in August at a height of 92 m gave C_n^2 approximately a log-normal random variable with mean

$$\langle C_n^2 \rangle = 7 \times 10^{-16} \text{ m}^{-2/3} \quad (30)$$

and variance

$$\text{var}(C_n^2) = 2.2 \times 10^{-30} \text{ m}^{-4/3} \quad (31)$$

during early morning hours. Afternoon data at this height had

$$\langle C_n^2 \rangle = 3.0 \times 10^{-15} \text{ m}^{-2/3} \quad (32)$$

and

$$\text{var}(C_n^2) = 4.0 \times 10^{-28} \text{ m}^{-4/3} \quad (33)$$

and deviated from a log-normal distribution.

An RADC study [14] has assembled a fairly large amount of temperature-strength (C_T^2) statistics at 3m height in upstate New York. These can be converted to C_n^2 via

$$C_n^2 = 10^{-12} C_T^2 \quad (34)$$

The RADC data does not fit a log-normal distribution. It does reveal diurnal trends and ranges over winter to spring weather conditions. Key results are summarized in Table 19. An AFCRL study [15] has found that the turbulence strength over land is a function of height (h) above the ground and obeys the relation

TABLE 19
RADC MONTHLY-AVERAGED TURBULENCE STATISTICS

		LOG C_n^2 STATISTICS (TYPE I)				LOG C_n^2 STATISTICS (ALL-WEATHER)			
		Mean	Std.Dev.	Skewness	Kurtosis	Mean	Std.Dev.	Skewness	Kurtosis
Feb	night	-14.1293	0.5818	-0.0193	1.8721	-14.1218	0.6750	0.0603	2.3967
	day	-12.7599	0.4071	-1.4601	4.7501	-13.6349	0.7631	0.2102	2.1841
	dusk	-13.5885	0.4554	-0.7393	2.3638	-13.8117	0.5895	-0.2495	2.6038
	dawn	-14.2593	0.6082	-0.0373	2.2389	-14.2997	0.7113	-0.0420	2.3398
Mar	night	-14.3290	0.6027	-0.2786	2.1450	-14.0482	0.7496	0.1822	3.1892
	day	-12.7031	0.5226	-0.8821	3.0298	-13.1210	0.8219	-0.3946	1.9218
	dusk	-13.8647	0.6043	0.5247	2.4447	-13.7303	0.6911	0.0951	2.2917
	dawn	-14.3422	0.6345	0.3018	2.4577	-14.1935	0.7008	0.2681	3.3321
Apr	night	-13.6654	0.4278	-0.3780	2.9456	-13.6394	0.5079	-0.2778	3.3083
	day	-12.7913	0.6151	-0.8924	3.1236	-12.8155	0.6286	-0.8228	2.9301
	dusk	-13.5856	0.5569	0.1467	2.0468	-13.6653	0.6370	-0.0915	2.4126
	dawn	-13.7922	0.5187	0.2501	3.1293	-13.7850	0.5109	0.1018	3.0319
May	night	-13.4911	0.5369	-0.1877	2.3367	-13.5387	0.5728	-0.6395	3.1334
	day	-12.5602	0.3703	-1.5192	5.9714	-12.8524	0.6315	-1.1269	3.6039
	dusk	-13.5285	0.4634	-0.2176	2.9851	-13.5110	0.5412	-0.3310	3.0026
	dawn	-13.6567	0.5986	0.0812	2.5258	-13.7145	0.6337	-0.2969	3.0355

$$C_n^2(h) = C_n^2(1) h^{-4/3} \quad (35)$$

for heights below a few hundred meters during the daytime. At night $C_n^2(h)$ falls off more slowly, perhaps slower than $h^{-2/3}$. Similar results have been obtained over the ocean by a group at the Naval Postgraduate School [16].

We have used the results cited in the preceding paragraph to obtain some crude estimates of σ_X^2 behavior at a wavelength of $10.6\mu\text{m}$. The results are given in Figures 23-33. The curves in Figure 23 are developed from Eqs.(9), (28), and (35) for a horizontal path 2m above the ground by assuming that C_n^2 is completely correlated (i.e., constant) along the propagation path. For a given L , the probability that σ_X^2 lies between the two curves is 0.84. As C_n^2 will not be completely correlated over many kilometers, these results may be pessimistic.

The curves in Figure 24 are obtained from Eqs.(9) and (29) and

$$C_n^2(h) = C_n^2(1) h^{-2/3} \quad (36)$$

for a nighttime horizontal path 2m above the ground by assuming C_n^2 is completely correlated along the propagation path. For a given L , the probability that σ_X^2 lies between the two curves is 0.70. These results may be pessimistic.

The curves in Figure 25 give $\langle \sigma_X^2 \rangle$ and $\langle \sigma_X^2 \rangle \pm (\text{var}(\sigma_X^2))^{1/2}$ for an early morning horizontal path 2m above the ground and are derived from Eqs.(9), (30), (31), and (35). These results were calculated assuming partial correlation along the optical path with a correlation length of

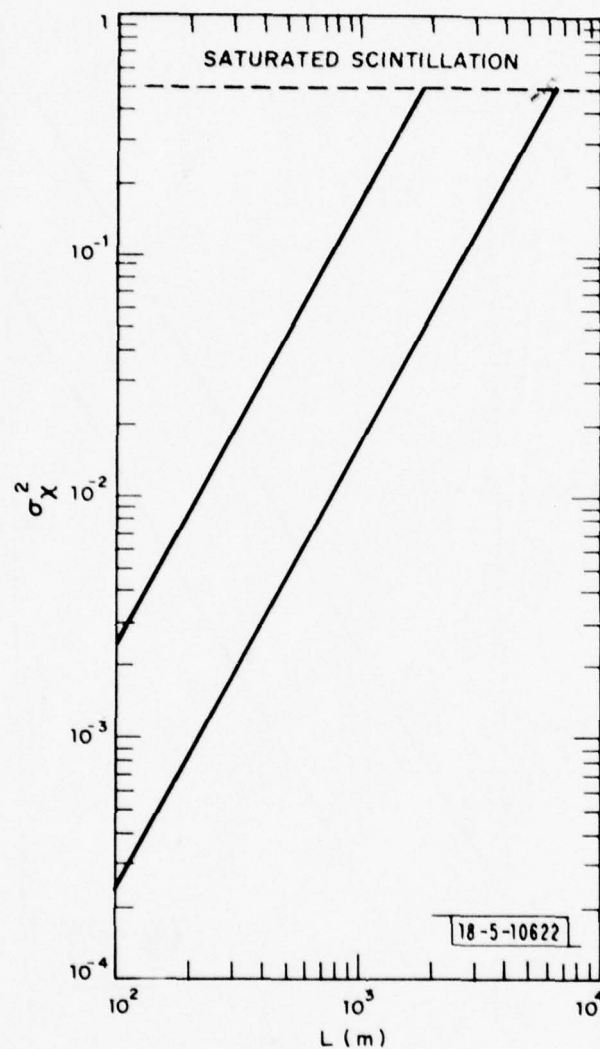


Fig. 23. Log-amplitude variance σ_X^2 vs. path length L for a horizontal path at a height of 2m assuming the Soviet daytime C_n^2 data and complete correlation along the path. For any given L , the probability that σ_X^2 lies between the two curves is 0.84.

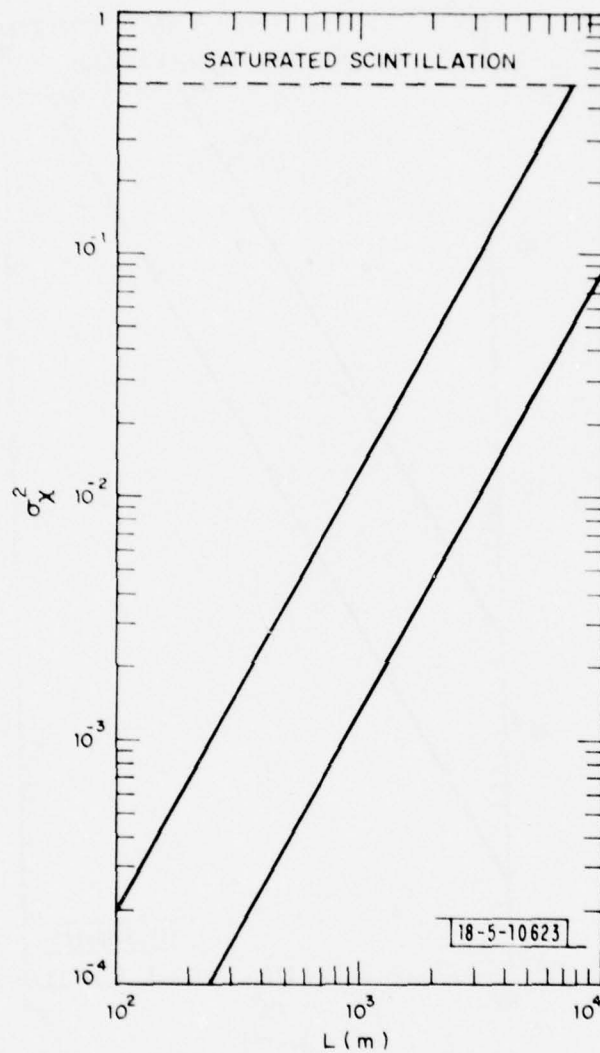


Fig. 24. Log-amplitude variance σ_{χ}^2 vs. path length L for a horizontal path at a height of 2m assuming the Soviet nighttime C_n^2 data and complete correlation along the path. For any given L , the probability that σ_{χ}^2 lies between the two curves is 0.70.

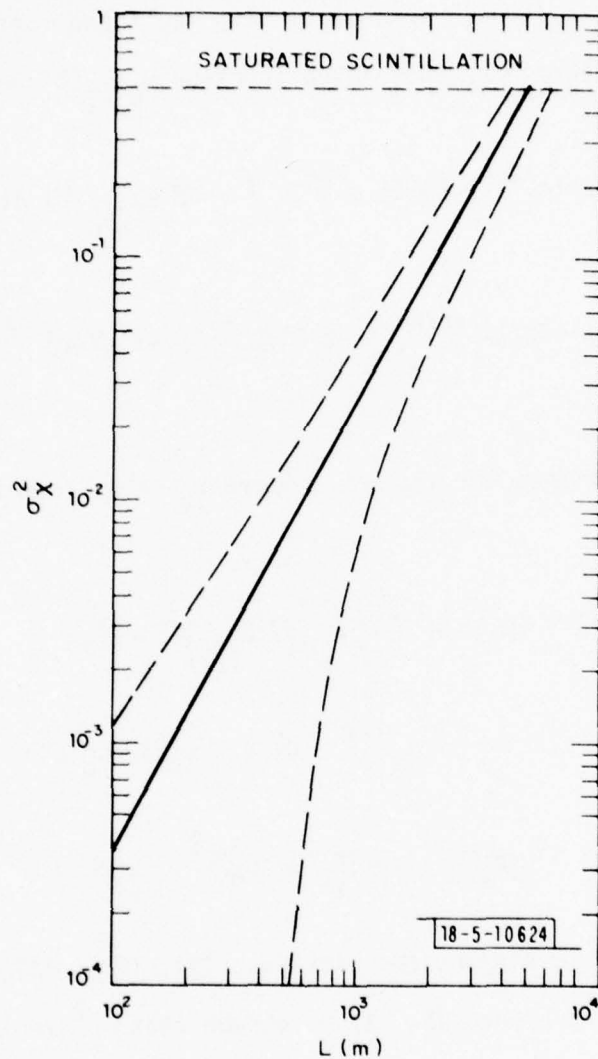


Fig. 25. Log-amplitude variance σ_X^2 vs. path length L for a horizontal path at a height of 2m assuming the NOAA early morning C_n^2 data and partial correlation along the optical path with a correlation length of 100m. The three curves represent calculations of $\langle \sigma_X^2 \rangle$ (solid curve) and $\langle \sigma_X^2 \rangle \pm (\text{var}(\sigma_X^2))^{1/2}$ (dotted curves).

100 m. Partial correlation is taken into account in the following manner. For a horizontal path with a constant mean $\langle C_n^2 \rangle$ and variance $\text{var}(C_n^2)$ along the path and a stationary covariance function $K_{C_n^2 C_n^2}(\tilde{z})$ we have that

$$\text{var}(\sigma_X^2) = (0.56 k^{7/6})^2 \int_{-L}^L d\tilde{z} K_{C_n^2 C_n^2}(\tilde{z}) K(\tilde{z}) \quad (37)$$

with

$$K(\tilde{z}) = \int_0^{L-|\tilde{z}|} dz' [(z'+\tilde{z}/2)/L]^{5/6} [(z'-\tilde{z}/2)/L]^{5/6} [L-z'-\tilde{z}/2]^{5/6} [L-z'+\tilde{z}/2]^{5/6} \quad (38)$$

If $K_{C_n^2 C_n^2}(\tilde{z})$ vanishes for $|\tilde{z}| > L_c$, where $L_c \ll L$, then Eqs. (37) and (38) give

$$\text{var}(\sigma_X^2) \sim (0.56 k^{7/6})^2 \int_{-\infty}^{\infty} d\tilde{z} K_{C_n^2 C_n^2}(\tilde{z}) K(0) \quad (39)$$

$$= 1.17 \langle \sigma_X^2 \rangle^2 L^{-1} \int_{-\infty}^{\infty} d\tilde{z} K_{C_n^2 C_n^2}(\tilde{z}) / \langle C_n^2 \rangle^2 \quad (40)$$

$$\sim 1.17 \langle \sigma_X^2 \rangle^2 [\text{var}(C_n^2) / \langle C_n^2 \rangle^2] (L_c/L) \quad (41)$$

Eq. (41) was used in conjunction with Eqs. (9), (30), (31), (35) and $L_c = 100$ m to yield Figure 25. If we assume that σ_X^2 is log-normally distributed, the data in Figure 25 may be re-expressed in a more useful fashion as shown in Figure 26. There is a 90% probability that σ_X^2 exceeds the lower curve and a 10% probability that it exceeds the upper curve.

The curves in Figure 27 are based on the RADC data for Type I (clear skies) turbulence obtained at 0100 EST and 1100 EST during the month of

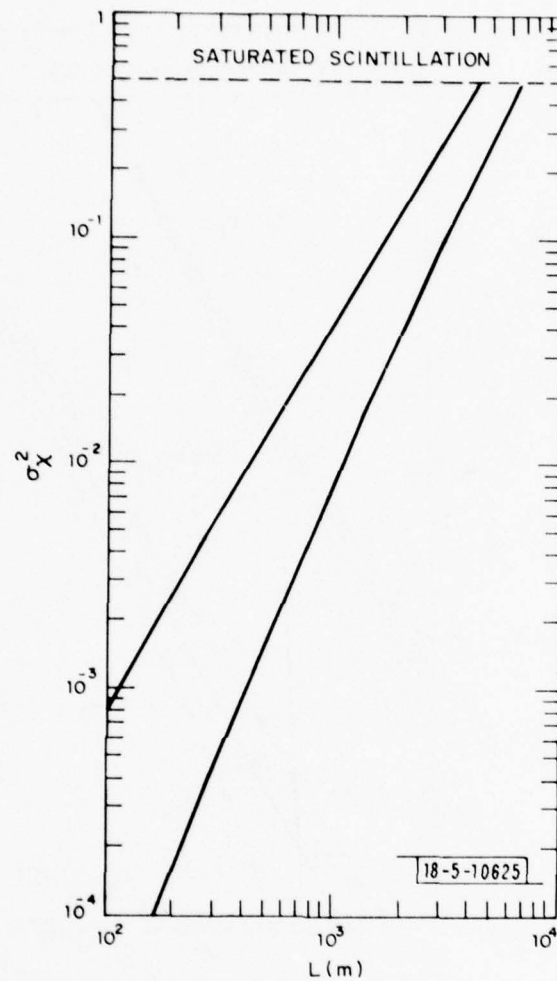


Fig. 26. Log-amplitude variance σ_X^2 vs. path length L for a horizontal path at a height of 2m assuming the NOAA early morning C_n^2 data, partial correlation along the optical path with a correlation length of 100m, and a log-normal distribution for σ_X^2 . This is a 90% probability that σ_X^2 exceeds the lower curve and a 10% probability that it exceeds the upper curve.

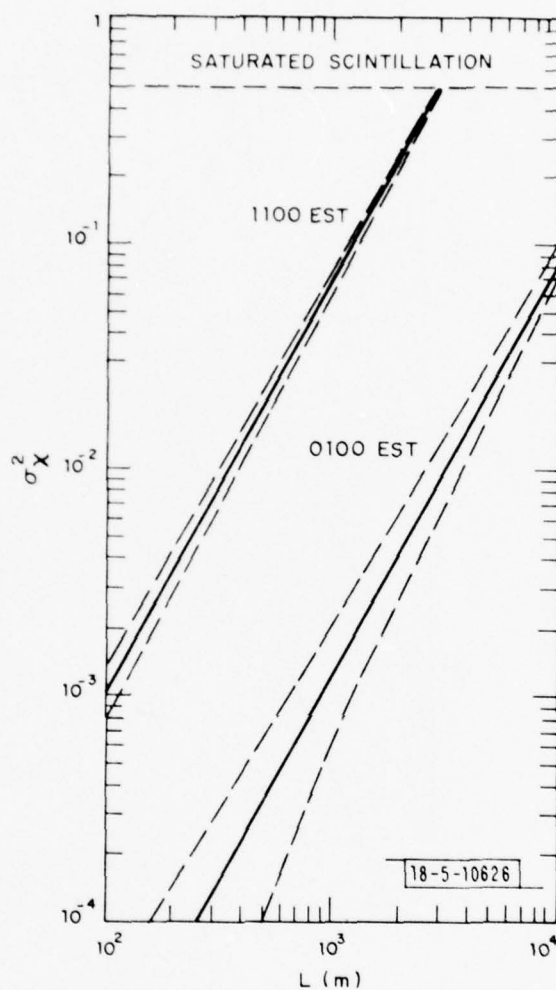


Fig. 27. Log-amplitude variance σ_X^2 vs. path length L for a horizontal path at a height of 3m assuming the RADC data for Type I turbulence obtained at 0100 EST and 1100 EST during the month of February and partial correlation along the optical path with a correlation length of 100 m. For each hour curves for $\langle \sigma_X^2 \rangle$ and $\langle \sigma_X^2 \rangle \pm (\text{var}(\sigma_X^2))^{1/2}$ have been plotted.

February. For each hour we have plotted $\langle \sigma_X^2 \rangle$ and $\langle \sigma_X^2 \rangle \pm (\text{var}(\sigma_X^2))^{1/2}$ for a horizontal path of 3m height and assuming a 100m correlation length.

In many applications of infrared radars slant paths through the atmosphere are utilized. Recalling Eqs. (27), (35), and (36) and assuming the slant path geometry of Figure 28 with target height h_0 , transmitter height H , and slant range L we obtain

$$\langle \sigma_X^2 \rangle = 0.56 k^{7/6} \langle C_n^2(h_0) \rangle \int_0^L dz (1 + (L-z)(H-h_0)/L h_0)^{-4/3} (z/L)^{5/6} (L-z)^{5/6} \quad (42)$$

for daytime propagation and

$$\langle \sigma_X^2 \rangle = 0.56 k^{7/6} \langle C_n^2(h_0) \rangle \int_0^L dz (1 + (L-z)(H-h_0)/L h_0)^{-2/3} (z/L)^{5/6} (L-z)^{5/6} \quad (43)$$

for nighttime propagation. The C_n^2 -dependence of Eq. (42) is illustrated in Figure 29 for paths with $H = 50\text{m}$ and $h_0 = 2\text{m}$. Since both Eqs. (42) and (43) are linear in C_n^2 , the slant path results (which will be obtained at a specific $C_n^2(h_0)$ value) presented in the figures to follow can be readily adjusted to any desired $C_n^2(h_0)$ value by simply shifting the curves along the vertical (σ_X^2) axis.

Figure 30 illustrates the dependence of $\langle \sigma_X^2 \rangle$ vs. L on the height of the transmitter for daytime propagation. These curves were obtained by numerical integration of Eq. (42). We have assumed a target height $h_0 = 2\text{m}$ so the $H = 2\text{m}$ curve corresponds to a horizontal path. A turbulence strength of $\langle C_n^2(2) \rangle = 10^{-13} \text{ m}^{-2/3}$ has been used since examination of Table 19

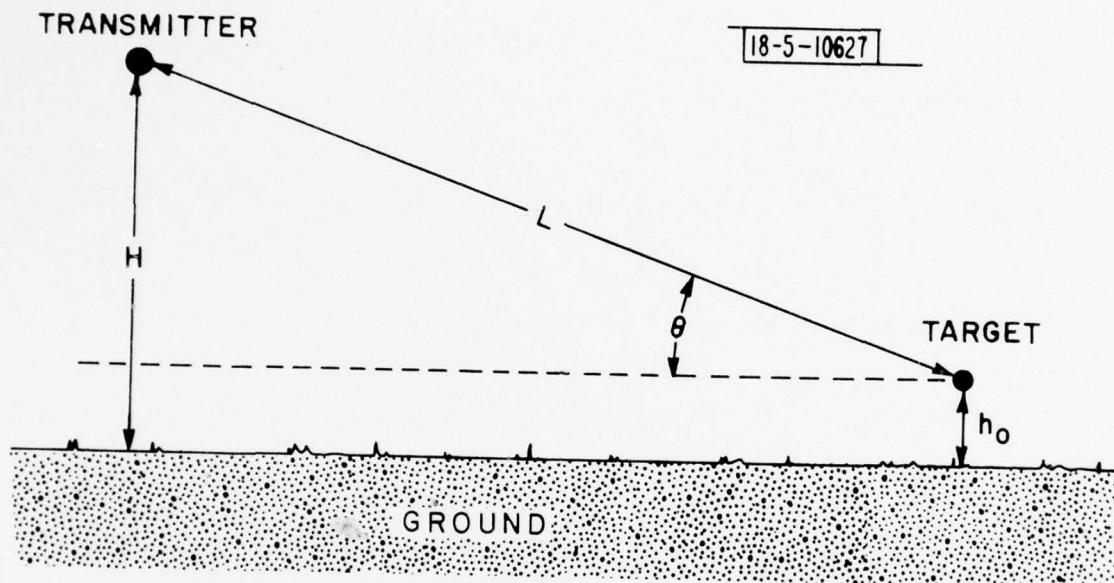


Fig. 28. Geometry involved in slant path propagation calculations.

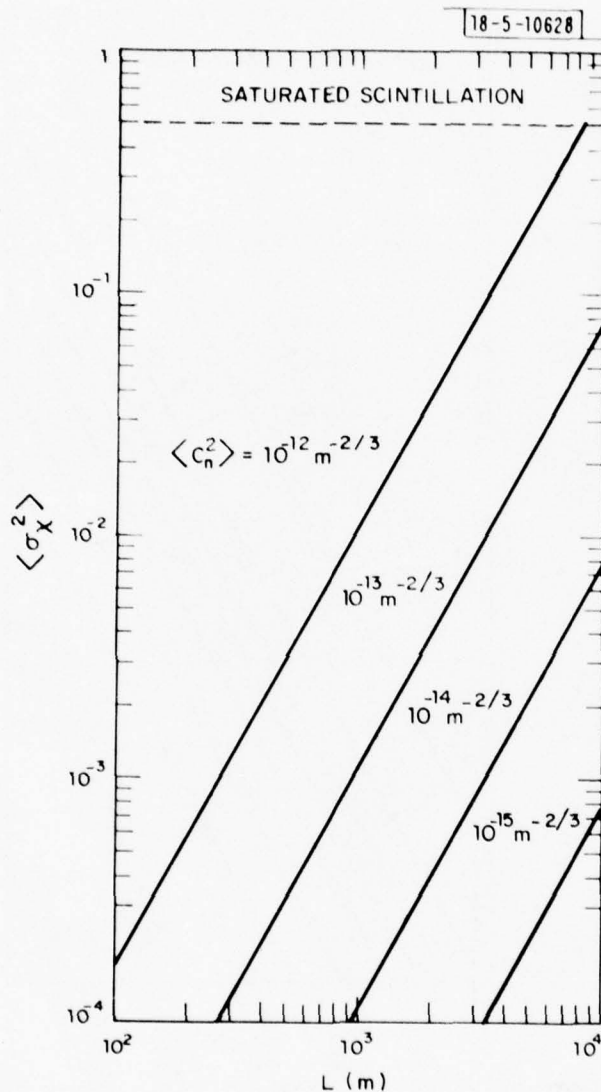


Fig. 29. Log-amplitude variance $\langle \sigma_X^2 \rangle$ vs. slant path length for paths with transmitter height $H_X = 50\text{m}$ and target height $h_0 = 2\text{m}$ assuming various values of $\langle C_n^2 \rangle$.

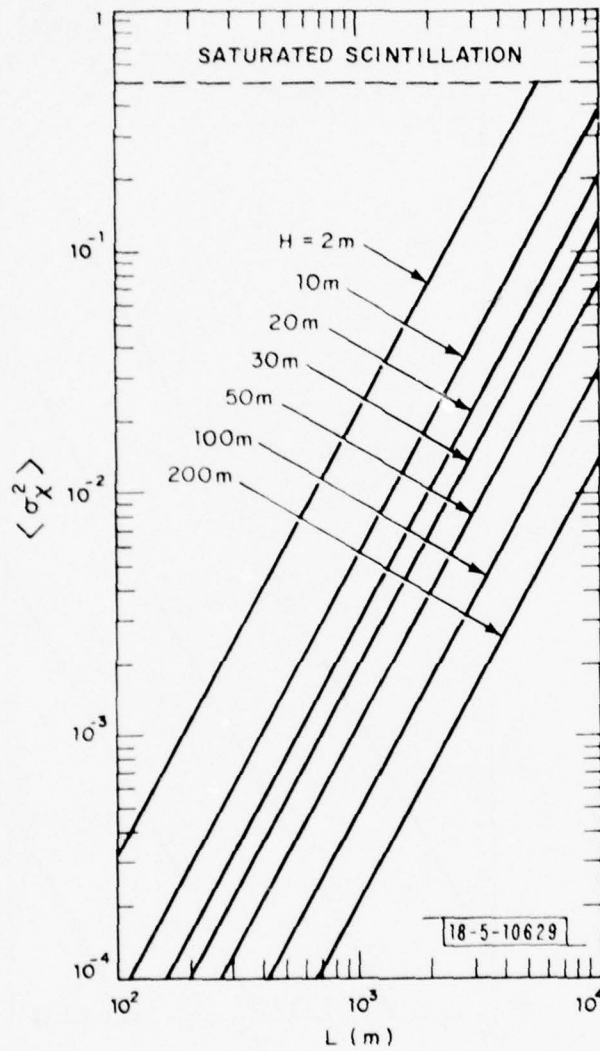


Fig. 30. Log-amplitude variance $\langle \sigma_X^2 \rangle$ vs. slant path length L for daytime slant paths with target height $h_0 = 2\text{m}$ and various transmitter heights assuming a typical daytime value of $\langle C_n^2 \rangle = 10^{-13} \text{ m}^{-2/3}$.

indicates that this is a reasonable average daytime value. Numerical integration of Eq. (43) yielded the curves in Figure 31, which illustrates the dependence of $\langle \sigma_X^2 \rangle$ vs. L on the transmitter height for nighttime propagation. We have assumed $h_0 = 2\text{m}$ and $\langle C_n^2(2) \rangle = 10^{-14} \text{ m}^{-2/3}$ (a reasonable average nighttime value).

The parameterization of Eqs. (42) and (43) in terms of transmitter altitude H is convenient in analysis of many airborne applications as typically the aircraft flies at a known altitude and searches for targets on the ground at unknown ranges. However, in the analysis of some ground-based applications it may be more convenient to parameterize in terms of the elevation angle θ . For a ground-based transmitter at height H looking for targets at elevation angle θ and slant range L , Eq. (42) may be rewritten as

$$\langle \sigma_X^2 \rangle = 0.56 k^{7/6} \langle C_n^2(H) \rangle \int_0^L dz (1 + z \sin\theta/H)^{-4/3} (z/L)^{5/6} (L-z)^{5/6} \quad (44)$$

and Eq. (43) may be rewritten as

$$\langle \sigma_X^2 \rangle = 0.56 k^{7/6} \langle C_n^2(H) \rangle \int_0^L dz (1 + z \sin\theta/H)^{-2/3} (z/L)^{5/6} (L-z)^{5/6} \quad (45)$$

In Figure 32 we have plotted curves showing $\langle \sigma_X^2 \rangle$ vs. L for various elevation angles and daytime propagation as obtained by numerically integrating Eq. (44). A transmitter height $H = 2\text{m}$ and a daytime turbulence strength $\langle C_n^2(2) \rangle = 10^{-13} \text{ m}^{-2/3}$ have been assumed. Figure 33 illustrates

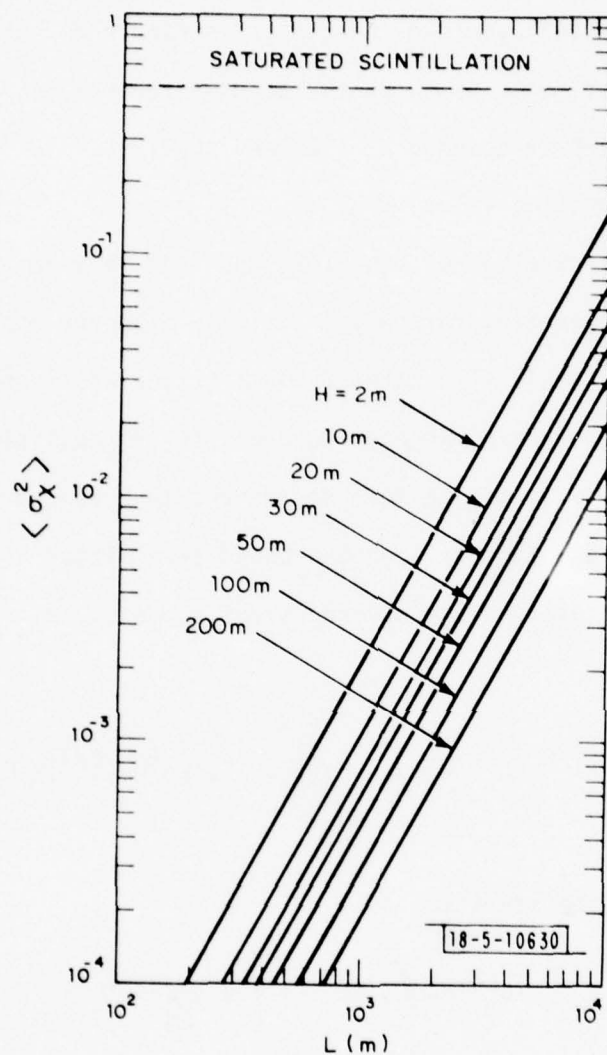


Fig. 31. Log-amplitude variance $\langle \sigma_X^2 \rangle$ vs. slant path L for nighttime slant paths with target height $h_0 = 2\text{m}$ and various transmitter heights assuming a typical nighttime value of $\langle C_n^2 \rangle = 10^{-14} \text{ m}^{-2/3}$.

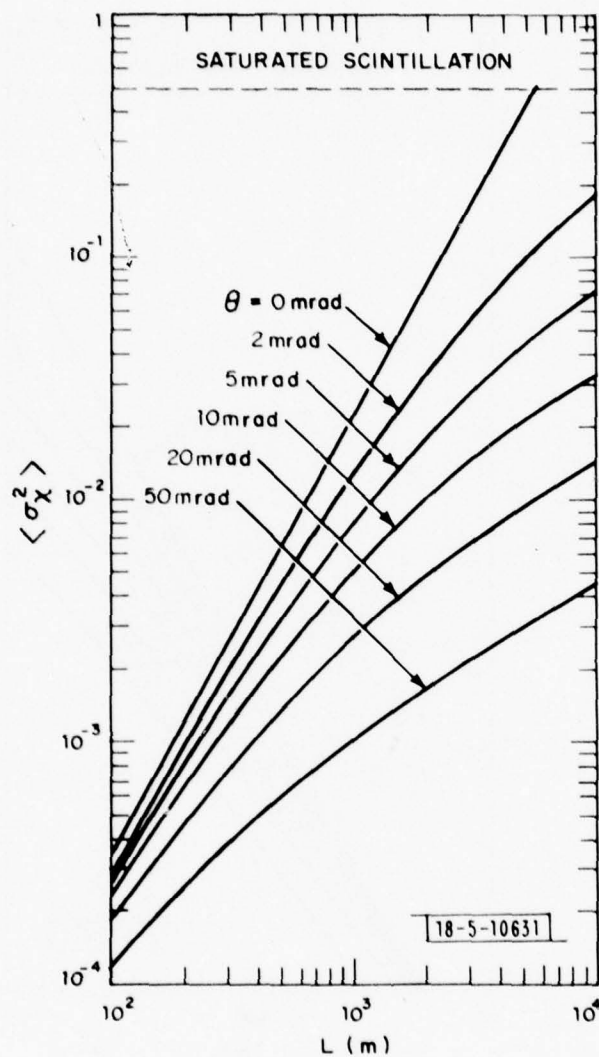


Fig. 32. Log-amplitude variance $\langle \sigma_X^2 \rangle$ vs. slant path length L for daytime slant paths with transmitter height $H = 2\text{m}$ and various elevation angles assuming a typical daytime value of $\langle C_n^2 \rangle = 10^{-13} \text{ m}^{-2/3}$.

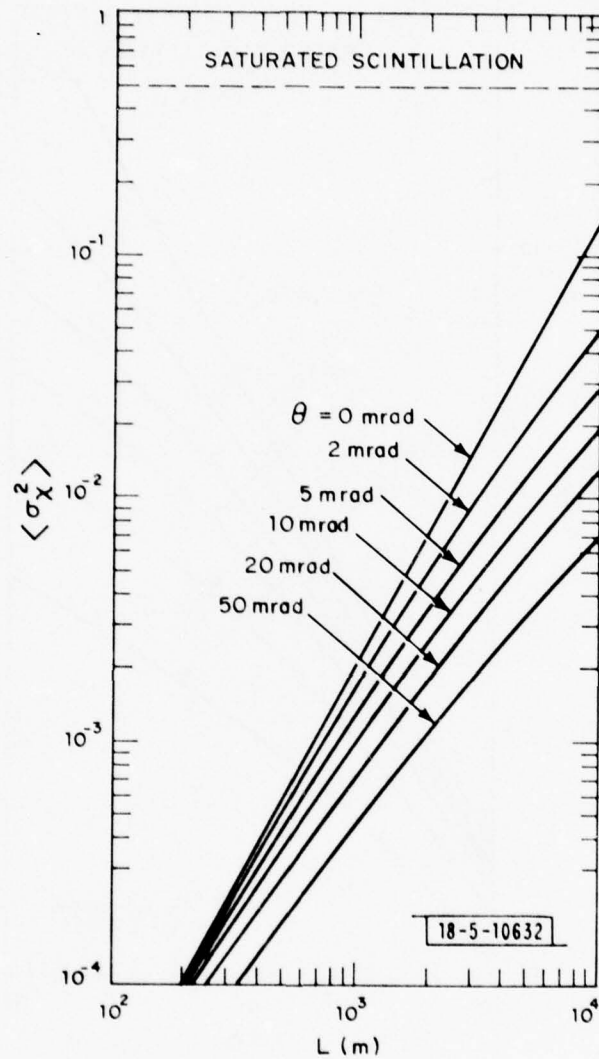


Fig. 33. Log-amplitude variance $\langle \sigma_X^2 \rangle$ vs. slant path length L for nighttime slant paths with transmitter height $H = 2\text{m}$ and various elevation angles assuming a typical nighttime value of $\langle C_n^2 \rangle = 10^{-14} \text{ m}^{-2/3}$.

similar results for nighttime propagation obtained by numerical integration of Eq. (45). Again $H = 2\text{m}$ has been assumed, however, a nighttime value of $\langle C_n^2(2) \rangle = 10^{-14} \text{ m}^{-2/3}$ has been used.

6. TURBULENCE EFFECTS ON RADAR PERFORMANCE-EXAMPLES

The results of the preceding two sections can be combined to estimate the performance of any given infrared radar system. Before attempting this for a few realistic examples, it is instructive to recast some of the results of Section 4 in a slightly more useful form. At high values of the detection probability the presence of atmospheric turbulence will cause an increase in the carrier-to-noise ratio required to achieve a given P_D value at a given P_F value. This increase may be expressed as

$$\Delta\text{CNR}(\sigma_X^2; P_D, P_F) = \text{CNR}(\sigma_X^2; P_D, P_F) / \text{CNR}(0; P_D, P_F) \quad (46)$$

In Figure 34 we have used Tables 1-8 to obtain ΔCNR vs σ_X^2 for glint targets and Tables 9-18 to obtain ΔCNR vs. $\sigma^2/4$ for speckle targets for $P_F = 10^{-7}$ and $P_D = 0.90$ and 0.99 . This figure clearly indicates that if high turbulence levels are encountered, very large CNR margins

$$M = \text{System CNR} / \text{CNR}(0; P_D, P_F) \quad (47)$$

must be available or performance will be degraded. The magnitude of the potential degradation becomes apparent in Figures 35 and 36.

In Figure 35 we have used Figures 5-12 to construct curves of P_D vs. σ_X^2 for glint targets with system carrier-to-noise ratio of 10, 15, 20, 30, and 40 dB at $P_F = 10^{-7}$. In Figure 36 we have used Figures 13-22 to construct

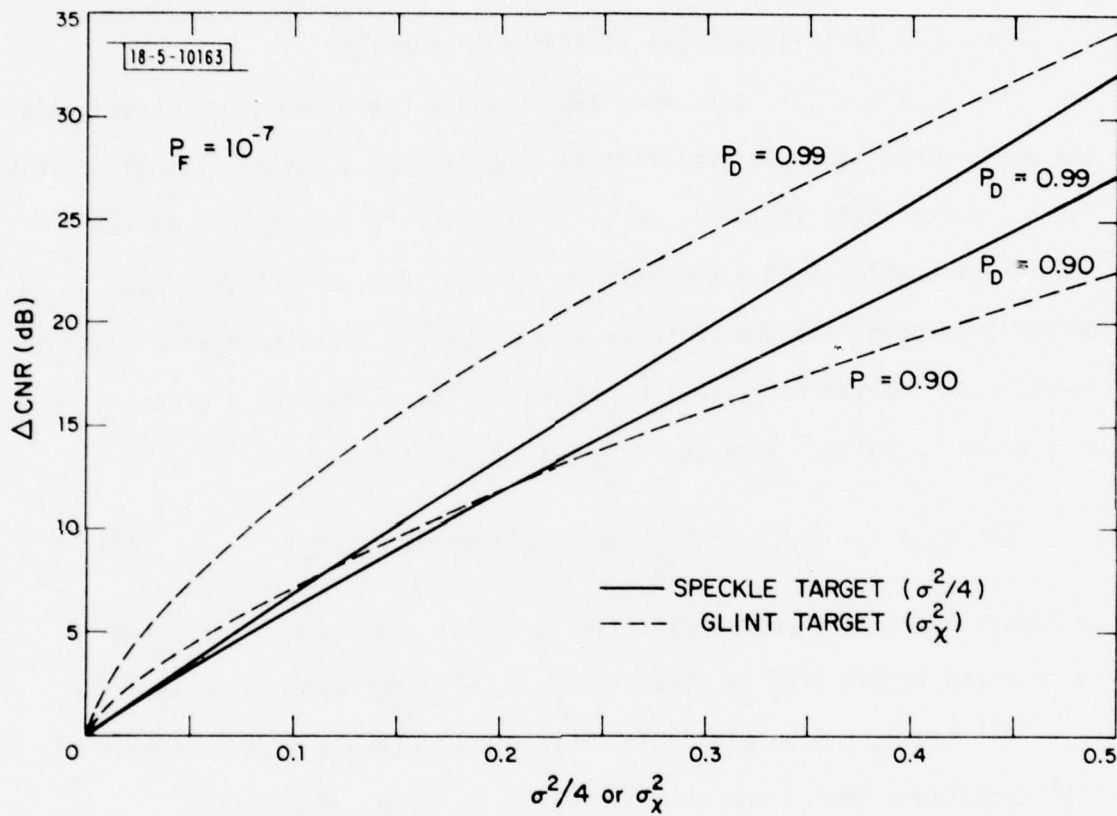


Fig. 34. Additional carrier-to-noise ratio ΔCNR required due to turbulence vs. log-amplitude variance, σ_X^2 or $\sigma^2/4$, for glint targets (σ_X^2) and speckle targets ($\sigma^2/4$) with $P_F = 10^{-7}$ and $P_D = 0.90$ and 0.99 .

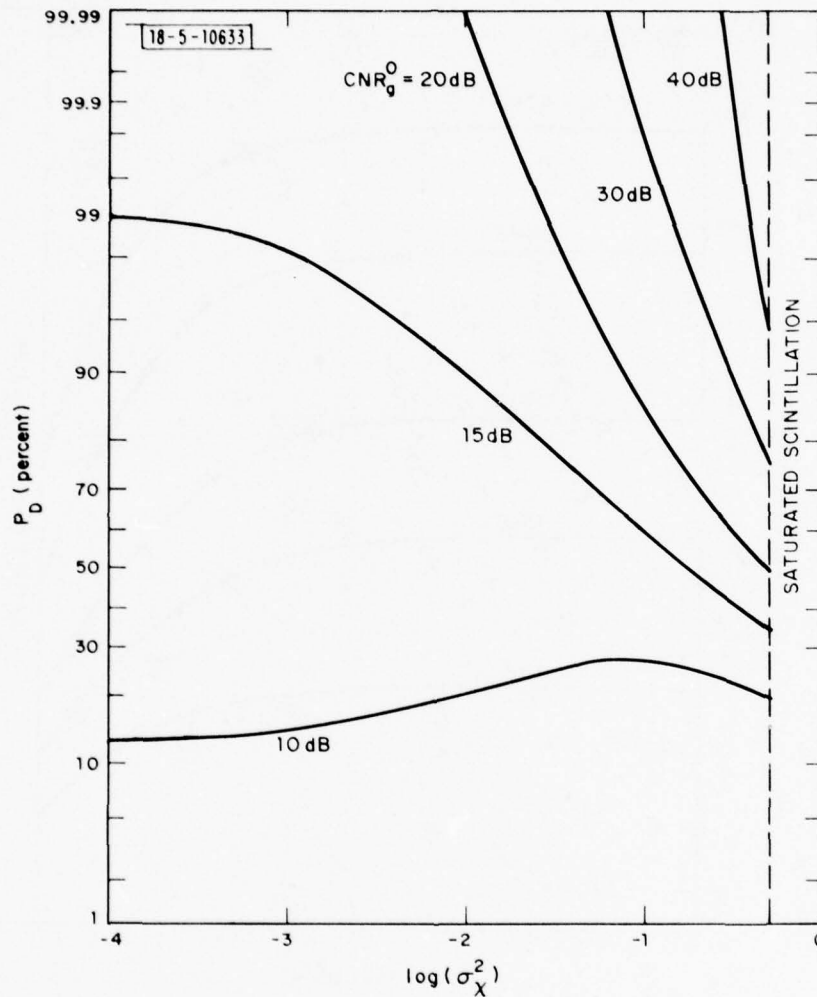


Fig. 35. Detection probability P_D vs. log-amplitude variance σ_X^2 for glint targets at $P_F = 10^{-7}$ and several values of the free-space propagation glint target carrier-to-noise ratio CNR_g^0 .

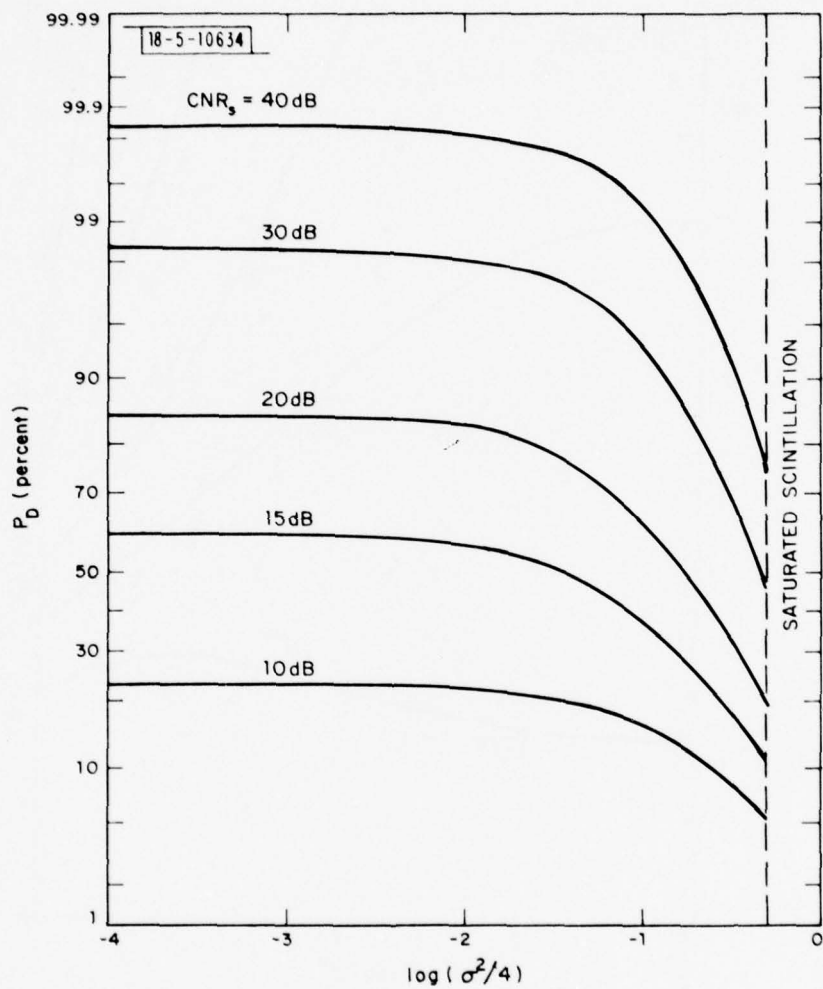


Fig. 36. Detection probability P_D vs. log-amplitude variance $\sigma^2/4$ for speckle targets at $P_F = 10^{-7}$ and several values of the turbulent-propagation speckle target carrier-to-noise ratio CNR_s .

similar curves of P_D vs. $\sigma^2/4$ for speckle targets at $P_F = 10^{-7}$ and the same CNR values. A brief examination of these figures indicates that significant changes in glint target detection performance can occur for quite low σ_X^2 values, while for speckle target detection, significant performance degradations do not begin to occur until much larger $\sigma^2/4$ values are reached. The magnitude of the maximum degradations encountered at saturation (of the scintillation), however, are not significantly different for glint and speckle targets if the free space P_D values are between approximately 0.50 and 0.9999.

The carrier-to-noise ratio of a coherent optical radar is given by the monostatic radar equation [2]

$$\text{CNR} = \frac{P_T}{h\nu_0 B} \frac{d^2}{4 L^2} \epsilon \rho \eta e^{-2\alpha L} \quad (48)$$

where P_T is the transmitted laser power, $h\nu_0$ is the photon energy, B is the IF bandwidth, d is the transmitter/receiver aperture diameter, L is the target range, ϵ is the optical efficiency of the system, ρ is the target reflectivity, η is the detector quantum efficiency, and α is the atmospheric extinction coefficient. In a pulsed laser radar using a matched filter detection scheme the quantity P_T/B in Eq. (48) may be replaced by the quantity P_{av}/PRF where P_{av} is the average transmitted power and PRF is the pulse repetition frequency. Table 20 lists typical parameters for a tactical infrared ($\lambda = 10.6\mu\text{m}$) radar. Using these values and assuming an atmospheric attenuation of 0.5 dB/km (a value consistent with propagation through clear, dry air) we have calculated CNR for this system as a function of L and plotted

TABLE 20
TYPICAL INFRARED RADAR PARAMETERS

Average Power (P_{av})	1 W
Pulse Repetition Frequency (PRF)	30 kHz
Transmitter/Receiver Diameter (d)	10 cm
Photon Energy ($h\nu_0$)	1.87×10^{-20} J
Optical Efficiency (ϵ)	0.1
Quantum Efficiency (η)	0.5
Average Target Reflectivity (ρ)	0.1

the results as the solid curves in Figures 37-39.

An indication of the magnitude of atmospheric turbulence effects on the performance of a radar in a realistic scenario can be obtained by comparing the CNR required to achieve a given P_D and P_F against the CNR available from the radar. Let us first consider a ground-based radar located at a height of 3m searching for targets on the ground. In this case a horizontal path is appropriate and we will use the RADC results of Figure 27. Combining these data with the Δ CNR curves of Figure 34 and the free-space values of CNR ($0, P_D, P_F$) from Tables 1 and 9 yields curves of $\text{CNR}_g^o(\sigma_x^2; P_D, P_F)$ and $\text{CNR}_s(\sigma^2/4; P_D, P_F)$. These are plotted in Figure 37 for $P_D = 0.90$ and $P_F = 10^{-7}$. In this example we find that in free space the radar can detect speckle targets out to 6 km and glint targets out to 10 km. If we assume the nighttime turbulence levels, the glint target detection drops to 7.5 km, a significant performance degradation. The speckle target detection range is only minimally affected by nighttime turbulence levels. This is partly the result of the higher CNR required for free-space speckle target detection over glint target detection and partly the result of speckle target aperture averaging which increases (ζ decreases) with increasing range. If we assume the daytime turbulence levels, the detection range is decreased to less than 2.5 km for both glint and speckle targets. This may be a catastrophic performance degradation in some applications.

It should be pointed out that at very large values of C_n^2 and large ranges the diameter of the transmitter may exceed the turbulence field coherence length ρ_0

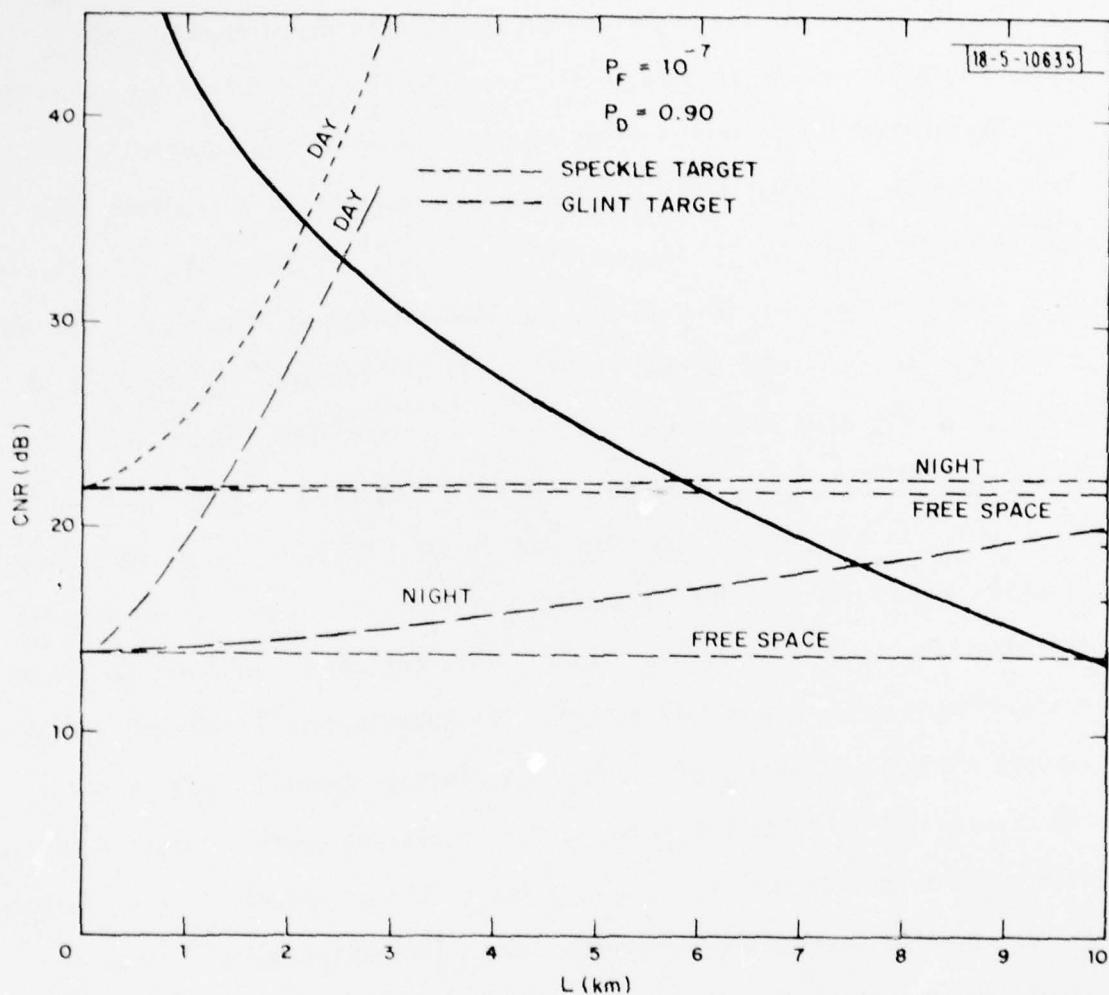


Fig. 37. Carrier-to-noise ratio CNR required to achieve $P_D = 0.90$ and $P_F = 10^{-7}$ vs. path length L for a ground-based radar located at a height of 3m searching for targets on the ground along a horizontal path. Curves are provided for both speckle (short-dashed lines) and glint (long-dashed lines) targets under daytime, nighttime, and free-space propagation conditions. The solid curve is the system CNR assuming 0.5 dB/km atmospheric attenuation.

$$\rho_0 = [2.91 k^2 \int_0^L dz C_n^2(z) (1 - z/L)^{5/3}]^{-3/5} \quad (49)$$

$$= [1.09 k^2 C_n^2 L]^{-3/5} \quad \text{for } C_n^2(z) = \text{constant} \quad (50)$$

If this occurs, transmitter beam spreading and receiver coherence loss will occur, effects which have been neglected in the theoretical analysis. Inclusion of these effects, however, only tends to increase the magnitude of the observed degradation.

Let us next consider an airborne infrared radar located at a height of 30m searching for targets on the ground. For this example we will assume the slant path data of Figures 30 and 31. The CNR values necessary to achieve $P_D = 0.90$ and $P_F = 10^{-7}$ are plotted as a function of target range in Figure 38. For speckle targets negligible effects on the detection range are observed under either daytime or nighttime conditions. For glint targets significant decreases in detection range are observed for both daytime and nighttime turbulence. However, the magnitude of the decreases are much less than those of the horizontal path example.

Finally, in Figure 39 we provide CNR results for a ground-based radar searching for airborne targets along a slant path of 5 mrad elevation angle assuming the data in Figures 32 and 33. The results for this example do not differ significantly from the airborne slant path example.

The preceding examples serve to indicate that typical turbulence levels can significantly degrade the target detection range performance of infrared radars. However, there is another more subtle way in which turbulence can

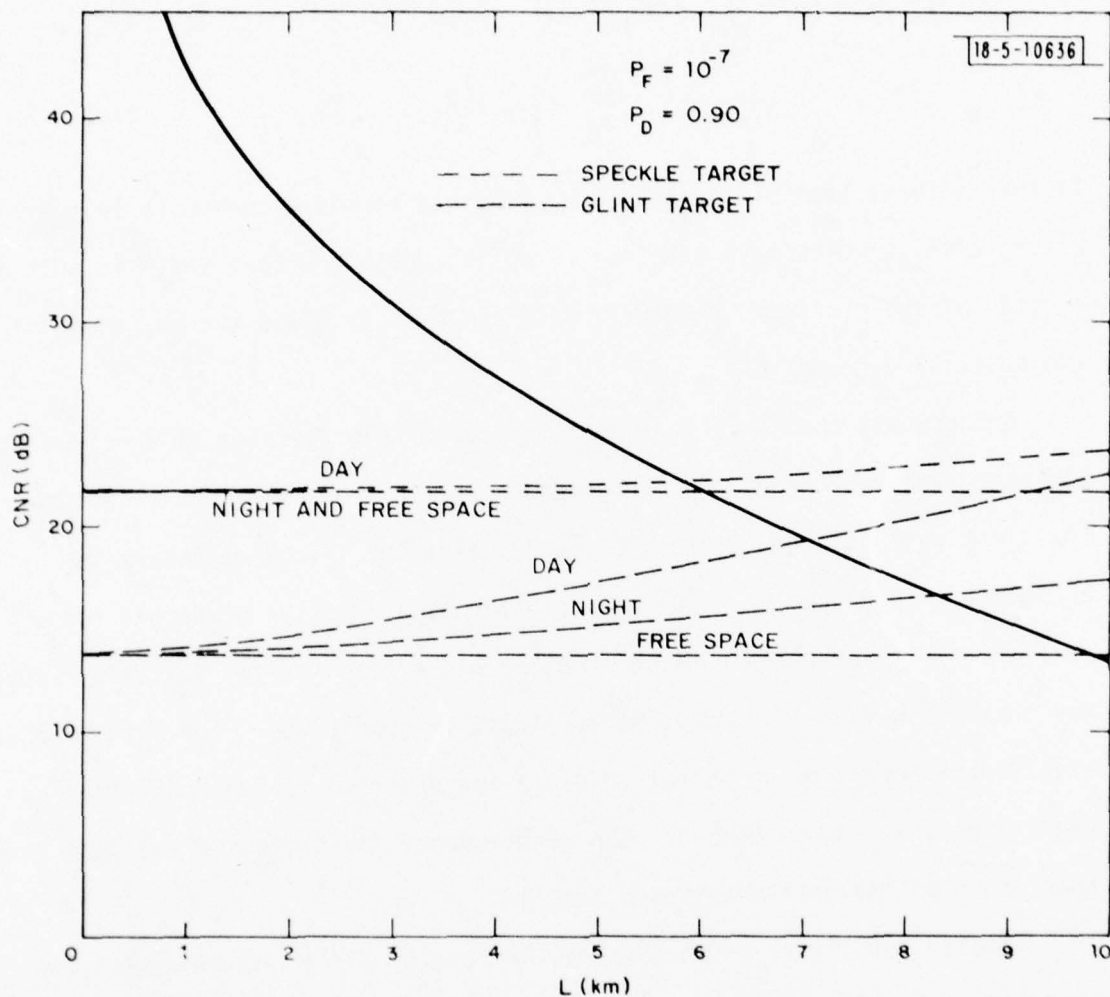


Fig. 38. Carrier-to-noise ratio CNR required to achieve $P_D = 0.90$ and $P_F = 10^{-7}$ vs. slant path length L for an airborne radar located at a height of 30m searching for targets on the ground. Curves are provided for both speckle (short-dashed lines) and glint (long-dashed lines) targets under daytime, nighttime, and free-space propagation conditions. The solid curve is the system CNR assuming 0.5 dB/km atmospheric attenuation. The speckle target nighttime and free-space curves are indistinguishable on this scale.

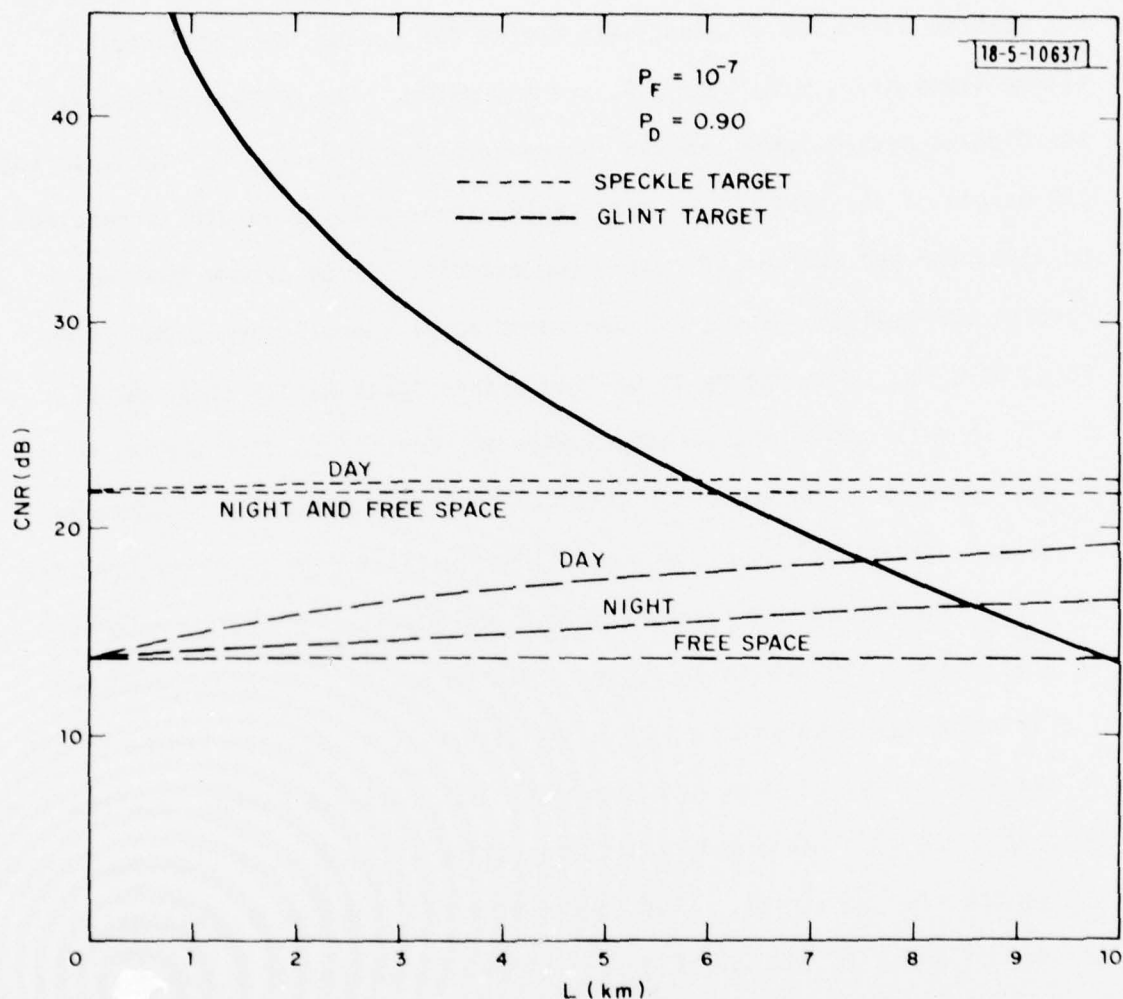


Fig. 39. Carrier to noise ratio CNR required to achieve $P_D = 0.90$ and $P_F = 10^{-7}$ vs. slant path length L for a ground-based radar located at a height of 2m searching for airborne targets along a slant path with an elevation angle of 5 mrad. Curves are provided for both speckle (short-dashed lines) and glint (long-dashed lines) targets under daytime, nighttime, and free space propagation conditions. The solid curve is the system CNR assuming 0.5 dB/km atmospheric attenuation. The speckle target nighttime and free-space curves are indistinguishable on this scale.

affect radar performance. In Figure 40 we have plotted the horizontal path CNR results of Figure 37 along with system CNR curves for atmospheric attenuations of 0, 0.5, 1.0, 2.0, and 4.0 dB/km. The difference between the 0 dB/km system curve and the appropriate CNR (σ_X^2 ; P_D , P_F) curve is the CNR margin of the system. In most applications a large margin is required to allow for bad weather effects. For example, let us assume that we require our radar to have a minimum operational speckle target detection range of 2 km. From Figure 40 we find a free space margin of 16 dB at 2 km. This is sufficient to accommodate an atmospheric attenuation of 4 dB/km or less. The degree of attenuation that a system can accommodate translates directly into system operational utility (the percentage of the time that the system will exceed minimum acceptable performance levels). This may be seen by examining Figure 41 which presents seasonal-averaged 10.6 μ m atmospheric attenuation data for Germany (the German climate is not unlike that of upstate New York where the RADC data was taken) obtained from Refs. [1] and [2]. An atmospheric attenuation of 4 dB/km or less occurs only 80% of the time in winter. Thus, our system will have an operational utility of 80%. If the margin were smaller, the amount of attenuation the system could accommodate would be smaller and the operational utility would be decreased.

Let us now look at the margins obtained when turbulence is present. For daytime turbulence the speckle target margin decreases from 16 dB to 4 dB. This implies a decrease in weather penetration capability (at 2 km) from 4 dB/km to 1 dB/km. This in turn implies a decrease in operational

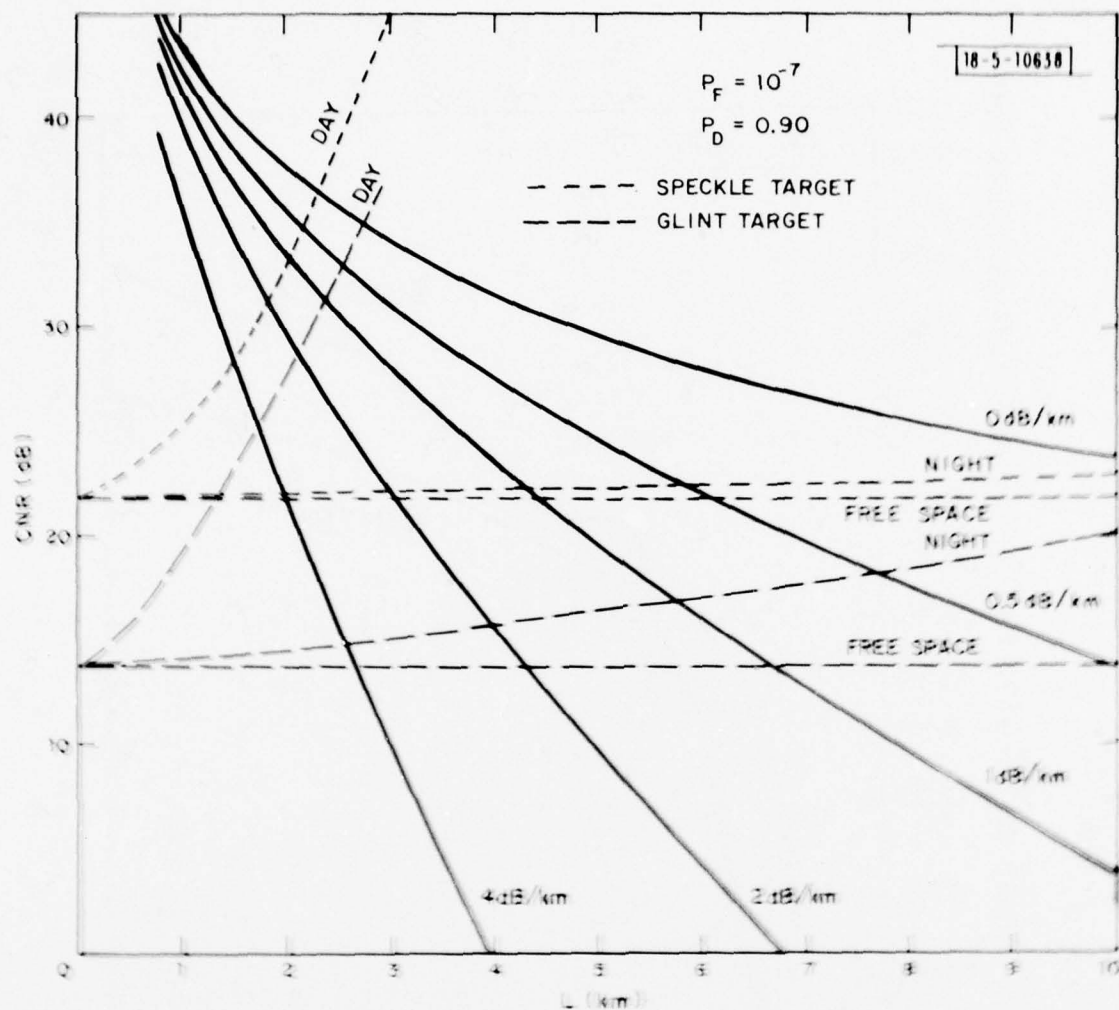


Fig. 40. Turbulence effects on infrared radar CNR margins. The dashed curves depict the carrier-to-noise ratio CNR required to achieve $P_D = 0.90$ and $P_F = 10^{-7}$ vs. path length L for a ground-based radar located at a height of 1m searching for speckle (short-dashed lines) and glint (long-dashed lines) targets on the ground along a horizontal path under daytime, nighttime, and free-space propagation conditions. The solid curves represent the system CNR obtained for atmospheric attenuations of 0, 0.5, 1.0, 2.0, and 4.0 dB/km.

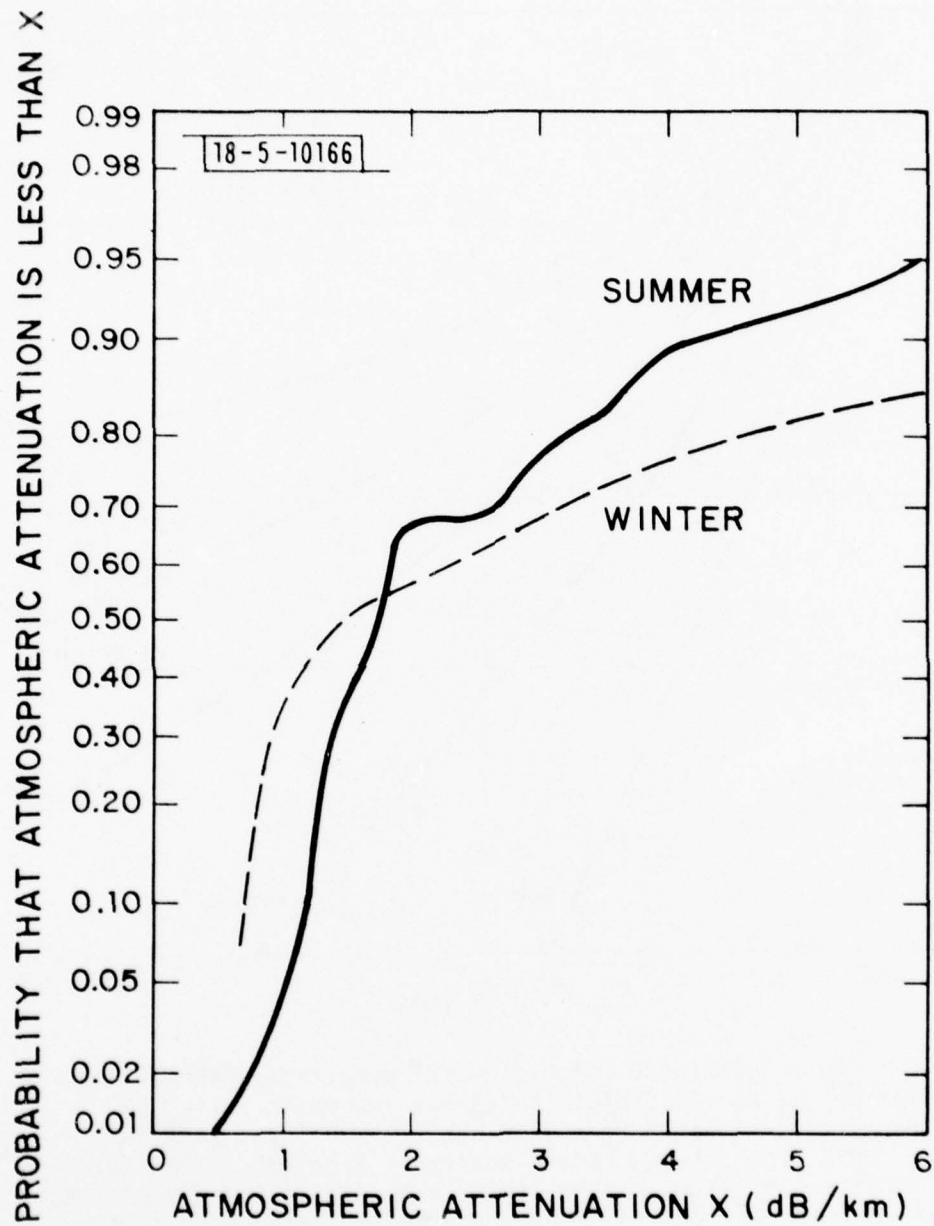


Fig. 41. Seasonal-averaged $10.6\mu\text{m}$ atmospheric attenuation statistics for Germany.

utility from 80% to only 35%, a truly significant performance degradation. Even in benign turbulence conditions, a margin reduction of a few dB is not unreasonable. Since even a small reduction in weather penetration capability can affect the operational utility by several percent and a 1% decrease in operational utility means 3.65 fewer days the system will operate, margin reduction effects may be significant even in turbulence conditions where detection range degradations are negligible.

The preceding analysis assumes that turbulence strengths and atmospheric attenuations are uncorrelated. Comparison of the Type I turbulence (clear weather) results in Table 19 with the all-weather results indicates that there is a correlation. In general, daytime turbulence strengths are lower in bad weather while nighttime, dawn, and dusk strengths are relatively independent of the weather. Although this will lessen the magnitude of the daytime effects, they will still be significant. A comprehensive treatment of radar performance will require detailed statistical analyses of the correlated effects of atmospheric attenuation and turbulence strength. Unfortunately, the simultaneous meteorological data needed for these analyses are not yet available.

It is important to note that in all of the examples in this section we have used mean or average values of σ_X^2 . However, in reality the observed σ_X^2 values will be randomly distributed about the mean. Thus, there is a nonzero probability that values greatly exceeding $\langle \sigma_X^2 \rangle$ may be obtained. Therefore, even if the mean turbulence performance degradations are acceptable (due to sufficient margin), unacceptable performance may be

obtained during some fraction of the time. Similarly, even if the mean performance is unacceptable, acceptable performance may be obtainable during a small fraction of the time. These statistical effects also need to be considered in a comprehensive study of coherent optical radar performance.

APPENDIX

PROGRAMMABLE HAND CALCULATOR PROGRAMS

Evaluation of the speckle target detection probability Eq. (21) is straightforward and yields excellent accuracy for quadratures with a relatively small number of points. This, coupled with the fact that most objects exhibit a significant diffuse reflection component at optical and infrared wavelengths, has prompted us to develop a program suitable for evaluation on a programmable hand calculator. In Table 21 we detail a program usable with either a Hewlett-Packard HP-67 or HP-97 calculator. This program calculates $P_D(\text{CNR}_S; P_F, \sigma^2)$ for P_F stored in register A, σ^2 stored in register B, and CNR_S entered as x using an 18-point Gaussian-Hermite quadrature. The quadrature points and weighing coefficients are entered via a data card. Computation time of this program is roughly 60 seconds and the relative accuracy in P_D is better than about 0.3% for $\sigma^2 = 2.0$ and improves rapidly as σ^2 decreases. Supplementary programs have also been outlined which convert numbers from decibels to decimal and vice-versa, evaluate the free-space detection probability according to Eq. (17), calculate σ^2 according to Eq. (14) given σ_X^2 and ζ , and determine ζ according to Eq. (15) given $N_F = d^2/\lambda L$.

The preceding programs were also modified for use with a Hewlett-Packard HP-29C calculator. The modified programs are detailed in Table 22. Because of the larger number of storage registers available, a 24-point Gaussian-Hermite quadrature was used. Computation time of this program is roughly 75 seconds and the relative accuracy in P_D is approximately 0.03% for $\sigma^2 = 2.0$ and improves rapidly as σ^2 decreases.

TABLE 21

SPECKLE TARGET TURBULENCE CALCULATIONS-HP67 PROGRAMS

STEP	KEY ENTRY	KEY CODE	COMMENTS	STEP	KEY ENTRY	KEY CODE	COMMENTS
001	f LBL A	31 25 11	PROGRAM A		0	00	
	STO C	33 13			z	81	converts x from
	9	09			g 10 ^x	32 53	decibels to decimal
	h STI	35 33	calculates speckle	060	h RTN	35 22	
	0	00	target $P_D(\sigma^2)$		f LBL C	31 25 13	PROGRAM C
	STO E	33 15			1	01	
	f LBL 1	31 25 01	$x = CNR_s$		+	61	calculates
	RCL (i)	34 24	$A = P_F$		h 1/x	35 62	
	g GSB a	32 22 11	$B = \sigma^2$		STO E	33 15	$P_D = P_F (1 + CNR_s)^{-1}$
010	STO 0	33 00	REGISTERS(data card)		RCL A	34 11	
	RCL (i)	34 24			RCL E	34 15	$x = CNR_s$
	CHS	42			h y ^x	35 63	$A = P_F^s$
	g GSB a	32 22 11	1 = 2.582677505E-01		h RTN	35 22	
	RCL 0	34 00	2 = 7.766829193E-01	070	f LBL D	31 25 14	PROGRAM D
	+	61	3 = 1.300920858		1	01	
	STO D	33 14	4 = 1.835531604		6	06	calculates σ^2
	f p \leftrightarrow s	31 42	5 = 2.386299089		x	71	given ϵ and σ_x^2
	RCL (i)	34 24	6 = 2.961377506		g e ^x	32 52	
	RCL D	34 14	7 = 3.573769068		1	01	
020	x	71	8 = 4.248117874		-	51	$x = \sigma_x^2$
	RCL E	34 15	9 = 5.048364009		RCL E	34 15	$E = \epsilon$
	+	61	11 = 4.834956947E-01		x	71	
	STO E	33 15	12 = 2.848072857E-01		1	01	
	f p \leftrightarrow s	31 42	13 = 9.730174764E-02	080	+	61	stores result in B
	f DSZ	31 33	14 = 1.864004239E-02		f LN	31 52	
	GTO 1	22 01	15 = 1.888522630E-03		4	04	
	RCL E	34 15	16 = 9.181126868E-05		z	81	
	h π	35 73	17 = 1.810654481E-06		STO B	33 12	
	f \sqrt{x}	31 54	18 = 1.046720580E-08		h RTN	35 22	
030	z	81	19 = 7.828199772E-12		f LBL E	31 25 15	PROGRAM E
	h RTN	35 22			STO E	33 15	
	g LBL a	32 25 11	SUBPROGRAM a		1	01	calculates ϵ given
	2	02	used in PROGRAM A	090	+	61	
	f \sqrt{x}	31 54			RCL E	34 15	$N_F = d^2/\lambda L$
	x	71			z	81	$x = N_F$
	RCL B	34 12			h 1/x	35 62	stores result in E
	f \sqrt{x}	31 54			STO E	33 15	
	-	51			h RTN	35 22	
	RCL B	34 12			g LBL b	32 25 12	PROGRAM b
040	f \sqrt{x}	31 54			f LOG	31 53	
	x	71			1	01	converts x from
	2	02			0	00	decimal to decibels
	x	71			x	71	
	g e ^x	32 52		100	h RTN	35 22	
	RCL C	34 13					
	x	71					
	1	01					
	+	61					
	h 1/x	35 62					
050	STO D	33 14					
	RCL A	34 11					
	RCL D	34 14					
	h y ^x	35 63					
	h RTN	35 22		110			
	f LBL B	31 25 12	PROGRAM B				
	1	01					

TABLE 22

SPECKLE TARGET TURBULENCE CALCULATIONS-HP29C PROGRAMS

STEP	KEY ENTRY	KEY CODE	COMMENTS	STEP	KEY ENTRY	KEY CODE	COMMENTS
001	g LBL 0	15 13 00	PROGRAM 1		g LBL 4	15 13 04	PROGRAM 4
	STO 2	23 02			1	01	
	2	02			+	51	
	9	09	calculates speckle	060	g 1/x	15 74	calculates
	STO 0	23 00	target $P_D(\sigma^2)$		RCL 3	24 03	$P_D = P_F^{(1+CNR_S)^{-1}}$
	0	00			x \leftrightarrow y	21	
	STO 1	23 01	x = CNR _S		f y ^x	14 64	x = CNR _S , 3 = P _F
	g LBL 1	15 13 01	3 = P _F		g RTN	15 12	
	RCL (i)	24 22	4 = σ^2		g LBL 5	15 13 05	PROGRAM 5
010	GSB 2	12 02			1	01	
	RCL (i)	24 22			6	06	
	CHS	32	DATA REGISTERS		x	61	calculates σ^2
	GSB 2	12 02			g e ^x	15 42	given ζ and σ_x^2
	+	51	29 = 6.015925561	070	1	01	
	g DSZ	15 23	28 = 1.664368497E-16		-	41	
	RCL (i)	24 22	27 = 5.259382928		RCL 2	24 02	
	x	61	26 = 6.584620243E-13		x	61	x = σ_x^2
	STO + 1	23 51 01	25 = 4.625662756		1	01	2 = ζ
	g DSZ	15 23	24 = 3.046254270E-10		+	51	
020	RCL 0	24 00	23 = 4.053664403		f ln	14 42	
	6	06	22 = 4.018971175E-08		4	04	stores result in 4
	f x ^y	14 41	21 = 3.520006813		:	71	
	GTO 1	13 01	20 = 2.158245705E-06		STO 4	23 04	
	RCL 1	24 01	19 = 3.012546138	080	g RTN	15 12	
	g π	15 73	18 = 5.688691636E-05		g LBL 6	15 13 06	PROGRAM 6
	f \sqrt{x}	14 63	17 = 2.523881017		ENTER +	31	
	:	71	16 = 8.236924827E-04		ENTER +	31	calculates ζ given
	g RTN	15 12	continued +		1	01	$N_F = d^2/\lambda L$
	g LBL 2	15 13 02			+	51	x = N_F
030	2	02	SUBPROGRAM 2		:	71	stores result in 2
	f \sqrt{x}	14 63	used in PROGRAM 1		STO 2	23 02	
	x	61			g RTN	15 12	
	RCL 4	24 04			g LBL 7	15 13 07	PROGRAM 7
	f \sqrt{x}	14 63		090	f LOG	14 43	
	-	41			1	01	converts x from
	RCL 4	24 04			0	00	decimal to decibels
	f \sqrt{x}	14 63			x	61	
	x	61			g RTN	15 12	
	2	02					DATA REGISTERS(cont)
040	x	61					15 = 2.049003574
	g e ^x	15 42					14 = 7.048355810E-03
	RCL 2	24 02					13 = 1.584250010
	x	61					12 = 3.744547050E-02
	1	01					11 = 1.126760818
	+	51					10 = 1.277396218E-01
	g 1/x	15 74					9 = 6.741711070E-01
	RCL 3	24 03					8 = 2.861795354E-01
	x \leftrightarrow y	21					7 = 2.244145474E-01
	f y ^x	14 64					6 = 4.269311639E-01
050	g RTN	15 12					
	g LBL 3	15 13 03	PROGRAM 3				
	1	01					
	0	00					
	:	71	converts x from				
	g 10 ^x	15 43	decibels to decimal				
	g RTN	15 12					

REFERENCES

1. A. P. Modica and H. Kleiman, "Statistics of Global IR Atmospheric Transmission," Project Report TT-7, Lincoln Laboratory, M.I.T. (8 March 1976), DDC AD-A024311/3.
2. R. J. Becherer, "System Design Study for Infrared Airborne Radar (IRAR)," Technical Note 1977-29, Lincoln Laboratory, M.I.T. (18 October 1977), DDC AD-A048979/9.
3. R. J. Hull and S. Marcus, "A Tactical 10.6 μ m Imaging Radar," Proc. 1978 National Aerospace and Electronics Conf. (IEEE, Dayton, Ohio, 1978), p. 662.
4. R. C. Harney, "Conceptual Design of a Multifunction Infrared Radar for the Tactical Aircraft Ground Attack Scenario," Project Report TST-25, Lincoln Laboratory, M.I.T. (25 August 1978), DDC AD-A061048.
5. R. C. Harney, "Design Considerations for the Infrared Airborne Radar (IRAR) MTI Subsystem," Project Report TST-26, Lincoln Laboratory, M.I.T. (to be published).
6. J. H. Shapiro, "Imaging and Target Detection with a Heterodyne-Reception Optical Radar," Project Report TST-24, Lincoln Laboratory, M.I.T. (13 October 1978), DDC AD-A063767.
7. A. H. Stroud and D. Secrest, Gaussian Quadrature Formulas (Prentice-Hall, Englewood Cliffs, 1966), Chapter 2.
8. J. I. Marcum, "Table of Q Functions," Report RM-339, Rand Corporation (1 January 1950).
9. J. V. DiFranco and W. L. Rubin, Radar Detection (Prentice-Hall, Englewood Cliffs, 1968), p. 316.
10. S. F. Clifford, "The Classical Theory of Wave Propagation in a Turbulent Medium," in Laser Beam Propagation Through The Atmosphere, J. W. Strohbehn, Ed. (Springer-Verlag, Berlin, 1978).
11. R. E. Hufnagel, "Propagation Through Atmospheric Turbulence," in The Infrared Handbook, W. L. Wolfe and G. J. Zissis, Eds. (Environmental Research Institute of Michigan, Ann Arbor, 1979), Chapter 6.
12. M. A. Kallistratova and D. F. Timanovskiy, "The Distribution of the Structure Constant of Refractive Index Fluctuations in the Atmospheric Surface Layer," Atmos and Ocean Phys. 7, 46 (1971).

13. W. D. Neff, "Quantitative Evaluation of Acoustic Echoes from the Planetary Boundary Layer," Technical Report ERL 322-WPL 38, National Oceanic and Atmospheric Administration (June 1975).
14. J. L. Spencer, "Long-Term Statistics of Atmospheric Turbulence Near the Ground," Report RADC-TR-78-182, Rome Air Development Center (August 1978).
15. J. C. Wyngaard, Y. Izumi, and S. A. Collins, Jr., "Behavior of the Refractive-Index-Structure Parameter Near the Ground," J. Opt. Soc. Am. 61, 1646 (1971).
16. A. W. Cooper, E. C. Crittenden, Jr., and A. F. Schroeder, "Height Dependence of Optical Scintillation Over the Ocean," Topical Meeting on Optical Propagation Through Turbulence (OSA, Boulder, Colorado, 1974), paper WB4.

AD-A076 535

MASSACHUSETTS INST OF TECH LEXINGTON LINCOLN LAB

F/G 17/9

TURBULENCE EFFECTS ON THE RECEIVER OPERATING CHARACTERISTICS OF--ETC(U)

JUL 79 B A CAPRON , J H SHAPIRO , R C HARNEY

F19628-78-C-0002

UNCLASSIFIED TST-33

ESD-TR-79-189

NL

2 OF 2

AD
A076535



END
DATE
FILMED

12-79

DDC

UNCLASSIFIED

SECURITY CLASSIFICATION OF THIS PAGE (When Data Entered)

19 REPORT DOCUMENTATION PAGE		READ INSTRUCTIONS BEFORE COMPLETING FORM
1. REPORT NUMBER 18 ESD-TR-79-189	2. GOVT ACCESSION NO.	3. RECIPIENT'S CATALOG NUMBER
4. TITLE (and Subtitle) 6 Turbulence Effects on the Receiver Operating Characteristics of a Heterodyne-Reception Optical Radar		5. TYPE OF REPORT & PERIOD COVERED 9 Project Report
7. AUTHOR(s) 10 Barbara A. Capron, Jeffrey H. Shapiro Robert C. Harney		8. CONTRACT OR GRANT NUMBER(s) 15 F19628-78-C-0002
9. PERFORMING ORGANIZATION NAME AND ADDRESS Lincoln Laboratory, M.I.T. P.O. Box 73 Lexington, MA 02173		10. PROGRAM ELEMENT, PROJECT, TASK AREA & WORK UNIT NUMBERS Program Element No. 65705F Project No. 649L
11. CONTROLLING OFFICE NAME AND ADDRESS Air Force Systems Command, USAF Andrews AFB Washington, DC 20331		12. REPORT DATE 11 26 July 1979
14. MONITORING AGENCY NAME & ADDRESS (if different from Controlling Office) Electronic Systems Division Hanscom AFB Bedford, MA 01731		13. NUMBER OF PAGES 98
16. DISTRIBUTION STATEMENT (of this Report) Approved for public release; distribution unlimited.		15. SECURITY CLASS. (of this report) Unclassified
17. DISTRIBUTION STATEMENT (of the abstract entered in Block 20, if different from Report)		15a. DECLASSIFICATION DOWNGRADING SCHEDULE
18. SUPPLEMENTARY NOTES None		
19. KEY WORDS (Continue on reverse side if necessary and identify by block number) infrared radar heterodyne reception target speckle target detection signal-to-noise ratio atmospheric turbulence glint atmospheric scintillation log-amplitude variance receiver operating characteristics		
20. ABSTRACT (Continue on reverse side if necessary and identify by block number) The theory of atmospheric turbulence effects on the receiver operating characteristics of coherent optical radars is reviewed and the theoretical results for the target detection probability are numerically evaluated. Graphs and tables are presented of the glint target and speckle target detection probabilities as a function of the carrier-to-noise ratio at various false alarm probabilities for different turbulence log-amplitude variances. Experimental turbulence strength measurements are reviewed and used to determine typical log-amplitude variances. These results are combined with the detection probability calculations to predict the performance of a realistic infrared radar under a variety of turbulent propagation conditions.		

UNCLASSIFIED

SECURITY CLASSIFICATION OF THIS PAGE (When Data Entered)

204650